UNIVERSITY OF TROMSØ UIT

FACULTY of Science and Technology
DEPARTMENT of Physics and Technology

Water and heat transfer in cement based materials

Hung Thanh Nguyen

A dissertation for the degree of
Philosophiae Doctor

February 2011

A DISSERTATION FOR THE DEGREE OF DOCTOR SCIENTIARUM

WATER- AND HEAT TRANSFER IN CEMENT BASED MATERIALS

Hung Thanh Nguyen

February 2011

Summary

While heat and mass transfer (transport phenomena) developed independently as branches of classical physics long ago, their unified study has found its place as one of the fundamental engineering sciences. This development, in turn, less than half a century old, continues to grow, and find applications in new fields such as biotechnology, microelectronics, nanotechnology, polymer science, and porous materials. The development of a model for transport phenomena in cement based material like concrete, is our primary consideration in this work.

Concrete has been one of the most useful building materials in the world in the past, and still is today. Therefore, transport phenomena in concrete are, and have been, an indisputable research theme in the building material sciences.

The evolution of models for the transport phenomena in concrete (both in theory and experimental work) has been rapid and extensive for many years. However, the great difficulties in constituting exact models for the transport phenomena in this material are well known. Why is the configuration of these models so difficult? There are several reasons for this, we will elucidate some aspects of this problem, and then pose out our main problems, which we will consider through this work.

For the mass transfer case (the absorption of moisture-water into concrete), the water content in concrete has a significant impact on its mechanical properties. Moisture transport in porous media, for example, plays an important role in the degradation of building materials such as mortars and concrete.

In general, there are two different models frequently used for this purpose, the Diffusion model and the Lucas Washburn model (LWE). Roughly speaking, the Diffusion model assumption, at the basis of the model, is that the transport mechanism during the initial phase of the absorption phenomenon is predominantly controlled by the diffusion of water. The LWE model, on the other hand, is based on the capillary transport mechanism. It models the capillary penetration of a liquid into pore space, initially empty. This is usually viewed as a spontaneous process driven by interfacial pressure differences. LWE is a simple relevant model that has been studied as a cylindrical capillary in contact with an infinite liquid reservoir. Moreover, this model predicts, for example, that the increasing of the water penetration has linear relationship with square root of capillary time (assuming a constant pipe diameter).

However, LWE ignores the complex pore structure and network, typically found in cement materials. Many earlier research works has shown clearly that complex pores structure of concrete, strongly impedes the water penetration. Following this line, we believe also that the changing of pore structure may impose a strong effect on the water capillary suction.

In this work we have also considered heat transportation in cement based materials. The used heat conduction transfer model with convection boundary conditions is a standard model for describing the distribution of energy in the building/building material (like concrete) and its exchange of energies (heating or cooling) with its surroundings. In this work we will focus on the surface convection heat transfer coefficient which is included in boundary conditions.

In recent years there has been a different strategy for handling the heat and moisture transfer in concrete. Both heat and mass transfer are dependent on each other. To study moisture movement in porous materials under temperature gradients is relevant and necessary in the building/ material science. The coupled transport of water/moisture and heat which occurs in concrete pore network, in general, is described by irreversible thermodynamics. An aspect of this transport process, namely the moisture transport from a wet concrete surface and into concrete exposed to frost is considered here. An analytical model for this purpose was developed. The model based on the simple reversible thermodynamics and the experimental data of experimental of water uptake during cyclic freeze/thaw action.

This work is a PhD-research program and it was carried out at the University in Tromsø (UiTø) and at the University College in Narvik (HiN). The aim of the research projects is: to construct or improve accurate models of the heat and mass transfer in concrete, and to compare the results with relevant experimental data. My contributions to the PhD-research program started in August 2005, and formally ended in February 2011. We hope and believe that this work will provide step stones for more insight in the complex transport phenomena in porous materials like concrete.

Acknowledgment

I would first and foremost like to thank my two supervisors Prof. Stefan Jacobsen and Prof. Frank Melandsø for involving me in research in one of the most interesting and important subjects in engineering work, the transfer of heat and mass in cement based materials like concrete.

I would like to express my sincere gratitude to all those who have assisted me in this study.

I am grateful to my supervisor Prof. Stefan Jacobsen, from Norwegian University of Science and Technology (NTNU), for his help with this thesis, resulting in insightful comments and guidance. I am grateful for his willingness to guide me and share his knowledge with me and for his patience with my English. Many of the ideas presented here are the fruits of numerous discussions with Stefan Jacobsen. He also used a lot of his time to assist me with my English writing. In addition, his open mind was a valuable contribution in helping me bring these ideas into practice.

I am also grateful to my other supervisor Professor Frank Melandsø, from University of Tromsø (UiTø), for his help with this thesis, especially in the Physics field. I came into contact with his group and began working with them in early 2003. My knowledge in this field was limited before I began working with him. It is through his encouraging support and guidance that my understanding of Physics has improved. His systematic work with the problem I address in my thesis is a continuing influence. I am grateful for having the opportunity to work with him before and during my PHD candidacy.

I would like to thank Professor Erik J. Sellevold, from NTNU, for sharing his expertise in material structures. Moreover, I am grateful to him, for introducing me to the model capillary absorption of the irregular pipe geometry. This has been a starting point in the development of the model in mass transfer addressed by this thesis.

The experimental work has been carried out in the University College in Narvik (HiN), and it was done with excellent work by senior engineer Svein Erik Sween. Thanks to my friend and colleague Raymond Riise (lecturer at HiN) for his encouragement and discussions with me. Moreover, I am grateful to him for never saying no, especially, when I asked about computer related problems. Special thanks to my colleague Tatjana Zivkovic (research fellow) and Alexander Biebricher (research fellow), from the Institute of Physics and Technology, UiTø, for many fruitful discussions in Physic.

My gratitude to my mother, Nguyen Thi Muoi Ba, for her support and for motivating me to stay focused during this whole process. She knows the true value of my work. Moreover, she often tells me that '' to reach the goal we must first of all get started, and don't forget that problem cannot solve themselves''. Thanks to my sisters Nguyen T. Phuong, Nguyen T. Lien and Nguyen T. Nguyet , for spending their time to take care of our mother.

Thanks to my wife Helene Eilertsen, for staying side by side with me this whole time. And she never let me down. I am grateful to my son Nguyen Thanh Bao Andre and my daughter Nguyen Thi Mai Emilie for their thoughtful and good relations between themselves, which in turn gives the family the harmony I need to focus on my work and complete my thesis.

'' Do not be afraid if it goes too slowly

But be afraid if it stops up ''

Tromsø February 2011

Hung Thanh Nguyen

CONTENTS

Publications:

List of symbols and abbreviations

A	Cross-section area of the specimen	m^2
B_i	Biot number	
$D(\emptyset)$	Water capillary diffusivity	m/s
G	Water absorbed	kg
g	Mass flux	m^2/s
H	Total potential hydraulic head	m
$h(t)$	Capillary penetration height/depth at time t	m
r	Radius of pore	m
Q	Heat flow	J/s
q	Heat flux	W/m^2
R_e	Reynolds number	
RH	Relative humidity	%
x, y, z	Cartesian coordinate system	m
u	Flow velocity (or flow flux density)	m/s
T	Temperature	^oC
T_s	Temperature of material surface	^oC
T_{amb}	Temperature of ambient	^oC
t	Times	s
Δx	Distance interval	m
Δt	Time interval	s
w/c	Water-to-cement ratio	kg/kg
α	Thermal convection heat transfer coefficient,(constant value)	W/m^2K
α	Degree of hydration	%
α_i	Ratio between the radius and the section length for section number i	

β_i	Ratio between the water front sectional area and the are of the other, passed, cross section,	
λ	Thermal conductivity	$W/m\ K$
ε	Total porosity	%
ε_{cap}	Capillary pores porosity	%
ε_{gel}	Gel pores porosity	%
$\emptyset$	Volumetric water content	m^3/m^3
θ	Contact angle between the pipe wall and the wetting water front	0^0
μ	Dynamic viscosity	$kg/m\ s$
ρ	Mass density	kg/m^3
σ	Surface tension between water and air	N/m
κ_s	Saturated hydraulic conductivity	m/s
$\kappa(\emptyset)$	Hydraulic conductivity as a function of water content	m/s

Chapter 1

Introduction: The structure of Concrete

1.1 Composite material

Concrete is a composite material mostly consisting of aggregate particles and hydrated cement paste as shown in Fig.1.1. A normal concrete typically contains the following parts [1]:

≈30% Volume of cement paste.

≈70% Volume of aggregate particles.

≈1-6 % of air voids.

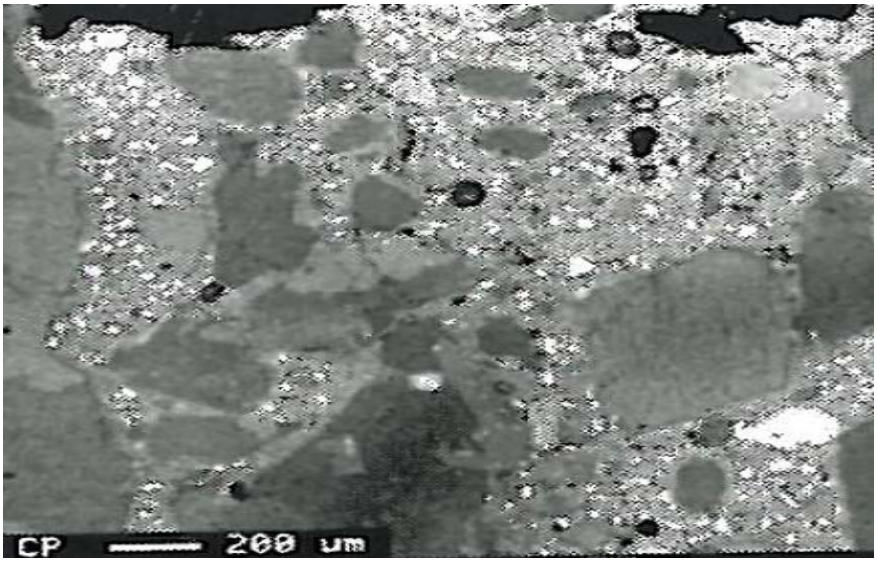

Figure 1.1. Backscatter electron image at the surface of concrete [2].

From the examination of the cross section of concrete (Fig.1.1), the two phases that easily can be distinguished are aggregate particles (of varying size and shape) and the hardened cement paste (hcp). A fourth phase, the interfacial transition zone (ITZ), represents the interfacial region between the particles of aggregate and the hcp. Each of the three phases aggregate, hcp and ITZ are in themselves multiphase in nature. For instance, each aggregate particle may contain several minerals, in addition to micro cracks and voids. Similarly both the bulk hcp and the transition zone generally contain a heterogeneous distribution of different types and amounts of solid phases and pores. Moreover, the two components of the structure, the hcp and the ITZ, are subject to change with time, environmental humidity, and temperature.

The pore structure is also complex including, for example, pores with irregular cross-sectional shapes and variations in size from micro till macro scale. Further, they are tortuous in nature, generally interconnected and randomly oriented. Finally, the pore structure may change over

time due to ageing effects by carbonation, leaching of components, irreversible drying/resaturation effects etc.

1.2 Porosity

The porosity of this material is in general defined as the ratio between the volume of the pore space and the bulk of the material. The defined porosity of a material can therefore take values in the range 0 to 1, and is a number. For many purposes, we may take the porosity as the average over the whole volume of a sample or specimen. For example, we may measure the porosity of concrete by exams of 100 mm concrete cubes [3]. The total porosity covers different kind of pores, and the network structure of them. Powers' model [4-5] is a classic model which divides porous system in hcp into two different kinds:

Capillary pores: Defined as the space not filled by the hydration products between water and cement where water may exist as capillary condensed (i.e. liquid and with under pressure or suction when less than saturated due to the surface tension between water and air). The capillary pores can obtain various dimensions ranging from $0.1\ \mu m$ to $100\ \mu m$.

Gel pores: These are very small pores with size up to a few nanometres, around $1 - 3\ nm$ (10 – 30 Å) and make up the rest of the porosity in hcp. A water molecule size is around $0.35\ nm$, e.g. gel pores are very small; only ≈3 - ≈10 times bigger than water molecules in diameter. They are regarded more as a part of the solid material structure than as normal pores. The nature of the CSH gel and state of its water (evaporable, interlayer, irreversible drying effects on porosity, shrinkage etc) has been much debated over the years. The topic was reviewed already 30 years ago [6]. Models are still published, like the recent nano-globule model in [7].

In addition, concrete also contains macro pores, or pores connected with the capillary pore system. The size of air pores is much larger than capillary pores; in the order 50 μm - > 1mm. Figure 1.2 shows microstructures of typical specimens of cement-based materials as seen in Scanning electron microscope (SEM) [3].

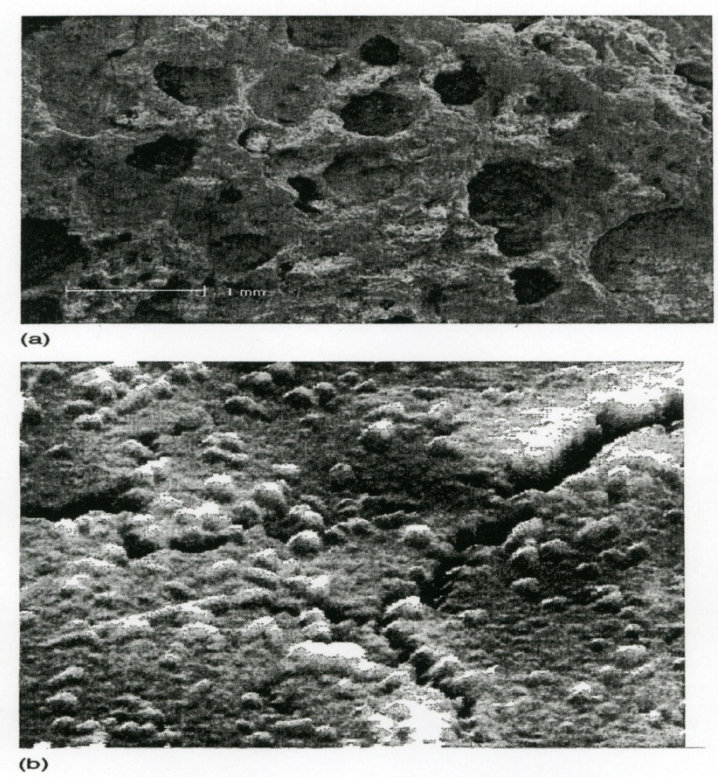

Figure 1.2. The porosity of cement materials. (a) Coarse structure of a fracture surface of autoclaved aerated concrete (normal density, ordinary Portland concrete) showing air voids Scale bar 1*mm. (b) Shrinkage cracks in a hydrated cement paste surface decorate with portlandite crystals. Image field* $14 \times 14\mu m$ *surface relief about* $1.4\ \mu m$ *[3].*

1.3 Open and closed porosity

In a porous medium, in general, it is obvious that the porosity can be connected – i.e. that there at some scale is a continuous path where a molecule or a fluid can move. In a disconnected porosity some of the pore space may be closed and isolated from the rest of the porosity and the surroundings. Such "closed porosity" or porosity where the movement of a specific fluid is restricted, contributes less or not to the transport of gases and liquids that cannot pass a certain lower threshold size value. This effect may or may not be counted for in the measured porosity, depending on practical use of the actual porosity measurement.

For transport of liquids and gases, only the part of the total porosity which is connected to the boundaries or surface is important. We will call this the open porosity, to mark the contrast between this and the closed porosity. Closed porosity can be hard to detect and it is often counted a part of the solid matrix [3-4]. Water can access most pores in concrete, though with different transport mechanisms, as observed in numerous studies [3-6].

1.4 The pores network-length of the tortuous path

From Figure 1.2, it seems that the length of the tortuous path through the pores to get from one side of a block of material to the other side may be much longer than the direct distance, but it is nevertheless finite (see distance AB in Fig. 1.3). The ratio (length AB)/(shortest distance) is one measure of the tortuosity of the pore system. The tortuosity depends on the shape of the connected paths of the pore system, where the shortest path is given by a straight line, e.g

through a straight pipe-shaped pore, having a tortuosity factor = 1, whereas a path around spheres (2D) has a tortuosity factor = π

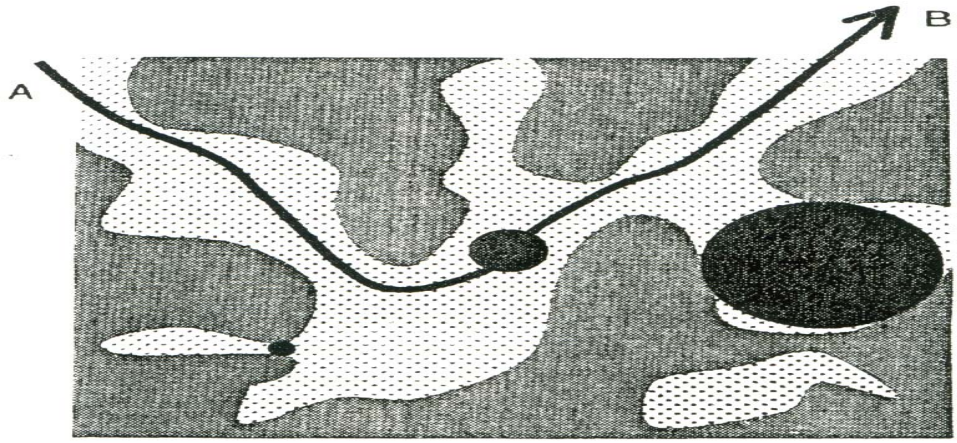

Figure 1.3. Cartoon of the porous material showing tortuosity of a part AB, and test spheres for passage along AB and for the smallest throat and the largest cavity [3].

In some cases, it is both useful and necessary, to make a clear distinction between the gel porosity (ϵ_{gel}) (where moisture is either part of the structure or perhaps moves by some diffusion-like mechanism), capillary porosity (ϵ_{cap}) (which fills by flow due to for example capillary suction), air porosity (which do not fill by capillary suction) and total porosity(ϵ). The suction porosity and air porosity may be measured, for example, by the (PF) test [5] which applies capillary suction on dried specimens followed by pressure saturation under very high hydrostatic pressure. Another measurement technique is Mercury Intrusion Porosimetry (MIP). An example of pore size distributions of hcp (determined by MIP) is showed in Fig.1.4. In Fig. 1.5, the total hcp porosity for a variety of $water/cement$-ratios (w/c) as a function of degree of hydration (α) is plotted as calculated with the classical Powers model.

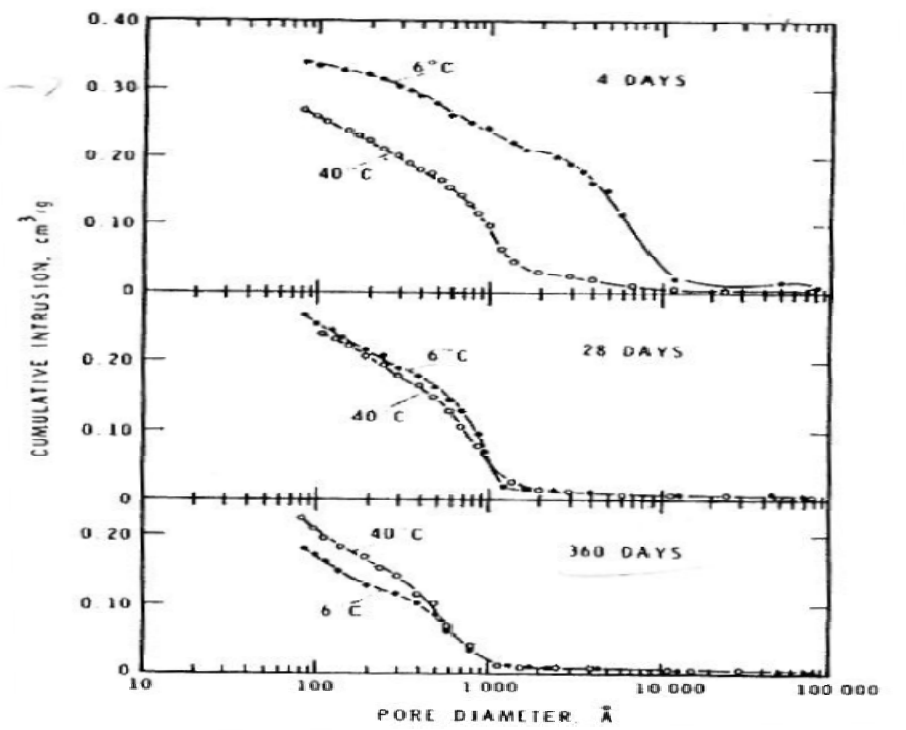

Figure 1.4. Cumulative pore-size distributions measured with MIP of w/c=0.60 cement pastes hydrated at different temperatures and periods [6].

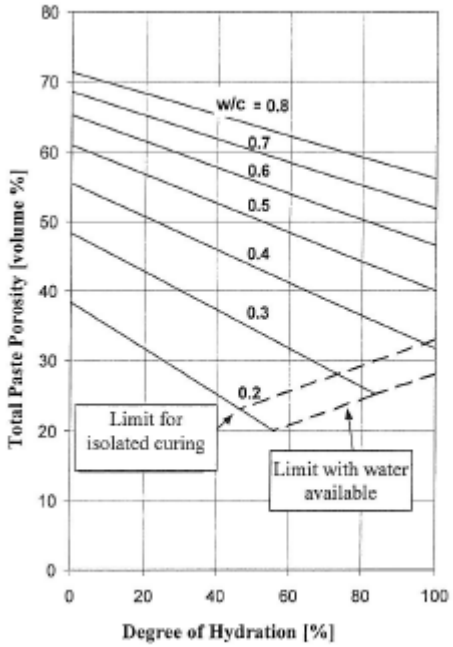

Figure 1.5. Total pasta porosity of cement for a variety of w/c-ratio as a function [8].

From the above it is clear that concrete is a porous composite material that has a highly heterogeneous and complex structure.

Chapter 2

Aim and scope

2.1 Mass transfer in porous materials (Water absorption of concrete)

In general, the water transport in a porous network like concrete is complex. This is due to many different kinds of transport mechanisms in combination with various types of pores that typically appears in the same porous system. For example, the capillary suction mechanism is a driving force in an empty or partly saturated capillary-pore network. On the other hand, up till today, it is still not clear which transport mechanisms that take place in the gel-pores. There is a general agreement in the material sciences that the pore sizes are too small in gel-pores for the capillary force to be active there. We may prefer to use the diffusion mechanism to describe the transport in these [9-10]. The role of the air voids in mass transfer in concrete is less clear. Air pores are much larger than capillaries and the capillary suction mechanism is not expected to be active there. On the contrary, the air pores could in fact play the role as a stop mechanism for the water transport process, [11-12]. However, a recent study found that entrained air voids can increase permeation and diffusion from 2 to 3 times [13] so their role in transport is not quite clear.

So far we have restricted our consideration of flow to a description of the different kinds of transport mechanisms in different pore sizes. In addition, the flow properties are depending on several material parameters like type of cement based material (Portland cement, pozzolanic, admixtures, impregnation etc), pore structure, w/c -ratio, initial water content, pre-treatment or ageing and drying and temperature/freezing [4][14-17]; it in turn may extend the problem into multi phase transport, for example with water and vapour and due to ice-water interfaces[18]. It is therefore a challenge to make a good model to predict the motion of the water in concrete under various types of exposure. In this study the transport modelling is therefore restricted to a very limited transport mechanism; namely liquid flow due to capillary suction.

Absorption of water in concrete is frequently modelled using the Lucas Washburn equation (LWE). This model is based on the capillary suction as driving force. It can be used to study the liquid rise in a cylindrical capillary pipe in contact with a water reservoir. Moreover, this model predicts, that the penetration depth, and therefore the amount of absorbed water, should be proportional to the square root of suction time (linear relation). However, many experiments of water absorption in concrete clearly illustrate some cases where the LWE fail to describe the phenomenon. Some examples of deviation from this rule are:

- Small pore structures of order of a few Angstroms where the concrete pore size varies widely. The very small calculated pore size representing the average capillary suction in concrete could indicate that the pore structure strongly impedes the water penetration, that the pores in the concrete are blocked, leading to the low permeability [14][19] or that the capillary suction mechanisms cannot alone explain the absorption.

- Capillary absorption experiments that run over long time. These falls below the linear suction [14][20-21].
- Absorption of water of dry concrete specimens seems to increase deviation from the linear suction as the thickness is larger than around 20 mm.

One objective of this work is to investigate the effect of the capillary pore structure on the above problems, particularly in the latter case.

2.2 Heat transfer in porous materials

To determine the temperature distribution in the concrete material, it is necessary to solve the appropriate form of the heat equation. However, such a solution depends on the physical conditions existing at the boundaries of the concrete and, if the situation is time dependent, on the condition existing in the concrete at some initial time. With regard to the boundary conditions, there are several common possibilities that can be expressed in mathematical form. Because the heat equation is of second order in the spatial domain, two boundary conditions much be expressed to obtain a well-defined system [22-23].

The convection heating (or cooling) boundary conditions at the surface are frequently used to describe the energy exchange at a solid- fluid (liquid or gas) interface. The heat transfer coefficient is included in heat convection boundary equations, and plays a fundamental role in material conduction problems that involve a surface effect. In fact, this must always be considered when determining heat flow to and from a concrete surface. The heat transfer coefficient is the proportionality coefficient between the heat flux and the thermodynamic driving force for the flow of heat (i.e. the temperature difference between the solid surface temperature and the ''bulk'' fluid temperature). It is also known as Newton's law of cooling. Therefore, in addition to knowing the heat conductivity and/or heat diffusivity in Fourier's law, an accurate estimation of the heat transfer coefficient is a necessary requirement to describe more correctly the energy exchange at the interface. However, this is not quite simple, since it depends on many parameters, such as heat flux term, the surface geometry and whether the gaseous/liquid flow near the surface is laminar, turbulent or transitional. In addition, gaseous flow mechanisms as convection, conduction, radiation, phase changes at the surface etc, [24], affect the flow of heat. These terms may be non-linear heat transfer phenomena affecting heat flow against the surface. In some real transfer problems it is difficult to say which heat transfer mechanism that should be taken into account, and for which reason. In addition, the transfer process is either a steady state or a transient process. An accurate model to estimate the heat transfer coefficient, which covers most of the physical parameters mentioned, is an ideal, and is very difficult to obtain in real experiments. The present work is limited to an investigation of a specific experiment with heat flow between air and a concrete surface.

2.3 Coupling heat and moisture transfer in porous materials like concrete

Concrete, like other porous materials, has the ability to absorb and retain moisture. This characteristic has an important consequence, since unprotected concrete structures in contact with water, are usually susceptible to frost damage. It has been clearly established that saturated concrete exposed to repeated freezing and thawing cycles can be affected by two types of deterioration: internal micro cracking and surface scaling (amplified by de-icers like salt)[25][26]. In recent years, the frost deterioration of concrete has been the focus of increased

research. The phenomenon is complicated to deal with. For example, still today we do not fully understand the deterioration mechanism in frost-salt scaling completely with quite different mechanisms proposed in the scientific literature [18][26-27]. To get an insight in how complicated this problem is, we refer to some physical parameters that are included in this process: the phase change, the triple-point, a chemical potential for all phases, freezing temperature can shift in porous materials, exchange of heat with surroundings, thermal incompatibility between ice and concrete [17][26][28], the effect of freezing of pore water on concrete permeability, the availability of water at the surface during freezing and thawing and so on. In the present work, we do study neither the depth nor the width of this problem; we consider only a part of these problems, namely, the effect of temperature gradient on the moisture movement assuming that the driving force for transport of water into concrete during freezing and thawing can be simplified to a frost suction created by the interface between water and ice in a saturated capillary pore [29]. In [29] the heat flow is not considered, only the local transport by capillary action between ice and unfrozen liquid. Thus the coupling is rather simple by connecting flow to phase change [29]. A more fundamental description is given for example in [30-31]. We have not pursued irreversible thermodynamics here, but simply compared measurements of absorption of water and salt solution during wet freezing and thawing in different freeze/thaw tests found in the literature with the mechanisms described in [29].

2.4 Objective of studies

We have in our study determined to focus on the following topics:

Capillary transport: The starting point for this study is the classical capillary model described by the LWE obtained by combining Laplace law for capillary suction with Poiseuille's equation for laminar flow. For a single uniform pipe size, this model predicts that the suction physics (suction velocity, suction height, and the suction volume) will all be linear functions of the square root of time. However, in many experiments on absorption of water into dry concrete specimens, a deviation from this law has been observed [19][32]. We pose the interesting question: "Why does thin slices ($\approx 20\ mm$) provide linear relations between absorbed water mass and capillary square root time ($(G - \sqrt{t})$ plots), whereas thick slices ($40 - 100\ mm$) does not (Fig.2.1) ? This has been investigated by several researchers and reviews of the problem are given by [3] and in publication 1 of this thesis.

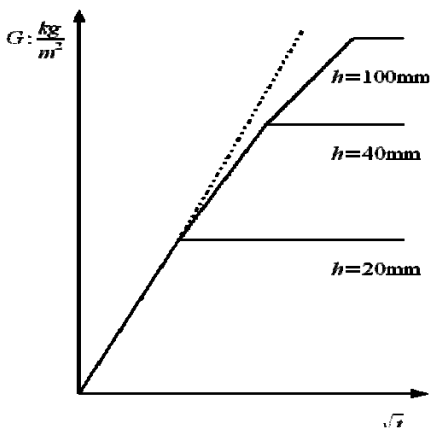

Figure 2.1. Absorbed water –weight as a function of the square root of time.

One main object for this study has been to investigate whether more complex and realistic capillary pipe models, can explain this deviation. We hypothesized that an important reason for this reduced transport is that the flow in the ''main capillary highway'' is reduced due to repeated contractions ("necks") or large capillary expansions and/or air voids. To investigate the proposed idea, pipes with repeated contractions and/or expansions were used in analytical model. Pipe models with varying cross-section along the length were constructed. The section sizes have both systematic and random values. All single pipe models are studied at the same volume fractions of the model material – similar to the total pore volumes measured on various concrete specimens.

Heat transfer coefficient: The aim is to investigate a method for a simple determination of the time-dependency of the heat transfer coefficient, $\alpha(t)$ based on measurements of temperature distribution in some light weight cement based materials at controlled air temperature. The method assumes conservation of energy at the concrete surface in finite-difference form combined with temperature measurements.

Frost suction: In the present work we investigate experimental data of measured absorption of water during wet freeze/thaw exposure of concrete specimens. We consider a simple reversible thermodynamic system where freezing causes pressure difference over the interface ice/water due to suction under the meniscus between ice and capillary water leading to moisture transport. Pressure difference and the resulting flow can be explained also by other mechanisms (e.g. hydraulic pressure from ice formation causing flow into concrete, cracking of concrete leading to volume increase, and filling of cracks with water). However, for our case only suction in capillaries with ice and water is used to explain the accelerated absorption during freezing and thawing of concrete in water. The sensitivity of the governing parameters is studied (water content, freezeable water content, enthalpy, coefficient of permeability, freezing temperature T and -gradient (dT/dx)).

CHAPTER 3

REVIEW-OF TRANSPORT LITERATURE

3.1 Mass transfer

In general, transport of liquid and gases take place in the pores, microcracks and voids of the concrete. Under normal conditions with medium moisture content and moderate temperature gradients, a moisture potential gradient in the porous medium is the main driving force of the transport process. At low moisture content, on the other hand, the main mechanism for moisture transport is through vapour diffusion and/or capillary suction when the pores are in contact with liquid water. However, at high relative humidity, surface adsorbed and capillary condensed water constitute the evaporable water in the saturated pore system of cement based material. Porosity and Relative humidity (RH)-sorption relation can simplified be described by the model of Powers and Kelvin's law. For a concrete surface continuously wetted or submerged, capillary suction is important.

Capillary suction is a fundamental transport mechanism to describe the water absorption in concrete. Furthermore, to describe this type of transport, it is important to measure the penetration depth and the absorbed water amount as a function of time. The amount of absorbed water can be determined easily by measuring the increase in weight of the test specimen as function of time. The determination of the penetration depth is more difficult.

Usually, the mathematical formulations used to express the water absorption in concrete are either capillary kinetics or diffusion models. The latter model can in steady state and in one dimensional flow ($1D$), be described by the moisture/water flux

$$g = \left[-D(\emptyset)\frac{\partial \emptyset}{\partial x}\right]. \tag{3.1}$$

In transient flow, a similar flow can be modelled by the 1D diffusion equation

$$\frac{\partial \emptyset}{\partial t} = \frac{\partial}{\partial x}\left[D(\emptyset)\frac{\partial \emptyset}{\partial x}\right] \tag{3.2}$$

where $\emptyset$ is the volumetric water content and $D(\emptyset)$ is diffusivity (a material property which is also a nonlinear function of the water content $\emptyset$ of the porous material). Partial derivatives are used because $\emptyset$ varies in both the x and t domain. Much of the effort in the past has been devoted to the determination of the 'material' property, $D(\emptyset)$ [33-34]. It has to be noted that such a formulation lumps all the information related to the pore structure and transport mechanisms into one parameter, D (diffusivity). Thus the multiphase transport dynamics of the porous medium and their relationship to physical characteristics are not adequately represented by equation (3.2). Transport properties of concrete have generally been analysed by treating concrete as an isotropic, homogeneous, and uniform porous medium [35]. In this approach, the physical characteristics of various components of concrete, such as aggregates, hcp, aggregate cement paste interface, and bleeding paths, are lumped into a single representative porous medium. One issue here has been how to quantify transport in the gel pores and to what extent water in these pores can flow. The gel pores are saturated in most real

situations (RH > 40 – 50 %) so possibly this is only a practical concern during freeze/thaw which can induce movement between capillary- and gel water [36].

Equation (3.2) is based on the extended Darcy's law (see Appendix A for more detail). The background is the experience that, for example in soil physics, permeability is strongly dependent on the degree of saturation of the material, just like diffusivity or vapour permeability of concrete varies with equilibrium RH or degree of saturation [37-38] as described by Eq.(3.2), and the assumption that capillary transport can be described as a diffusion like process. So that mathematically both concentration difference and pressure difference can be used as potential. Physically there is of course a big difference between the two forms of transport.

Another possibility for the description of water transport in porous materials like concrete is capillary suction. The simplest theoretical model, which relates time and the height or depth of penetration of a liquid into an empty capillary with pore radius r (see Fig. 3.1) is

$$h(t) = \sqrt{\frac{r\sigma cos\theta}{2\mu}}\sqrt{t} \qquad (3.3)$$

where h is the capillary penetration depth, σ is surface tension, θ is contact angle, r is the radius of pore and μ is the dynamic viscosity. Equation (3.3) is well known as the LWE. The penetration depth, (and therefore the amount of absorbed fluid), should be proportional to the square root of time. Therefore it is also called the square root of time law in literature.

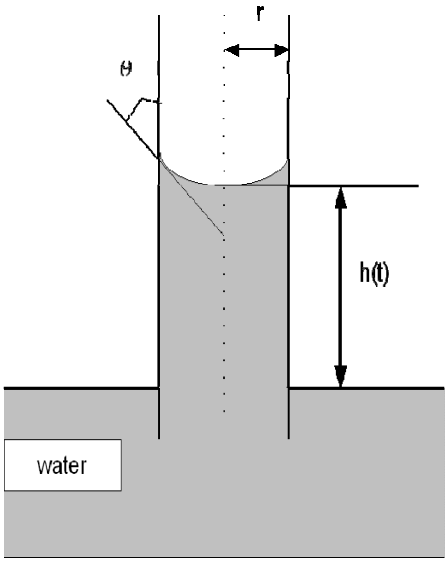

Figure 3.1. Forces acting on water transport due to capillary rise in concrete pore. A contact angle θ is obtained where the water-air interface meets a solid surface.

Equation (3.3) is based on a single pipe model representing the porous media, and cannot accurately model capillary suction in a complex and/or random porous material like concrete. The pore surface topology is far more complex so that, as the air/water interface moves through the porous medium, there are many orientations of the local interface which may be stable

despite varying pore size. In addition, the above theory of capillary suction applies to the case where the medium is initially dry. Cleary, the rate of capillary sorption will depend on degree of saturation of the porous medium [3], just like diffusion does.

3.2 Heat transfer coefficient

Heat transfer at surface of the concrete will in general, affects the total heat flow through the material and must therefore be taken into account in a broad range of practical engineering problems.

The most common approach to describe the surface heat exchange is by using Newton's law of cooling. This law can be expressed as

$$q = \alpha(T_s - T_{amb}) \qquad (3.4)^1$$

where q is heat flux , α is the heat transfer coefficient, T_s and T_{amb} are temperatures of the surface and ambient air (or other fluid) respectively. It should be noticed that the heat transfer coefficient α is influenced by the characteristics of the flow. This means not only by the temperature distribution in the fluid near the solid surface, but also by the flow properties like for example convection, turbulence, wind speed, etc. This coefficient may also be influenced by other processes such as phase change, condensation, evaporation, and sublimation/"frosting".

In the literature [22][39] the heat transfer coefficient is often assumed to be a constant quantity that can be measured, or a given coefficient for the flow system of interest. Examples here are empirical correlation like the Nusselt number (a dimensionless wall heat flux or heat transfer coefficient) or a function of the relevant dimensionless quantities, such as the Reynolds and Prandlt number [22-24]. However, it should be emphasized that all these approaches are simplifications [23]. In addition, previous research has been made to understand the mechanism of the heat transfer, but the knowledge of transient contact between building material and ambient is still inadequate [40]. Therefore more research is needed in this field. In this work a technique based on time series methods is used to estimate α from experimental data.

3.3 Coupling heat and mass transfer

It has been and is currently a large interest for moisture transportation in porous media under the influence of a temperature gradient. Current research topics involving simultaneous heat and mass transfer with/without phase change in porous media stem, have a large spectrum of applications ranging from drying technology to building material exposure to moisture and freeze/thaw in different environments, like frost deterioration of concrete [43-44].

---

[1] *Historically, Eq. (3.4) was written down by Fourier [41], who introduced in this way the concept of heat transfer coefficient (" external conductivity," in his terminology). More than 100 years earlier, Newton had published an essay [42] in which he reported that the rate of temperature decrease* (dT/dt) *of a body immersed in a fluid is at all time proportional to the body –fluid temperature difference* $(T - T_{amb})$*. This is why, beginning with Fourier's contemporaries, the name "Newton's law of cooling" was acquired*

The thermodynamical knowledge of coupled irreversible processes dates back to the early twentieth century [30-31]. For thermoelectric phenomena involving two or more irreversible transport processes (e.g. heat conduction, electrical conduction and diffusion) the processes may influence each other. They will then be connected by so-called reciprocal relations which can be expressed as

$$J_1 = L_{11}X_1 + L_{12}X_2$$

$$J_2 = L_{21}X_1 + L_{22}X_2. \qquad (3.5)$$

Here J_1, J_2 are for example electric and heat flow respectively, X_1, X_2 are electromotive force and force which drives the flow of heat respectively, while $L_{11}, \cdots, L_{22}$ denotes the conductance coefficients.

A simplification of Eq.(3.5) can be used to describe the coupling between heat and mass transfer. Let q and g express the heat and mass flow, respectively. These may then in a steady-state condition be described by the two equations

$$q = L_{qq}X_q + L_{qg}X_g$$

$$g = L_{gq}X_q + L_{gg}X_g \qquad (3.6)$$

where X_q, X_g are the flow potential of heat and mass flow, $L_{qq} \cdots L_{gg}$ are phenomenological transport coefficients. Examples of applications of Onsager's reciprocal relations in temperature induced moisture transport can be found in [45].

In this work the coupled heat and mass transfer in concrete is treated very simplified as frost suction.

CHAPTER 4

Summary and conclusions

Publications

The results of the research work in this thesis are published in the following papers:

Paper 1 Hung. T. Nguyen; Frank, Melandsø; Stefan, Jacobsen: Capillary suction in concrete with analytical pipe model-part 1: numerical study of flow conditions. Publication in Nordic Concrete Research (NCR), No.42_2/2010, pp. 71-87.

Paper 2 Hung. T. Nguyen; Frank, Melandsø; Stefan, Jacobsen: Capillary suction in concrete with analytical pipe model-part 2: expansion-, contraction- and random sized sections compared with experiments. Publication in Nordic Concrete Research (NCR), No.42_ 2/2010, pp. 89-107

Paper 3 Hung, T. Nguyen; Stefan, Jacobsen; and Frank Melandsø: Time dependent surface heat transfer in light weight arrogate cement based materials. Engineering (2010) 2, pp. 307-317.

Paper 4 Stefan Jacobsen; Frank Melandsø, Hung T. Nguyen: Flow calculation and thermodynamics in wet frost exposure of cement based materials, Presented at Int RILEM symposium Adv in Concrete through Science and Engineering March 22 - 24 2004 North Western University, USA, 14 pp.

4.1. Analytical and numerical models for capillary velocity in pipes with multiples sizes

This section refers to the study of capillary velocity in circular pipes with multiples sizes in paper 1.

In this work we have looked at various pipe geometries as model for capillary flow in concrete. Circular pipes with multiple sizes are also "building blocks" for our capillary flow study. An analytical model of capillary velocity is developed. The analytical approach allowed us to describe the capillary velocity uniquely in terms of dimensionless geometry parameters, α_i and β_i of the pipes defined through Eq. (25) in Paper 1. Furthermore, each cross section in the pipe was characterized by the term $\beta_i \frac{1}{\alpha_i}$. The parameters α_i describe the local characteristics of a section, which is a ratio between the radius and the length for each section number i. On the other hand, the parameters β_i describe the relationship between the water front cross sectional area and the area of the other, passed, cross sections.

The analytical model is very useful to gain an overview of how various geometrical models will influence the capillary velocity flow. Several physical assumptions are made in the analytical approach, for example, the flow is assumed to obey the Hagen-Poiseuille relation. Numerical testing in terms of solving either Stoke (SE) or Navier-Stokes (NSE) equations is therefore required to gain insight in the breakdown of these assumptions. Numerical solutions are also an important complementary tool, in order to investigate flow not covered by the analytical theory, like for instance, flow in a turbulent regime or flow in pipe systems where the cross section change very rapidly. In order to test the validity of the Analytical Equation (AE) for the varying pipe geometries, a simple pipe model describing a local pipe contraction (model C) and a similar model describing an expansion section (model E) were introduced. For both models C and E, we kept the radii of the sections constant, $r_1 = 10^{-6}\ m, r_2 = 0.5 \times 10^{-6}\ m$, while the lengths varied with shortest and longest section $l_1 = l_2 = 10^{-6}\ m$ and $l_1 = l_2 = 10^{-2}$ m. From this study we obtained the following mains results.

The velocity of AE is in a very good agreement with NSE and SE for almost all changes of pipe geometries. However, the velocity of AE deviates from the other models when the section length is dramatically reduced to around$10^{-6}m$, (see Tables 3 and 4 in paper 1 for more details). In other words, the velocity of AE, NSE and SE are almost identical for most of the studied laminar flow. On the other hand, the velocities of AE deviate from the other models when the flow is turbulent, (see Figs.5-6 in paper 1 for more details about the velocity profile of NSE and SE respectively). It is noted that the flow became turbulent for very small Reynolds number(Re), i.e., $Re = 3.16 \rightarrow 6.32$ for NSE.

All velocities of the contraction models are faster than in the corresponding expansion models. That is, the suction at the front is more important than the flow resistance behind the front for the actual geometries.

Based on these results, it is clear that the AE is a very good model for the approximation of flow as fluid passes a sudden change (contraction or expansion) in the cross section area of a capillary pore, in spite of a large variation of the section length.

The AE is very simple to apply to evaluate the dynamic capillary flow of any other irregular well-defined pipe geometry. Furthermore, the AE is a very useful tool to study the effect of variation of section geometries on the capillary velocity, by simple analyses of the velocity as a function of the parameters α_i and β_i, $for\ i = 1, \cdots, N$ (where N is total number of sections).

4.2 Effect of pore structure on capillary suction

This section refers to the study of capillary suction in circular pipes with multiples sizes described in paper 2. As already stated, we hypothesized that an important reason for the reduced transport below the linear square root time vs. absorption curve is that the flow in the "main capillary highway" is reduced due to repeated necks. In order to test this hypothesis, we constructed a pipe model with several contraction-expansions sections (model C), and expansion-contraction sections (model E) as described above. In addition a model with random geometries was also investigated (model R). For each set of models C, E and R, there is a corresponding model-U with constant uniform mean volume radius. We modified the well known LWE to include a pipe model with multiple sizes. The dimensions of the pipe model sections area were selected in the capillary size range as $r_i \in [10^{-7}, 10^{-6}m], i = 1, \cdots, N$. The results of the calculations are shown as absorbed weight (kg/m^2) vs. square root of time ($\sqrt{s}$). The capillary suction experiments are based on the regular weighing of pre-dried specimens exposed to water on one side. The capillary absorption experiments consist of our own data and data from the literature. The tested concrete specimens had different $w/c = 0.45$ and 0.60 with different thickness 20, 30, 40 and 100 mm.

It is known that the capillary rise in a uniform tube (model U) is a straight line function of square root of time, By comparing the capillary suction of the varying models to this standard line, we can see how the effect of the different geometries are on the capillary rise. In addition, the paper also includes a comparison between simulations of capillary rise of models C-E with experimental data. This showed that within the chosen variables of capillary pipe sections it was possible to make models with similar suction behavior as observed in real concrete specimen predried at 105 °C.

Comparing the results of models C, E, R with model U:

An investigation was also made of how capillary absorption varies with the pipe sections length and cross section area. In order gain insight in this rather complicated problem, the ratio between the cross section area $[r_1 : r_2]$ was increased from [1: 0.8] to [1: 0.1], while the section length was kept equal, $[\ l_1 : l_2\ ] = [1: 1]$. The results show clearly that the capillary flow in the C and E models practically stop when passing one or several narrow/large-contraction/expansion sections compared to model U. For example, the times for the three models to reach the total suction volume or capillary nick point ($L = 0.04m$) are $\sqrt{t_U} \approx 6.95\sqrt{s} < \sqrt{t_C} \approx 7.5\sqrt{s} < \sqrt{t_E} \approx 5.6\sqrt{s}$, when $[r_1 : r_2] = [1: 0.8]$, while $\sqrt{t_U} \approx 7.85\sqrt{s} < \sqrt{t_C} \approx 326\sqrt{s} < \sqrt{t_E} \approx 336\sqrt{s}$, when $[r_1 : r_2] = [1: 0.1]$. Clearly, there is some kind of blocking phenomenon. On the other hand, the capillary suction for both models C-E are almost linear like the uniform pipe model-U.

When both section length and section area were varied with $[\ l_1 : l_2\ ]$ increasing from [1: 1] to [1: 2], and $[r_1 : r_2]$ was increased from [1: 0.8], to [1: 0.5] and to [1: 0.1], the same tendency of blocking phenomenon was observed here. In addition, an even more interesting capillary

suction curve was now observed. The capillary suction curves of model E obey the linear behaviour until the flow passes around 2/3 of the total suction volume, where after that, the curves deviate from the linear behaviour (see Fig.5 (d-e-f) for more detail). The same trend is observed for model C where the ratio of section length switched into $[l_1 : l_2] = [2: 1]$. For the random size model the frequent and random change of cross section gave little effect on the capillary absorption compared to the uniform model. However, random combination of varying both section length and radius did not give the same effect on capillary suction curves as the C and E-model did.

The comparison of the results of models C, E with experimental data also show that the AE capillary suction time with $[r_1 : r_2] = [1: 0.1]$ micrometer is of the same order of magnitude as the experimental nick point times of all tests; It was also found that the calculated capillary suction seems to give the right kind of increasing anomaly at increasing total pipe length (corresponding to specimen thickness).

The above results can be summarized by saying that the pipe geometry has a strong effect on the capillary flow. However, this does not allow us to conclude that the varying of the capillary pore size is the only reason for the capillary suction deviation from the square root of time proportionality law. The capillary suction may slow down by other reason than the capillary pore structure. For example, the effect of some kind of slow diffusion mechanism filling the gel-type pores in the tube walls ("side flow" from main capillary highway). We believe, however, that the kind of narrowing or pore-neck effect proposed and investigated in paper 1 and 2 can at least partly explain the deviation from the square root time law (LWE).

4.3 Time dependant heat transfer coefficient

This section refers to the study of time dependant surface heat transfer in light weight concrete in paper 3.

A simple technique for determining the heat transfer coefficient at the concrete specimen surface was developed based on experimentally acquired interior, surface and air temperature – time data of specimens mounted between a cold and a warm side.

For the analysis, two different numerical methods were applied: Finite different (FDM) and Taylor polynomial (TLM). The first method expressed heat transfer coefficients at the instantaneous time $\alpha(t_i)$, while the other method expressed the heat transfer coefficients as depending on the varying time steps t_{i-1}, t_{i+1}. Furthermore, the TLM expressed heat transfer coefficients as function of the dimensionless quantity the Biot-number$[\alpha(Bi(t_i))]$.

To calculate the value of heat transfer from FDM-TLM, it is necessary to have the local heat flux at the surface, the time-dependant surface temperature and the bulk ambient temperature. The ambient temperature and the surface temperature are measured values. The heat flux may be expressed in terms of the material thermal conductivity which was measured in a separate experiment for the five investigated cement based materials and the temperature gradient that is driving the flux (see paper Eq.(3.4)). Hence, heat flux has only one variable, the temperature gradient when the convective and radiative effects are neglected. The temperature gradient can be measured and used to determine α.

The laboratory experiments consisted of measurement of one dimensional heat flow on cylindrical specimens of light weight aggregate concrete (LWA). Five LWA concrete specimens with different compositions were tested. Each specimen was 10 cm long and 10 cm in diameter. The specimens were placed horizontally in a polystyrene pipe with a very low thermal conductivity ($\lambda = 0.04\ w/mK$). The pipe was placed in a 10 cm thick vertical polystyrene wall between a warm and a cold room. The thermocouples were molded into the concrete, positioned along the central axial of the cylindrical LWA concrete (see Fig.2 paper 3 for more details). The heat conductivities of the concretes that were measured in a separate experiment are applied to calculate the time dependant surface heat transfer coefficients.

The surface heat transfer coefficients $\alpha(t_i)$ were calculated based on a combination of the measured temperatures and FDM-TLM. The $\alpha(t_i)$, at the cold side is an increasing function of time, while it is a decreasing function of time at the warm side. Both the heat transfer curves at the cold and warm sides converged to a constant value after six and a half hours (this period is approximately equal to the transient period of the air temperatures on the cold and warm sides). Apparently, the value of the surface heat transfer coefficient varies under unsteady or transient state period. On the other hand, $\alpha(t_i)$ will reach a constant value when a steady-state temperature distribution of ambient air is reached. The physical explanations for this is reviewed in the paper including effects of varying wind and phase transfer as frosting forms or disappears on the surface. The results of the FDM are almost equal with the results of the TLM and there is no systematical differences in a (t) for the five different cement based materials studied.

In order to study the effect of the time dependant heat transfer coefficient on the accuracy of numerical simulations of temperature distribution in the same concrete specimens we compared the solution of heat diffusion equation with $\alpha(t)$ and constant heat transfer coefficient (α) with the experimental data. The result show clearly that the temperature-profile using $\alpha(t)$ better fit the experimental data than when using constant α, especially during short periods at start of temperature change, where heat flow in the material is non-stationary. Over longer periods the two solutions using α and $\alpha(t)$ converge.

The work demonstrated how a simple experiment can be used to estimate values of heat transfer coefficients. It should be noted that this study has some limitations that are discussed under future work. However, it is believed that this work has provided valuable insight on the significant role of the surface heat transfer coefficient on the complex surface energy exchange process with the following advantages:

- The local, time dependent heat transfer coefficient can be determined simply
- It is economical because it is easy to perform the measuring procedure, does require neither advanced equipments nor excessive time to carry out experiment.
- The model is very simple to use

4.4 Frost suction

This section refers to the study of flow calculation and thermodynamics in wet frost exposure of concrete in paper 4.

Moisture transport with phase change (water-ice) in concrete pore structure is a complex multi scale mechanical- physical process. Furthermore, it is a well known phenomenon that the water

uptake increases under freeze/thaw conditions compared to absorption at constant temperature above zero [17][18][29]. In this work, we consider an interesting part of this problem, here termed as frost suction.

The frost suction flow can be measured, during freeze/thaw tests and show that the rate of flow is in the range of $\approx 8.10^{-7} - 6.10^{-6}\ kg/(m^2 s)$, but to predict this suction flow by an analytical model is more difficult. This is due to the complexity of this transport phenomenon as already stated in chapter 3.

In paper 4 the frost suction was created during phase transition of pore water to ice [29][46], and assumed to be the only driving force for water transport into concrete during freezing. The suction mechanism was described by [29] and is due to the curved interface formed between water and ice in a saturated capillary pore. A further simplification of the frost suction transport process was made by assuming a reversible thermodynamics process with ice and water in contact and combining Clausinus-Clapeyron under a thermal gradient with Darcy's law. Assuming constant permeability the frost suction flow was calculated by analytical means. The analytical model expresses the frost suction as a function of the enthalpy of freezing, volume of ice phase, volume of water phase, temperature and permeability. All parameters were measured or estimated from the literature.

The results show clearly that the frost suction is significant and proportional with the decrease of temperature. Illustrated by numbers; frost suction is increased from 0.0 (Pa) to $50^6(Pa)$ when temperature is decreased from 273 (K) to 255 (K). Comparing the calculation of frost flow with measured data show clearly that the experimental value can be simulated by choosing realistic material- and thermodynamic data. The experimental data on flow during frost exposure (frost suction) were based on four different wet frost exposure laboratory test condition with varying gradient, number of cycles, wet period, pure water or salt solution etc. Illustrated by number, the measured weight showed the rate of flow in the range of $8.10^{-7} - 6.10^{-6}\ kg/m^2 s$.

Note that the frost flow may depend on more physical parameters than those included in our model (enthalpy, volume of water, volume of ice, freeze able water, permeability, temperature gradient), like irreversible thermodynamic effects , other transport mechanisms like diffusion, effects of frost damage in the material (cracking, volume increase etc). However, this work has demonstrated the existence of frost suction under phase change water-ice in the pore structure of concrete. Moreover, this suction is at least one mechanism causing the flow observed in wet freeze-thaw experiments.

Chapter 5

Further work

5.1 Capillary suction

The purpose of this study has been to investigate the effect of different model capillary pore structures on the capillary suction. However, both the pore models and transport mechanism in this study are still limited compared to real transport which will include a large amount of very small pores (gel) and also some very large ones, as well as inclusions of practically non-permeable aggregate particles with a porous interfacial transition zone between paste and aggregate.

Further modelling of these type of systems should include pore systems with various pore types and include a varying volume fractions matching the proportions of real materials as determined for example by experimental pore structure analysis. One approach is to model the diffusion-loss of water from the pipe ”main capillary highway” into the pipe walls or ” sidewalk” made of gel material. This introduction of a multi-scale mechanism and multi-scale pore size will be both more complex and more realistic from a physical point of view.

5.2 Time dependant heat transfer coefficient

This study has showed clearly that a combination of a simple numerical finite different method and temperature measurements can be successful for calculation of the surface heat transfer coefficient. However, improvements of both the analytical model and the measuring techniques are needed. Further modeling may be based on the type of dicretization of conservation of surface energy that was studied here. In addition, the calculation of heat flux should take material properties as porosity and non-linear processes into account and this could form the basis of a semi-empirical field theory, e.g.[47-50].

Furthermore, heat flow conditions vary from point to point on the surface, including both heat flux and heat transfer coefficient. Therefore, future modeling should investigate the total heat flux and average heat transfer coefficient for the entire surface. It is also necessary to further investigate and analyse the error of the temperature measuring technique.

5.3 Frost suction

An improvement of the model is necessary to make a better description of the complexity of frost transport. Such an improved model could for example, be applied to study effects of ice on the surface of the concrete, frost damage in the concrete, and other transport mechanisms such as diffusion, non-linear material properties such as permeability, irreversible thermodynamics, etc. The pipe suction model in papers 1 and 2 could perhaps be included.

Experimentally one should first make extended instrumented tests observing temperature gradients more accurately, as well as observing the ice free period of the surface and measuring

the permeability under varying frozen conditions. Then more advanced experimental studies could be made such as measuring freezeable water or ice with calorimeter, MRI (Magnetic Resonance Imaging) etc, and observing the motion of water and ice over time during freeze/thaw.

Appendix A

Darcy's law[2] for flow through porous media

For one dimension, flow through a saturated homogenous material may be described by the well known Darcy's law

$$u = -\kappa_s \frac{\partial \mathrm{H}}{\partial \mathrm{x}} \qquad \text{(A.1)}$$

where u is flow (m/s), κ_s is saturated hydraulic conductivity (m/s), H is the total potential or pressure head, (m) and x is length (m). This equation is used for porous materials like soil, concrete

Unsaturated flow is described by the extended Darcy equation

$$u = -\kappa(\emptyset) \frac{\partial H}{\partial x} \qquad \text{(A.2)}$$

where κ is a function of local water content $\emptyset$. Buckingham [51] was the first that had described the dependence of the unsaturated flow upon the potential gradient $(\partial \mathrm{H}/\partial \mathrm{x})$ so therefore equation (A.2) is often referred to as the Darcy-Buckingham equation [52]. (Eq.3.2) is analogous to A.2 but uses concentration difference as potential instead of hydraulic head.

[2] *Henry Philibert Gaspard Darcy (1803-1858) [23] studied in Paris and became famous for designing the municipal water-supply system in Dijon, the city of his birth. H. Darcy, Les Fontaines Publiques de la Ville de Dijon, Victor Dalmont, Paris (1856).*

Appendix B

Authorship declaration

Paper 1 and 2: Hung Thanh Nguyen developed the analytical model based on the physical concepts, performed numerical simulations, drafted the papers and also did capillary suction experiments at the HiN lab i Narvik. Frank Melandsø made a few suggestions to the analytical model and the approach to investigate local flow conditions numerically to verify the analytical model, reviewed and corrected drafts. Stefan Jacobsen supervised the experiments (capillary suction, porosity), reviewed and corrected drafts.

Paper 3: Hung Thanh Nguyen carried out the experiments in Narvik with assistance from the HiN-lab, analysed all data and developed the model. Stefan Jacobsen supervised the experiments, reviewed and corrected drafts. Frank Melandsø reviewed and corrected drafts.

Paper 4: Stefan Jacobsen reviewed available data on absorption of water in concrete during wet freeze/thaw exposure at the very start of the PhD work as input to further experiments and modeling and drafted a paper. Frank Melandsø reviewed the draft. Hung Thanh Nguyen co-authored, reviewed and corrected the paper and participated at the conference in Chicago.

Tromsø, February 2011

Nguyen Thanh Hung

Hung Thanh Nguyen(sign) – Place and date

References

[1] Rolf Andre Bohne, Arne Aalberg, Stefan Jacobsen, and Per Jostein Hovde. Bygnings- og konstruksjonsmaterialer, Høsten 2010. Institutt for bygg, anlegg og transport & Insitutt for konstruksjonsteknikk, NTNU, 456 pp.

[2] Ragnhild Holen Relling. (1999). Coastal concrete bridges: Moisture state, Chloride permeability and Aging effects. Doktor ingeniøravhandling. Institutt for konstruksjonsteknikk. Norge tekinisk-naturvitenskapelige universitet (NTNU).

[3] Christopher Hall, and William D. Hoff. Water transport in brick, stone and concrete. 2002, Spon Press Inc. 318 pp.

[4] Powers T. C., and Brownyard T. L. (1948): *Research Lab. Portland Cement association, bull 22.*

[5] Jounu Punkki and Erik J. Sellevold (1994): Capillary suction in concrete: Effects of drying procedure. *Nordic concrete research;No.15.2,* 59-74.

[6] Ramachandran V.S., Feldman R.F.and Beaudoin J.J., (1981): Concrete Science, Heyden&son, 427 pp.

[7] Hamlin M. Jennings, Jeffrey J. Thomas, Julia S. Gevrenov, Georgios Constaintinides, Franz-Josef Ulm, (2007): A multi-technique investigation of the nano-porosity of cement paste. Cement and concrete research 37, pp. 329-336.

[8] Erik J. Sellevold and Tom Farstad (2005): The PF-method- A simple way to estimated the w/c-ratio and Air content of Hardened Concrete, Mindness Symposium Conference Vancover, Canada.

[9] Brennan J. K., Dong W. (2003): Molecular simulation of the vapour-liquid phase behavior of lennard-Jones mixtures in porous solids. *Physical review E67, 031503*, 1-6.

[10] Marty N. S., and Chen H. (1996): Simulation multi-component fluids in complex three-dimensional geometries by the lattice Boltzmann method. *Physical review, E 53 1*, 743-750.

[11] Per Gunnar Burstrøm, Byggnadsmaterial, Sweden, Sudentlitteratur 2001. 546 pp.

[12] Kaufman J., Studer W., and Schenker K. (1997): Study of water suction of concrete with magnetic resonance imaging methods. *Magazine of concrete research 49*, No. 180, 157-165.

[13] Wong, Pappas, Zimmermann, Buenfeld et al, Imperial College, draft paper submitted to Cement and Concrete Research november 2010.

[14] Bulu Pradhan, Nagesh M., and Bhattacharjee B. (2005): Prediction of the hydraulic diffusivity from the pore size distribution of concrete. *Cement and concrete research 35*, pp. 1424-1733.

[15] Christopher Hall, William D. Hoff, and Wilson, M. A. (1993): Effect of non-sorptive inclusions on capillary absorption by a porous material. *Journal of Physics, D: applied Physics* 26, pp. 31-34.

[16] Max J. Setzer (2001): Micro-Ice-Lens Formation in porous solid. *Journal of colloid and interface science 243,* 193-201.

[17] Stefan Jacobsen., and Sellevold E.J, (1994) 'Frost/salt scaling testing of concrete-importance of absorption during test', Nordic Concrete Research Vol.14, pp. 26-44.

[18] Stefan Jacobsen, Jacques Marchand, and Hugues Hornain (1995): Sem observations of the microstructure of frost deteriorated and self-healed concretes. *Cement and concrete research,* 25, pp. 1781-1790.

[19] Nikhil Barbare, Arun Shukla, Arijit Bose, (2003): Uptake and loss of water in a chemosphere-concrete composite material*. Cement and concrete research 33,* pp. 1681-1689.

[20] Lockingston D.A., and Parlange J.Y. (2004): A new equation for macroscopic description of capillary rise in porous media. Colloid and Interface Science, Vol.278, pp. 404-409

[21] Marty N. S., and Chen H. (1996): Simulation multi-component fluids in complex three-dimensional geometries by the lattice Boltzmann method. *Physical review, E 53 1*, pp. 743-7580.

[22] Frank P. Incropera and David P.Dewitt, Fundamentals of heat and mass transfer, Fifth edition, 2002, John Wiley&-Son, Inc.

[23] Edwin N. Lighfoot, R. Byron and Warren E. Steward, Transport phenomena, Second edition, 2002, John Wiley&-Son, Inc.

[24] William Kays, Michael Crawford, and Bernhard Weigand, Convective heat and Mass transfer, Fourth edition, 2005, McGraw-Hill Education, Inc.

[25] Claesson P. M., and Christenson H. K. (1988): Very long range attractive forces between uncharged hydrocarbon and fluorocarbon surface in water, *Journal of Chemistry 92(6*), pp. 1650-1655.

[26] Max J. Setzer. (2001): Micro-Ice-Lens Formation in porous solid. *Journal of colloid and interface science 243,* pp. 193-201.

[27] John J. Valenza, and George W. Scherer. (2007): Mechanism for salt scaling of a cementitious surface. Material and Structures Vol. 40, pp. 259-268.

[28] Zuber B, and Marchand. (2000): Modeling the deterioration of hydrated cement systems exposed to frost action. Part 1: Description of the mathematical model. Cement and concrete research, Vol. 30, pp. 1929-1939.

[29] Farrokh Fariborz Radjy. (1970-1974): Freezing and frost damage, kompendium i bygningsmateriallære, Teoretisk del, The Tecnhnical university of Denmark, Dept. Of civil engineering building materials laboratory.

[30] Lars Onsager, (1930): Reciprocal relation in irreversible process. I. Physical review, Vol. 37. pp. 405-426.

[31] Lars Onsager, (1931): Reciprocal relation in irreversible process. II. Physical review, Vol. 38, pp. 2265-2279.

[32] Nicos S. Martys and Chiara F. Ferraris, (1997): Capillary transport in mortars and concrete. Cement and concrete research *27,* 747-760.

[33] Kaufman J., Studer W., and Schenker K. (1997): Study of water suction of concrete with magnetic resonance imaging methods. *Magazine of concrete research 49*, No. 180, pp. 157-165.

[34] Christopher Hall. (2006): Anomalous diffusion in saturated flow: Fact or fiction?. Cement and concrete research, 37, pp. 378-385.

[35] Koichi Maekawa, Rajesh Chaube, and Toshiharu Kishi, Modeling of concrete performance, Hydration, Microstructure formation and mass transport, 1999, E&FN Spon, an imprint of Routledge 11 New Fetter Lane, LondonEC4P 4EE.

[36] Powers T.C., Helmuth R.A. (1953): Theory of volume changes in hardened portland cement paste during freezing, Proc Ann. Meet Highw Res Board V.32, Wash. DC pp 285-297.

[37] Lars Olof Nilsson, (1980): Hydroscopic Moisture in concrete- Drying, measurements & Related material properties, Report TVBM-1003. Lund Institute of Technology, Sweden.

[38] Gøran Hedenblad, (1993): Moisture permeability of mature concrete, Cement mortar and cement Paste. Division of building materials, Lund Institute of Technology, Sweden.

[39] Adrian Bejan, Heat transfer.(1993) John Wiley & Sons, Inc.

[40] Hong. G; Irving A. D; Dewson T.; and Day B. (2993): Comparison of time series response factor estimators. *Energy and buildings, 20,* pp. 179-186.

[41] Fourier J. (1878): Analytical theory of heat, translated, with notes, by A. Freeman, G. E. Stechert & Co., New York.

[42] Newton I., Scala Graduum Caloris, Calorum Descriotiones & Signa, Phil. Trans. Roy. Soc. London, Vol.8, 1701, pp. 824-829; translated from Latin til Phil. Trans. Roy. Soc. London, Abridged, Vol. IV (1694-1702),1809, pp. 552-575.

[43] Andrew P. Shapiro, and Shahryar Motakef, (1990): Unsteady heat and mass transfer with phase change in porous slabs: analytical solutions and experimental results. Int. J. Heat Mass Transfer, Vol.33, No.1, pp. 163-173.

[44] Stefan Jacobsen, Ge'rard B., and Marchand, (1996): Prediction of short time drying for OPC and Silica fume concrete frost/salt scaling test. Durability of building materials and components 7 (Volume one) Edited by C. Sjøstrøm.

[45] Cary J. W. (1962): Onsager's relation and the non-isothermal diffusion of water vapour. Soil and water conservation research division, USDA, Logan, Utah. Vol. 67, pp. 126-129.

[46] Bager D. H., and Stefan J., (1999): A conceptual model for the freeze/thaw damage of concrete in ' Frost resistance of building material' K Fridh (ed) Proc 3^{rd} Nordic res seminar, Lund Sweden rep TVBM-3087 ,pp. 1-18

[47] Jan Taler, (1996): Theory of transient experimental techniques for surface heat transfer. Int. J. Heat Mass transfer. Vol. 39, No. 17, pp. 3733-3748.

[48] Suresh R. Sunderesan and Nigel N. Clark, (1995): Local heat transfer coefficients on the circumference of a tube in a gas fluidized bed. Int. J. Multiphase flow Vol. 21 No. 6,pp.1003-1024.

[49] Irving A.D., T. Dewson, G. Hong and B. Day (1993): Time series analysis of test cell field data. Building and Environment , Vol, 28, No. 2, pp. 167-173.

[50] Shuja S.Z., Yibas B.S., Kassas M., (2009): Flow over porous block in a square cavity: influence of heat flux and porosity on heat transfer rates. International Journal of Thermal Sciences 48, pp. 1564-1573.

[51] Narasimhan T. N., (2005): Bukingham, 1907: An appreciation. Vadose Zone Journal Vol.4, pp. 434-441.

[52] Nimmo John R., and Edward R. Landa, (2005): The soil physics contributions of Edgar Buckingham. Soil. Sci. Soc. Am J. 69, pp. 328-342.

Paper 1

Capillary suction in concrete with analytical pipe model-part 1: numerical study of flow conditions

Capillary suction in concrete with analytical pipe model - part 1: numerical study of flow conditions

Hung Thanh Nguyen
University of Tromsø, Department of physics, 9000 Tromsø, Norway &
Narvik University College, P. 8500 Narvik, Norway
E-mail: hung.thanh.nguyen@uit.no

Frank Melandsø
University of Tromsø, Department of physics, 9000 Tromsø, Norway
E-mail: frank.melandso@uit.no

Stefan Jacobsen
Norwegian University of Science and Techn., Dept. of Structural Engineering,
7491 Trondheim, Norway.
E-Mail: stefan.jacobsen@ntnu.no

Abstract

Absorption of water in concrete is often described by the simple linear water uptake vs square- root-of-time law. However, a deviation from this behavior is frequently seen depending on factors such as initial water content, water/binder ratio and specimen thickness. The increasing deviation at increasing thickness is seen even for very dry specimens with a significant fraction of capillary pores when the specimen thickness increases from around 25 to around 100 mm. In this paper, we have combined Navier-Stokes flow equation with Laplaces law for suction created under a curved meniscus between air and water, and applied it to series of pipes with different lengths and radii, (the analytical model). The analytical model is in good agreement with the numerical models at abrupt reduction or increase of pipe radius, even at very small radii, and our analytical pipe model made with different radii and lengths thus works satisfactorily in terms of flow conditions.

Key Words: Concrete, capillary, surface tension, Analytical, and numerical modelling, Navier Stokes and Stokes models, pipe geometry.

1 INTRODUCTION

Capillary transport of water in porous materials like concrete has kept the attention of researchers world wide for many years. Capillary transport is considered a basic transport mechanism in concrete and similar porous materials [1] where suction is created under water meniscii in partly filled capillary pores. During the last decade an increasing portion of the applied concrete qualities have very little capillary porosity. This is due to the increasing use of high performance concrete and supplementing cementing materials that refine and make the pore structure less continuous [2]. However, in spite of the reduced capillary continuity of the pore system of HPC with low w/b and/or supplementary cementing materials like fly ash and condensed silica fume, such concretes may after some predrying show the typical nick point on the water uptake vs square root of time plots in one sided (unidirectional) capillary suction experiments. The severity of drying has a very clear effect, and this has been found to relate to the degree of saturation of the pore system at start [3]. By re-plotting these results they actually fit well into the kind of saturation-sorptivity plots suggested [1] for use in solving Richards equation. However, in experiments there is a size effect on capillarity that is problematic compared to the capillary

mechanism since there is an increasing deviation from the linear absorption vs square root of time relation of capillary theory as the sample thickness is increasing. The size dependant deviation from the square root-law effect has sometimes been ascribed to the replacement of interstitial water and subsequent swelling of the gel [1]. We believe that capillary discontinuities in the form of narrow passages or larger capillary voids along the flow path of the capillary pore system can be involved in the phenomenon (as some sort of pipe geometry effect on the water transport). This deviation from the square-root law has been observed in concrete with a significant amount of capillary porosity [4] as well as in materials with theoretically no capillary porosity, depending on the severity of the drying [3]. The deviation has also been observed in capillary absorption experiments with an organic fluid [5]. It is therefore probable that the proposed gel swelling [1] cannot be a general explanation for the anomaly. Figure 1 shows the results of one of our experiments on cylindrical mortar specimens with diameter 100 mm and w/c = 0.60 after drying at 105 C. The three graphs show how real capillary absorption deviates increasingly from the square-root of time law as the specimen thickness increases from 20 to 40 to 100 mm height. We also see how the nick-points vanish at increasing specimen height.

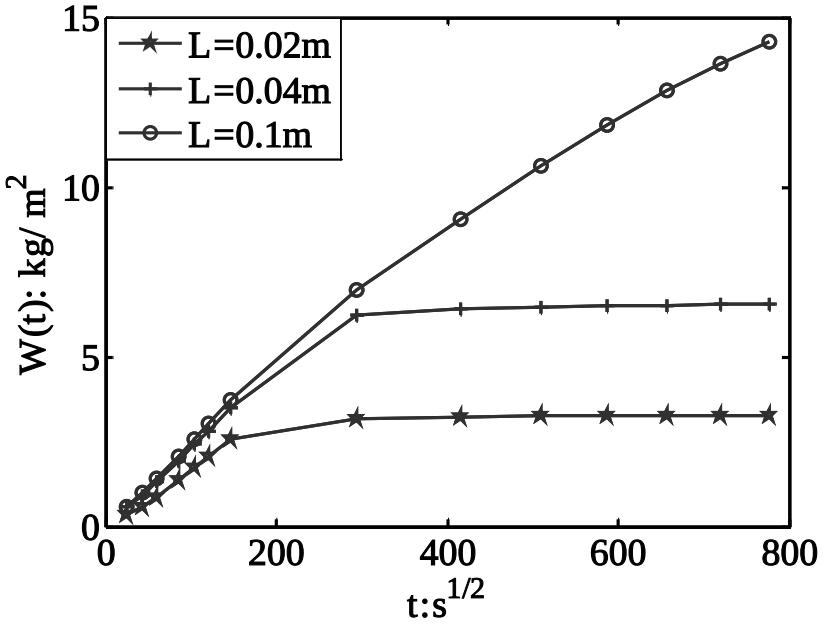

Figure 1- Capillary absorption in w/c 0.60 mortar with increasing deviation from linear absorption vs square-root-of-time law at increasing specimen thickness 20 to 40 to 100 mm.

The kind of narrowing and widening discontinuity-effects we propose may be compared with percolation thresholds which have so far mainly been used in diffusion studies [4]. That is, accounting only for transport in the capillaries and not in the very fine gel structure of the cement based material. For the very fine, nano sized gel pores molecular simulation is probably a suitable way of modelling the transport [6],[7]. To investigate to what extent the proposed capillary discontinuities affect the size dependant deviation from the linear square root time - absorption law, we have in this paper developed an analytical solution to a multiple pipe model. The objective has been to investigate the reliability of this model compared to a numerical solution of the continuum approach. Then, in part 2 of this study we will calculate absorption with varying combinations of pipes and also compare the calculated pipe absorption with experiments from other researchers, as well as our own capillary absorption experiments. All capillary absorption experiments were made at ambient temperatures on specimens after drying at 50 or $105\ C$.

2 FLOW MODELS

Varying pipe flow approaches have been taken in earlier studies of this kind of problem. Some have been based on pipe flow according to Hagen-Poiselle with capillary suction due to the under-pressure caused by the surface tension between liquid and gas (l-g - water-air in our case) and the curvature of the water meniscus between air and the liquid wetting the pipe wall (concrete in our case). One example of pipe flow modelling can be found in [8] and early efforts to model capillary suction in sandstone and concrete in this way are [9],[10]. However, these studies did not analyze the reasons for the increasing deviation from the square root of time law.

2.1 Navier Stokes equation

As a starting point for our capillary system, we will assume an incompressible and stationary flow in an axial-symmetric pipe system. For such a system the mass conservation equation can be reduced to the incompressibility requirement

$$\frac{\partial u}{\partial x}+\frac{1}{r}\frac{\partial}{\partial r}(rv)=0 \tag{1}$$

while the momentum conservation equations can be expressed as

$$\rho\left(u\frac{\partial u}{\partial x}+v\frac{\partial u}{\partial r}\right)=-\frac{\partial p}{\partial x}+\mu\left[\frac{\partial^2 u}{\partial x^2}+\frac{1}{r}\frac{\partial}{\partial r}\left(r\frac{\partial u}{\partial r}\right)\right] \tag{2}$$

and

$$\rho\left(u\frac{\partial v}{\partial x}+v\frac{\partial v}{\partial r}\right)=-\frac{\partial p}{\partial r}+\mu\left[\frac{\partial^2 v}{\partial x^2}+\frac{1}{r}\frac{\partial}{\partial r}(rv)\right]. \tag{3}$$

Here u and v are the velocity components in the axial direction (denoted by x) and radial directions (r), respectively, while p denotes the fluid pressure. The two other parameters ρ and μ describing the mass density and dynamic viscosity coefficient, are both assumed to be constants.

In the rest of the paper we will refer to Eqs. (1)-(3) as the Navier-Stokes equation (NSE), while the non-linear terms on the left hand side of Eqs. (2) and (3) will be referred to as the flow acceleration terms or the convective terms.

In order to obtain consistent solutions for the NSE, boundary conditions that incorporate the basic physics, have to be specified. For our case, a capillary suction or under-pressure p_c described above in front of the water column created at the meniscus is driving the flow trough the pipe system. Such a driving force can be imposed through the pressures

$$p(r, x=0)=0 \quad and \quad p(r, x=L)=-p_c \tag{4}$$

at the pipe ends $x=0$ and $x=L$. In addition, we also assume non-slip boundary conditions at

the pipe wall at $r = r_x$, or

$$u(r = r_x, x) = 0 \quad and \quad v(r = r_x, x) = 0 . \tag{5}$$

2.2 Stokes equation

For cases where the flow velocity is sufficiently small and well within the laminar regime, it is possible to approximate the NSE with models which are easier to handle both by numerical and analytical means. In Stokes approach for example, the convective terms in Eqs. (2) and (3) are neglected. This yields the Stokes equation (SE)

$$0 = -\frac{\partial p}{\partial x} + \mu\left[\frac{\partial^2 u}{\partial x^2} + \frac{1}{r}\frac{\partial}{\partial r}\left(r\frac{\partial u}{\partial r}\right)\right] \tag{6}$$

and

$$0 = -\frac{\partial p}{\partial r} + \mu\left[\frac{\partial^2 v}{\partial x^2} + \frac{1}{r}\frac{\partial}{\partial r}(rv)\right]. \tag{7}$$

2.3 Hagen-Poiseuilles equation

Further simplification may be possible, for example for pipes with constant radius where so-called fully developed flows will occure. Fully developed flows are characterized by both zero lateral velocity v and gradient of axial velocity component $(\partial u/\partial x)$. The latter velocity relates to the pressure p through Eq. (6), and gives

$$\frac{\partial p}{\partial x} = \mu\left[\frac{1}{r}\frac{\partial}{\partial r}\left(r\frac{\partial u}{\partial r}\right)\right]. \tag{8}$$

This equation points out a simple balance between shear and pressure forces in the flow [11].

It should be emphasized that Eq. (8) which is the basis for the Hagen-Poiseuille equation (HPE), also can be used as an approximation for pipes with a slowly changing radius, or in pipes with a stepwise changing radius. However, a Hagen-Poiseuille (HP) flow approximation requires that the changes are sufficiently small, or do not happen too often (for a stepwise change), so that a fully developed flow will dominate on a local scale. The latter assumption is also fundamental for the analytical theory presented in the next section.

2.4 Analytical equation: Pipe flow velocity - N -sized pipe model

In order to develop an analytical capillary model for a pipe system with a stepwise changing cross section, we will start with the two sized (binary) model shown in Fig. 2. This figure illustrates how a physical flow pattern shown in the upper Fig. 2(a), can be approximated with the stepwise model shown in the upper Fig. 2(b). For this binary model we assume a HP flow in both sections, which changes abruptly at the interface ($x = x_1$), and thereby neglecting the regions indicated with the

darkest shading in the upper figures, where the flows are not fully developed. This approach will also lead to a stepwise flow velocity and a linear pressure as indicated in the lower Fig. 2(b), acting as approximation for the physical mean fields shown in the lower Fig. 2(a). The field u_x and p_x should be considered as mean values over the pipe cross section, given by the integrals

$$u_x = \frac{2}{r_x^2}\int_0^{r_x} u(r,x) r dr \tag{9}$$

and

$$p_x = \frac{2}{r_x^2}\int_0^{r_x} p(r,x) r dr \tag{10}$$

for an axial-symmetrical flow.

In addition to the radius parameter r_x which has the value r_1 and r_2 in section 1 and 2, respectively, the geometry is also characterized by the sections length l_1 and l_2, and h which is the current position for the water front.

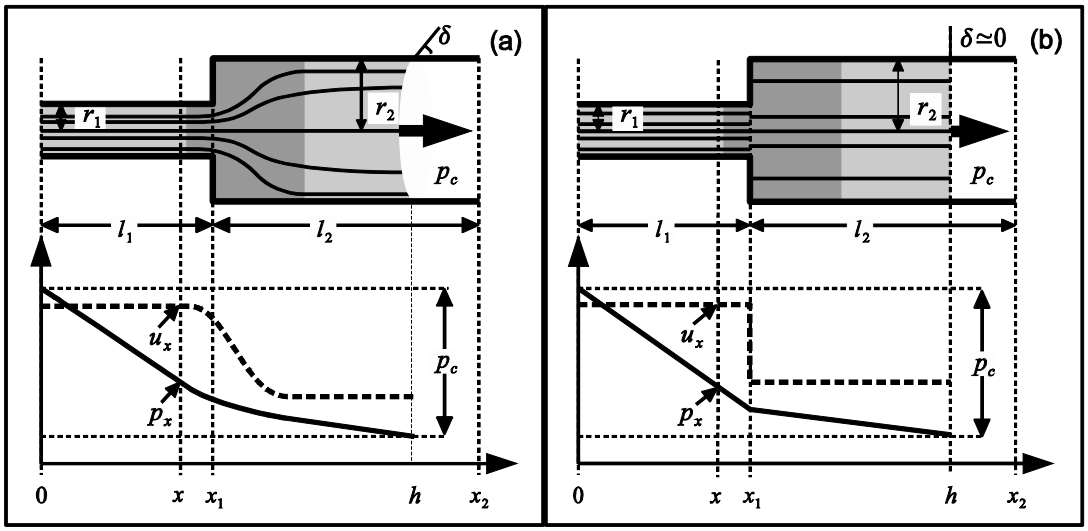

Figure 2- A circular tube divided into two sections and the balance force between the capillary force and the moving-body-force.

Local expressions for the HP flow now can be obtained by intergrating Eq. (8) twice and imposing the non-slip boundary conditions Eq. (5). This yields the well known parabolic profile [11]

$$u(x,r) = -\frac{1}{4\mu}\left(\frac{dp_x}{dx}\right) r_x^2 \left[1 - \left(\frac{r}{r_x}\right)^2\right] \tag{11}$$

inside each pipe section.

The foregoing result may be used to determine the mean velocity of flow. After substituting Eq.

(11) into Eq. (9) and integrating, we obtain

$$u_x = -\left(\frac{r_x^2}{8\mu}\right)\left(\frac{dp_x}{dx}\right). \tag{12}$$

It should be emphasized that both the pipe radius, the pressure gradient and the velocity in Eq. (12) are local quantities changing between the individual pipe sections. Therefore, in order to determine the velocity at the fluid-front u_h based on Eq. (12), we need two additional constraints.

The first of these constraints can be found by looking at the total pressure fall from position $x = 0$ to h. This pressure fall has to be balanced by the capillary pressure p_c in the water front as shown in Fig. 2. The capillary pressure, on the other hand, can for fluids with moderate velocities, be approximated with the stationary pressure given by the Laplace equation

$$p_c = -\frac{2\sigma_{l-g}cos\delta}{r_h} \tag{13}$$

obtained from static conditions. Here σ_{l-g} is the surface tension between water and air and δ the contact angle between the pipe wall and the wetting water front (see for example [1],[12]).

The second constraint can be imposed by assuming that the water flux entering the left hand side of the pipe interface, has to equal the right hand value. This constraint which has to be fulfilled in order to conserve the water mass in a stationary flow [13] , gives

$$u_x A_x = u_h A_h \Rightarrow u_x = u_h \frac{r_h^2}{r_x^2}. \tag{14}$$

Here A_x and A_h are the cross section areas at position x and h, respectively, as shown in Fig. 2(b).

After rearranging Eq. (12) and then integrating from $x = 0$ to h we obtain

$$\int_0^h u_x \frac{dx}{r_x^2} = \frac{1}{8\mu}\left(-\int_{p_0}^{p_h} dp_x\right).$$

A further reformulation of this equation can be done by inserting expressions for the pressure $p_c = p_h - p_0$ and velocity u_x given by Eqs. (13) and (14), respectively. This yields

$$u_h = \frac{k}{f(h)r_h^3} \tag{15}$$

for the capillary front velocity where we have introduced a constant k as

$$k = \frac{\sigma_{l-g} cos\delta}{4\mu}. \tag{16}$$

and a function

$$f(h) = \int_0^h \frac{dx}{r_x^4} \tag{17}$$

which depends on the position h of the capillary front.

One should notice that the velocity u_h and radius r_h at the location h, are constants and that the evaluation of Eq. (17) involves integration of $f(h)$. In order to evaluate this function which may be interpreted as the area under the graph of $(1/r_x^4)$ from 0 to h, a numerical integration can be used [14] . However, in our approach where a step fuction is assumed, a simple analytical solution can be found, as

$$f(h) = l_1 \frac{1}{r_1^4} + (h - x_1) \frac{1}{r_2^4}. \tag{18}$$

Now, Eq. (18) can be substituted into Eq.(15), to give

$$u_h = \frac{k}{\left(\frac{r_2}{r_1}\right)^3 \frac{l_1}{r_1} + \left(\frac{r_2}{r_2} = 1\right)^3 \frac{h - x_1}{r_2}}. \tag{19}$$

In this equation the first terms in the denominator of Eq. (19) is a constant while the second term depends on the position h.

It is relatively straight forward to expand the two-pipe capillary model to a pipe system containing N sections. By repeating the previous steps for a N-pipe system, it can be shown that the velocity of the capillary front in an arbitrary section j, is

$$u_h = \frac{k}{f(h) r_h^3}. \tag{20}$$

This expression is identical to the one found for the two pipe model (Eq. (15)), but with $f(h)$ substituted with the general expression

$$\begin{aligned} f(h) = \int_0^h \frac{dx}{r_x^4} \quad &= \frac{l_1}{r_1^4} + \cdots + \frac{l_{j-1}}{r_{j-1}^4} + \frac{h - x_{j-1}}{r_j^4} \\ &= \sum_{i=1}^{j-1} f_i + \Delta f_j, \end{aligned} \tag{21}$$

where

$$f_i = \frac{l_i}{r_i^4} \;\; and \;\; \Delta f_j = \frac{(h - x_{j-1})}{r_j^4}. \tag{22}$$

Here r_i and l_i are the pipe radius and pipe lengths, respectively for section i (expanding from position x_{i-1} to x_i) while h is the position of the capillary front assumed to be in pipe section j.

In many pipe geometries it is useful to describe the flow in terms of dimensional variables. For our case, we will introduce dimensionless variables α_i defined as

$$\alpha_i = \frac{r_i}{l_i} \;\; for \;\; i = 1,2,\cdots, j-1, \;\; and \;\; \Delta\alpha_j = \frac{r_j}{h - x_{j-1}} \tag{23}$$

which provide information about how rapidly the cross sections change with respect to the pipe section lengths. Our approach which assumes Hagen-Poiseuille in all pipe sections and thereby neglecting the non-developed regions of the flow, are based upon sufficiently small α_i values. These parameters are therefore very useful when the breakdown of the analytical approach will be tested in the next section.

In addition to the α-parameters, we will introduce a set of β-parameters (also dimensionless) defined as

$$\beta_i = \left(\frac{r_j}{r_i}\right)^3 \;\; for \;\; i = 1,2,\cdots, j. \tag{24}$$

The latter parameters relate the cross sections of previous pipe sections ($i = 1,2,\ldots, j-1$) to the current section ($i = j$). It should be noticed that $\beta_j = 1$ due to its definition.

After inserting Eq. (23) and (24) into Eq. (20) and rearranging, the velocity can be expressed in terms of the new variables as

$$u_h = \frac{k}{\beta_1/\alpha_1 + \beta_2/\alpha_2 + \ldots + \beta_{j-1}/\alpha_{j-1} + \beta_j/\Delta\alpha_j}. \tag{25}$$

We call Eq. (25) the Analytical equation (AE).

3 RESULTS AND DISCUSSION

3.1 Flow velocity in contraction- and expansion sections

In order to evaluate the solution of the flow velocity for NSE, SE, and AE as shown in Eq. (25), we have introduced a testing model geometry as shown in Fig. 3. Here, the pipe has a contraction (model C) and expansion sections (model E). Data for the section length and radius are given in Tabs. 1 and 2 respectively. Figure 3- Tube with contraction and expansion sections.

Table 1- Geometry data for contraction-model

Idenfication	$r_1(m)$	$r_2(m)$	$l_1 = l_2 = l(m)$	α_1	α_2	β_1
$C_{l=10^{-2}}$	1×10^{-6}	0.5×10^{-6}	1×10^{-2}	0.0001	0.00005	0.125
$C_{l=10^{-3}}$	1×10^{-6}	0.5×10^{-6}	1×10^{-3}	0.001	0.0005	0.125
$C_{l=10^{-4}}$	1×10^{-6}	0.5×10^{-6}	1×10^{-4}	0.01	0.005	0.125
$C_{l=10^{-5}}$	1×10^{-6}	0.5×10^{-6}	1×10^{-5}	0.1	0.05	0.125
$C_{l=3.0\times10^{-6}}$	1×10^{-6}	0.5×10^{-6}	3.0766×10^{-6}	0.3250	0.1625	0.125
$C_{l=1.8\times10^{-6}}$	1×10^{-6}	0.5×10^{-6}	1.8180×10^{-6}	0.5500	0.2750	0.125
$C_{l=1.2\times10^{-6}}$	1×10^{-6}	0.5×10^{-6}	1.2902×10^{-6}	0.7750	0.3875	0.125
$C_{l=10^{-6}}$	1×10^{-6}	0.5×10^{-6}	1×10^{-6}	1.0	0.5	0.125

Results of velocity, where:

$$e_{NSE} = \frac{|u_h^{NSE} - u_h^{AE}|}{u_h^{NSE}} \; and \; e_{SE} = \frac{|u_h^{SE} - u_h^{AE}|}{u_h^{SE}}$$

Table 2: Geometry data for expansion-model

Idenfication	$r_1(m)$	$r_2(m)$	$l_1 = l_2 = l(m)$	α_1	α_2	β_1
$E_{l=10^{-2}}$	0.5×10^{-6}	1×10^{-6}	1×10^{-2}	0.00005	0.0001	8
$E_{l=10^{-3}}$	0.5×10^{-6}	1×10^{-6}	1×10^{-3}	0.0005	0.001	8
$E_{l=10^{-4}}$	0.5×10^{-6}	1×10^{-6}	1×10^{-4}	0.005	0.01	8
$E_{l=10^{-5}}$	0.5×10^{-6}	1×10^{-6}	1×10^{-5}	0.05	0.1	8
$E_{l=3.0\times10^{-6}}$	0.5×10^{-6}	1×10^{-6}	3.0766×10^{-6}	0.1625	0.3250	8
$E_{l=1.8\times10^{-6}}$	0.5×10^{-6}	1×10^{-6}	1.8180×10^{-6}	0.2750	0.5500	8
$E_{l=1.2\times10^{-6}}$	0.5×10^{-6}	1×10^{-6}	1.2902×10^{-6}	0.3875	0.7750	8
$E_{l=10^{-6}}$	0.5×10^{-6}	1×10^{-6}	1×10^{-6}	0.5	1.0	8

As shown in Tabs. 1 and 2, for both models C and E, we kept the radius of the sections constant, $r_1 = 10^{-6}m$, $r_2 = 0.5\times10^{-6}m$, while the lengths varied with the shortest and longest section $l_1 = l_2 = 10^{-6}m$ and $l_1 = l_2 = 10^{-2}m$. Hence, these section lengths give $\alpha_1 \in [10^{-4},1]$, $\alpha_2 \in [5\times10^{-5},0.5]$ or $\alpha_1 \in [5\times10^{-5},0.5]$, $\alpha_2 \in [10^{-4},1]$, for model C or E in Fig.3 respectively.

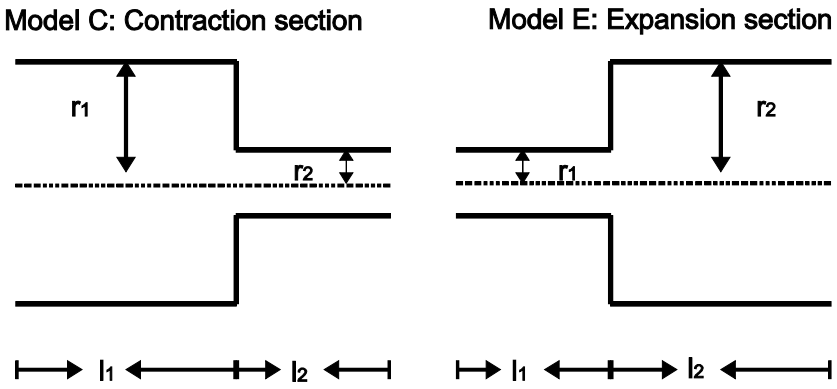

Figure 3- Tube with contraction and expansion sections

The results for NE, SE and AE presented in this section are based on $\rho = 1000\, kg/m^3$, $\sigma_{l-g} = 0.073\, mN/m$, $\mu = 0.001\, kg/ms$, and the effect of the contact angle δ on AE is ignored by setting $\delta = 0$. Numerical solutions for NSE and SE were obtained using the FEM-based software [15]. The velocity results are based on the time for the flow front to reach the end of the last section (e.g section two).

In the following we have performed a series of parametric studies of the analytical model and compared with numerical solutions. The objective is to find out when the analytical models "break down" in terms of deviating from the numerical solutions of the not fully develop laminar flow shown at the darkest shading in Fig.2. This may happen when $\alpha_{1,2}$ increases or, as in our case, the section length is dramatically decreased with respect to the cross section area, for example $l_i \approx r_i,\ \ i = 1,2$.

Figure 4(a) and (b) illustrate the velocity as a function of α_2 for model C (where $\beta = 0.125$) and E (where $\beta = 8$), respectively. Tabs. 3 and 4 give the corresponding results of velocity in numbers and some other necessary information of the flow properties, like the Reynolds numbers for NSE. The Re – number is determined by the following equation [8]:

$$Re_i = \frac{u_i D_i}{\nu};\ \ i = 1,2, \tag{26}$$

where u_i, and D_i are the mean velocity and diameter for section number i, while ν is the kinematic viscosity, $\nu = \frac{\mu}{\rho}$.

Table 3: Velocity for the NSE, SE and AE models, $C_{l=10^{-2}\to 10^{-6}}$

Id.	$u_h^{NSE}(\frac{m}{s})$	$u_h^{SE}(\frac{m}{s})$	$u_h^{AE}(\frac{m}{s})$	e_{NSE}	e_{SE}	Re_1^{NSE}	Re_2^{NSE}
$C_{l=10^{-2}}$	0.00085	0.00085	0.00085	0.00001	0.00001	0.0004	0.0008
$C_{l=10^{-3}}$	0.00858	0.00858	0.00858	0.00016	0.00016	0.004	0.008
$C_{l=10^{-4}}$	0.08573	0.08574	0.08588	0.00166	0.00164	0.04	0.08
$C_{l=10^{-5}}$	0.84274	0.84473	0.85882	0.01908	0.01667	0.42	0.84
$C_{l=3.0\times10^{-6}}$	2.58647	2.64539	2.79137	0.07922	0.05518	1.29	2.58
$C_{l=1.8\times10^{-6}}$	4.07184	4.31063	4.72400	0.16016	0.09589	2.03	4.07
$C_{l=1.2\times10^{-6}}$	5.30450	5.85890	6.65611	0.25480	0.13606	2.65	5.30
$C_{l=10^{-6}}$	6.32553	7.31211	8.58823	0.35770	0.17452	3.16	6.32

Table 4: Velocity for the NSE, SE and AE models, $E_{l=10^{-2}\to 10^{-6}}$

Id.	$u_h^{NSE}(\frac{m}{s})$	$u_h^{SE}(\frac{m}{s})$	$u_h^{AE}(\frac{m}{s})$	e_{NSE}	e_{SE}	Re_1^{NSE}	Re_2^{NSE}
$E_{l=10^{-2}}$	0.00010	0.00010	0.00010	0.00018	0.00019	0.00042	0.0002
$E_{l=10^{-3}}$	0.00107	0.00107	0.00107	0.00018	0.00019	0.00429	0.0021
$E_{l=10^{-4}}$	0.01071	0.01071	0.01071	0.00189	0.00190	0.04285	0.0214
$E_{l=10^{-5}}$	0.10548	0.10536	0.10736	0.01770	0.01888	0.42192	0.2109
$E_{l=3.0\times10^{-6}}$	0.33156	0.32789	0.34893	0.05237	0.06415	1.32623	0.6631
$E_{l=1.8\times10^{-6}}$	0.54748	0.53143	0.59005	0.07857	0.11114	2.18992	1.0949
$E_{l=1.2\times10^{-6}}$	0.75953	0.71846	0.83206	0.09548	0.15812	3.03841	1.5190
$E_{l=10^{-6}}$	0.97741	0.89257	1.07352	0.10196	0.20273	3.89716	1.9483

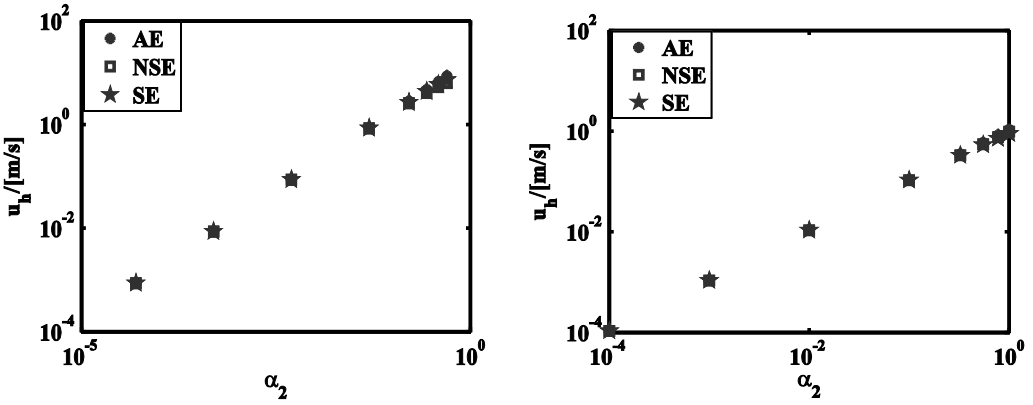

a) Models $C_{l:10^{-2}\to10^{-6}}$ *b) Models* $E_{l:10^{-2}\to10^{-6}}$

Figure 4: Velocity for contraction and expansion models, (as parameters $\alpha_i = r_i/l_i$ *) in log.-scala in both axis*

We illustrate the velocity field for NSE and SE for some models in Figs. 5 and 6. As shown in Figs. 5(a-b-c) and (d-e-f), for model C and E respectively, the NSE-velocity field is regular or straight-lined for almost all section lengths $l_{1,2} = 10^{-3} \to 10^{-5}$, while irregular fields, are seen at a sudden change in section geometry as Figs.5(c) and (f) for $l_1 = l_2 \approx 10^{-6}$. This observation of the flow profile of SE are the same for model C and E as also shown in Figs. 6(a-b-c) and Figs. 6(d-e-f). That is, when the section length is too short the irregular flow region has a noticeable effect. Based on the Reynolds number, these results indicate that the flow velocity fields are still regular for Reynolds number of approximately $10^{-4} \le Re_1^{NSE} \le 2.65$ for section one and $8\times10^{-4} \le Re_2^{NSE} \le 5.30$ for section two. The velocity fields became irregular for $Re_1^{NSE} = 3.16$ to $Re_2^{NSE} = 6.32$. In other words, the irregular flow started at very small Reynolds numbers, (see Fig.5(c) and (f) for more detail).

The change of the laminar flow velocity profile at sudden contraction of cross sectional area was studied in [8]. Experiments using Laser-Doppler system (LDA) were employed for detailed velocity measurements of the incoming flow close to the change in the cross sectional area and also of the flow redeveloping in the smaller pipe (pipe material was glass and fluid consisted of warm oil and palatinol). The incoming flow had parabolic profile corresponding to a fully developed laminar flow. Only about one to two step-heights before the sudden change in cross sectional area, the longitudinal velocity profile starts to deform providing higher velocities in the center part of the test section. This work also showed the deformed velocity profiles redeveloping into a parabolic profile in subsequent longer section, for Reynolds number in the range $23 \le Re_D \le 1213$ for the large section and $42 \le Re_d \le 2294$ for the small section. With deformation of flow profile starting at $Re_D = 196$ and $Re_d = 371$. The authors also carried out LDA-measurements to obtain information of the geometry of the separation bubble developing just downstream of the inlet of the smaller pipe. The separation region started at a Reynolds number of approximately $Re_D = 300$. The actual pipe geometry was, however, very large: $r_D = 9.5mm, l_D = 720mm$ and $r_d = 5.1mm, l_d = 880mm$. (Or, $\alpha_D = 0.0132 \text{and} \alpha_d = 0.0058$). The author, found a good agreement between the experimental and numerical results for NSE for all Reynolds numbers but a small systematic deviation occurred just downstream of the plane of contraction in the region where the velocity overshoot occurs.

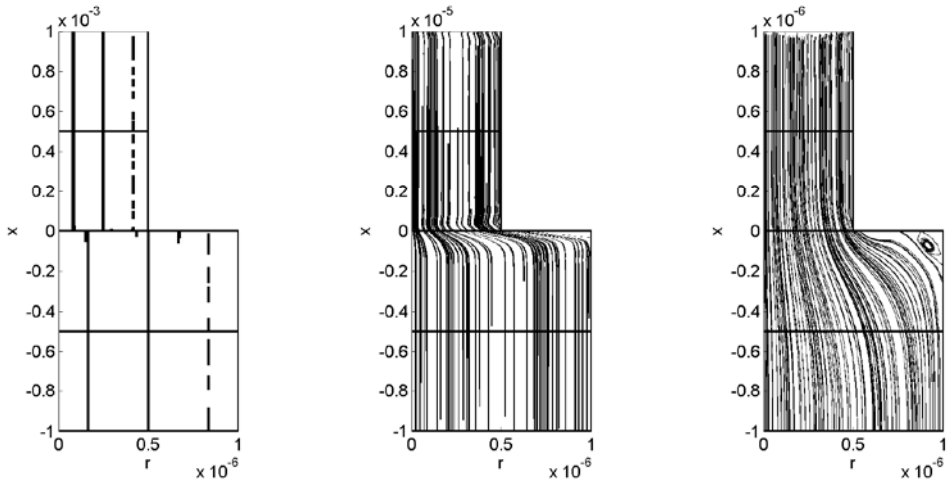

a) Model $C_{l=10^{-3}}$ b) Moodel $C_{l=10^{-5}}$ c) Model $C_{l=10^{-6}}$

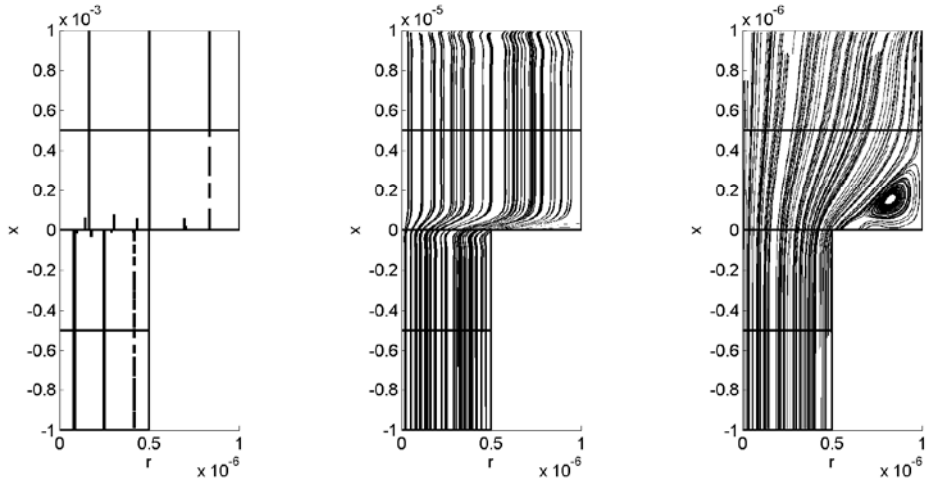

d) Model $E_{l=10^{-3}}$ e) Model $E_{l=10^{-5}}$ f) Model $E_{l=10^{-6}}$

Figure 5: NSE-Streamline velocity field for models C- $E_{l=10^{-3},10^{-5},10^{-6}}$ *, (water flows upwards)*

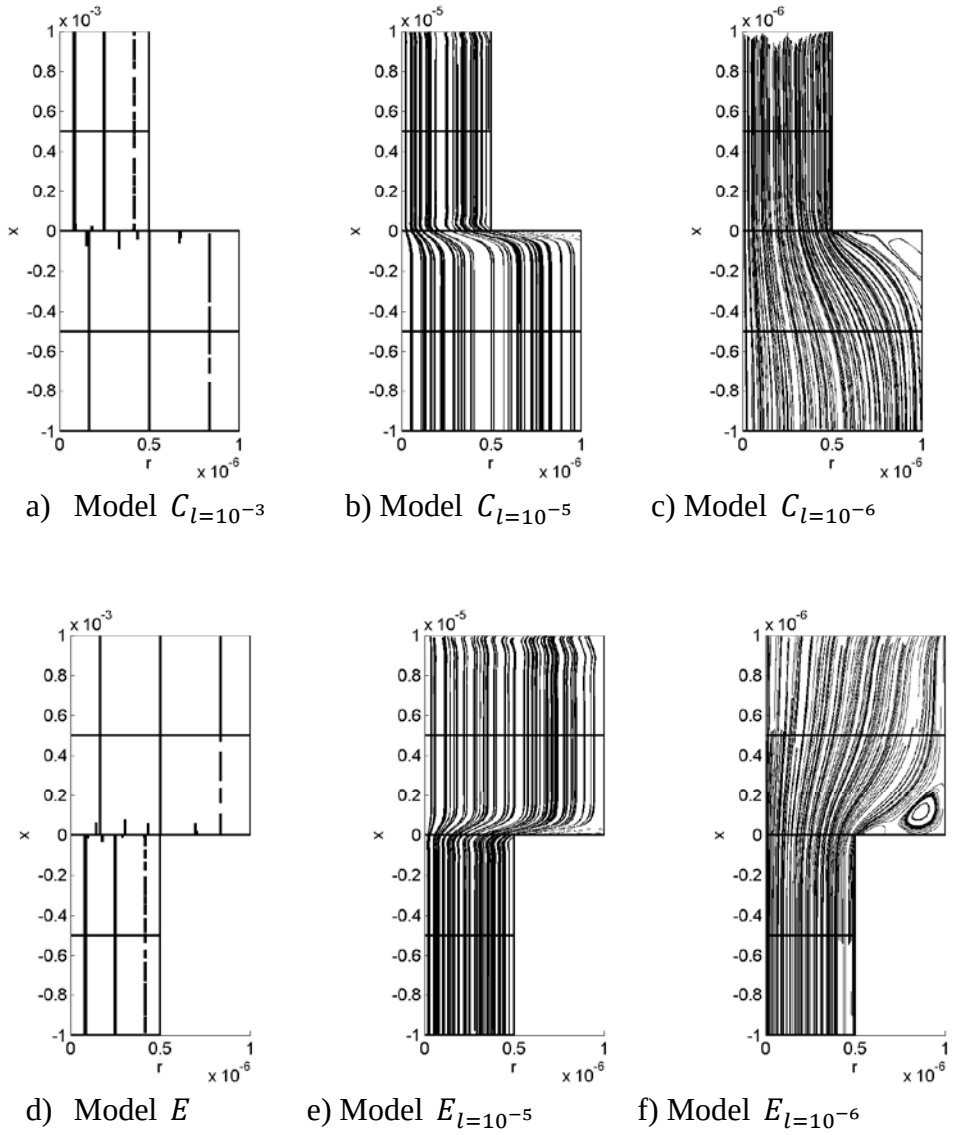

a) Model $C_{l=10^{-3}}$ b) Model $C_{l=10^{-5}}$ c) Model $C_{l=10^{-6}}$

d) Model E e) Model $E_{l=10^{-5}}$ f) Model $E_{l=10^{-6}}$

Figure 6: SE-Streamline velocity field for models C- $E_{l=10^{-3},10^{-5},10^{-6}}$

As shown in Fig. 4, the velocity of AE is in very good agreement with NSE and SE for almost all values of α_2, for both models C and E. However, a difference between the AE-velocity and the two other equations occurred as the section length is reduced to around $10^{-6}m$. Illustrated by numbers, for example, we have for model-C, when α_2 varies between 10^{-4} and 0.5 at equal section lengths and vary between 10^{-2} and 10^{-6} then the flow according to Navier Stokes u_h^{NSE} varies from 0.00085 to 6.32 m/s, whereas the flow according to Stokes u_h^{SE} varies from 0.00085 to 7.31 m/s, and the flow according to the analytical expression u_h^{AE} varies from 0.00085 to 8.58 m/s, The relative error-terms increase from $e_{NSE} = 10\times10^{-5}$ to 0.35 , and e_{SE} increase from 10×10^{-5} to 0.17, (see Tables 3 and 4 for more details). These results fall in line with the observation of the velocity fields of the NSE and the SE models. All velocities of the contraction models $C_{l=10^{-2}\to10^{-6}}$ are faster than the corresponding expansion models $E_{l=10^{-2}\to10^{-6}}$

That is, the suction at the front is more important than the flow resistance for the actual geometries.

Based on these results, it is clear that the AE is a very good model for the approximation of flow as the fluid passes section changes, for almost all the chosen pipe geometries in Tables 1 and 2. Figures 5 and 6 indicate that when the cross section of a pipe is relatively small for example $r_1, r_2 = (1\times10^{-6}, 0.5\times10^{-6}\, m)$, the flow still is laminar with a sudden contraction/expansion in cross sectional area, in spite of a large variation of the section length, $l_{1,2} = 10^{-3} \rightarrow 10^{-5}\, m$.

It is also worth noting that the velocity depends on the parameters α_i and β_i, $i = 1,2$, with the AE-velocity being proportional to the logarithm of α_2 (Fig. 4). For the AE-velocity, it may be shown that the velocity function generally depends on the parameters α_i and β_i, by function analysis of u_h in Eq. (25).

3.2 Limiting pore size for capillary suction with Laplace equation

There is a possible physical limitation to the use of capillary rise simply calculated from the suction created in the pore water under the curved meniscus, Eq. (13). This limitation is the minimum size of a water meniscus when it is no longer possible to talk about a curved meniscus creating capillary suction.

The tensile strength of water σ_{H_20} is a physical limitation to this problem. The net lifting force due to the capillary suction or under-pressure p_c of Eq. (13) is limited by the tensile strength of water which has been foud to be: $\sigma_{H_20} \approx 0.5 N/mm^2$ at $20^o C$ [16]. Equilibrium of vertical forces at the water surface, combined with Eq. (13) gives:

$$max\ p_c = \sigma_{H_2o} = \frac{2\sigma_{l-g}}{r_{min}} \Rightarrow r_{min} = \frac{2\sigma_{l-g}}{\sigma_{H_2o}} \tag{27}$$

giving

$$r_{min} = \frac{2\times0.073\frac{N}{m}}{0.5\frac{N}{mm^2}} \approx 3\times10^{-4}\, mm \approx 0.3\mu m$$

The minimum capillary radius with a meniscus creating suction calculated this way is a bit smaller than the minimum radius used in the numerical examples in tables 1 and 2 and in figures 5 and 6. We therefore assume that capillary theory based on Laplaces law applies to our pipe models.

4 CONCLUSION

An analytical pore suction model was developed based on Navier-Stokes equation and Laplaces law with multiple sized pipes in series simulating the water flow in a porous material like concrete. The analytical model is very simple to apply to evaluate the dynamic capillary flow of

any other irregular well-defined pipe geometry. Furthermore, the parameters α_i and β_i are used in the model to account, for variations in pipe geometry in relation to the pressure-conditions under the meniscus at the water front.

The results of the analytical model were compared with numerical solutions of the Navier Stokes and Stokes models. This showed good agreement of the analytical model to the more complex flow at abrupt reduction or increase of pipe radius at very small radii. For the chosen geometries of contracting and expanding straight tube sections the maximum deviation in flow between analytical and numerical solutions were in the order of $20-35\%$ whereas the majority of geometries had practically equal flows, when comparing the analytical and numerical models. The analytical model was applied for pipes large enough to avoid tensile fracture of water (approximately $300nm$).

REFERENCES

[1] Hoff, W. D.; Hall, C.(2002): Water transport in brick, stone and concrete. *Spon press London and New York.* , 318p.

[2] Hazrathi , K. (1998): Etudes des mechanismes de transport de l'eau par absorption capillare dans des materiaux cimentarles conventionels et de haute performance. PhD, Laval University.

[3] Sellevold, E.J.; Punkki, J. (1994): Capillary suction in concrete: Effects of drying procedure. Nordic Concrete Research. 15, 59--74.

[4] Garboczi, E. Bentz, D. (1999): Computer simulation and percolation theory applied to concrete. Annual reviews of computational Physics VII, World Sc. Publ. comp. 85--123. www.nist.gov.

[5] Hansic, L. (2005): Capillarity in concrete. PhD, University of Lubljana.

[6] Martys, N.S.; Chen H. (1996): Simulation of multicomponent fluids in complex three-dimensional geometries by the lattice Bolzmann method. Physical review E 53 1, 743--750.

[7] Brennan, J.K.; Dong, W. (2003): Molecular simulation of the vapour-liquid phase behaviour of Lennard-Jones mixtures in porous solids. Physical review E 67, 031503 , 1--6.

[8] Durst, F.; Loy, T. (1985): Investigation of laminar flow in a pipe with sudden contraction of cross sectional areal. Computers and Fluids. 13, 15--36.

[9] Dullien, F. A. L.; El-Sayed, M. S.; Batra V. K. (1976): Rate of Capillary Rise in Porous Media with Nonuniform Pores. Journal of Colloid and Interface Science. 60, 497--506.

[10] Fagerlund, G.(1991): Unpublished data cited by E.J Sellevold in course compendium post graduate course Concrete Structure. Norway Univ. Science and Technology.

[11] Frank, P. Incropera; David, P. DeWitt (2002): Fundamental of Heat and Mass Transfer, Fifth Edition *John Wiley and Sons. Inc*.

[12] Chatterje, S. (2002): An explanation for the unsaturated state of water stored concrete. Cement and Concrete Composites. 26, 75--79.

[13] Merle, C. Potter; David, C. Wiggert (1991): Mechanics of Fluid. Prentice Hall, Inc.

[14] Wen-Bin Young. (2004): Analysis of capillary flows in non-uniform cross-sectional capillaries. Colloids and Surfaces A: Physicochem. Eng. 234, 123--128.

[15] (2005): Comsol Multiphyscis 3.2. COMSOL AB .

[16] Crum, L. A. (1979): Tensile strength of water. Nature. 278, 148--149.

Paper 2

Capillary suction in concrete with analytical pipe model-part 2: expansion-, contraction- and random sized sections compared with experiments

Capillary suction in concrete with analytical pipe model - part 2: expansion-, contraction- and random sized sections compared with experiments

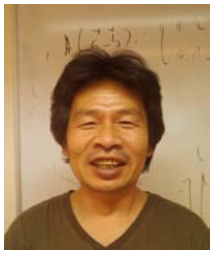

Hung Thanh Nguyen
University of Tromsø, Department of physics, 9000 Tromsø, Norway &
Narvik University College, P. 8500 Narvik, Norway
E-mail: hung.thanh.nguyen@uit.no

Frank Melandsø
University of Tromsø, Department of physics, 9000 Tromsø, Norway
E-mail: frank.melandso@uit.no

Stefan Jacobsen
Norwegian University of Science and Techn., Dept. of Structural Engineering,
7491 Trondheim, Norway.
E-Mail: stefan.jacobsen@ntnu.no

Abstract

The Lucas-Washburn equation (LWE) is based on laminar flow within the simple geometry of a single pipe with a uniform radius. We studied the effect of different pipe geometries on capillary suction by modifying the LWE to be able to handle pipes with multiple sizes (the analytical model). To do this a complete second order equation describing the relation between the capillary suction and the suction time was developed. Varying geometries of the pipes of the capillary system were investigated including the effects on the flow rate of varying combination of lengths, radius and sequence (expansion $\rightarrow$ contraction and contraction $\rightarrow$ expansion series). The results showed that largest flow reductions occurred with very narrow sections causing a blocking, reducing the capillary flow rate vs. square root of time several ten folds compared to uniform pipes without diameter variations. Similar results were also obtained for the random size models. The often observed phenomenon of reduced flow below the straight line water uptake vs. square root of time could be simulated with the multiple diameter pipe model, as seen by comparing simulations with experiments with varying concrete qualities and sample thicknesses in simple capillary absorption tests.

Key Words: Concrete, Capillary absorption, Pore necks, Modeling and Experiments

1 INTRODUCTION

Following the suggested analytical model previously developed and investigated in terms of flow conditions [1] we here further investigate the capillary absorption in concrete. We particularly investigate the deviation from the square root time vs absorption law. This deviation or anomalous capillary absorption has been observed and investigated by several, see for example [2],[3],[4] and [5]. In this second paper we proceed by investigating the behavior with our new model. This is done by investigating absorption vs square root of time relationships of three different types of pore- or pipe systems, contraction model (water going from large to small pore or pipe),

expansion model (vice versa) and a random sized system where pipes of different radii and lengths follow each other up to a desired total length. The expansion- and contraction models are coupled in series so that they are repeated a sufficient number of times to give a desired total length, comparable to the thickness of a concrete specimen tested for capillary suction, without tortuousity network or branches etc.

The models investigated only consider straight pipes, which is a simplification since real concrete can have some kind of network with interconnections distributed at varying angles and lengths in space. Our straight pipe model is designed to investigate whether narrow passages between capillary size pores may slow down capillary suction rate and cause the anomalous absorption behavior discussed in part one of this study. Are such pore necks sufficient to explain the behavior often seen in experiments with increasing deviation from the straight line absorption vs square root time as specimen thickness and the number of necks increase?

Other effects have also been proposed as explanation. Air can be entrapped, compressed and/or dissolved in voids during capillary suction in concrete [6]. Furthermore, there is a significant volume fraction of gel pores in concrete that are too small for the capillary suction mechanism [7]. Neither effects of air nor gel are taken into account in our study. Still we believe that since the fraction of capillary active porosity in most concrete is quite large, the present model will give a useful illustration of the problem.

2 FLOWMODELS

Consider laminar flow in a circular pipe with with $N-$ subsections (Figure 1, where, r_i and l_i , $i = 1,2,...,N$ are section radius and length respectively). And, assume that the water front reaches the position h.

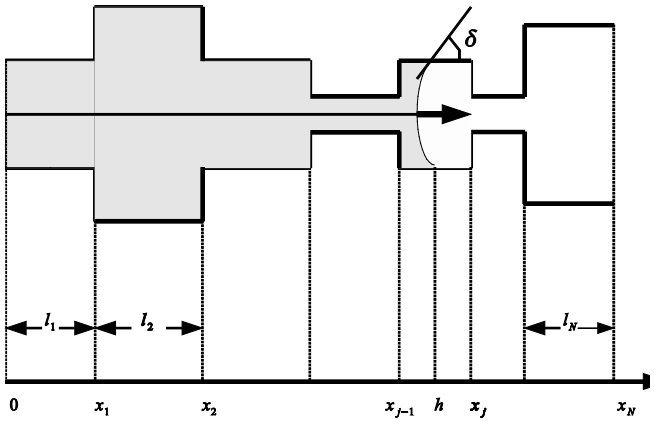

Figure 1- Pipe with $N-$ irregular subsections

Analyticale formulas for the capillary flow height $h(t)$ based on the velocity u_h were developed the previous paper [1]. The velocity of the water flow at the front in an arbitrary section j as shown in Fig. 1, can be determined with the following equation

$$u_h = \frac{k}{f(h) r_h^3} \tag{1}$$

where

$$k = \frac{\sigma \cos\delta}{4\,\mu} \tag{2}$$

Here, σ is the surface tension between water and air, μ is viscosity coefficient and δ the contact angle between the pipe wall and the wetting water front (Figure 1). And

$$\begin{aligned} f(h) = \int_0^h \frac{dx}{r_x^4} \quad &= \frac{l_1}{r_1^4} + \cdots + \frac{l_{j-1}}{r_{j-1}^4} + \frac{h - x_{j-1}}{r_j^4} \\ &= \sum_{i=1}^{j-1} f_i + \Delta f_j, \end{aligned} \tag{3}$$

$$f_i = \frac{l_i}{r_i^4} \;\; and \;\; \Delta f_j = \frac{(h - x_{j-1})}{r_j^4}. \tag{4}$$

The relation between the capillary velocity and the capillary height is given by the differential equation

$$u_h = \frac{dh}{dt}$$

which can be inserted in Eq. (1) and then integrated. This yields

$$\int_0^h r_s^3 f(s) ds = kt. \tag{5}$$

where s is an integration variable running over the tube sections with a stepwise changing radius r_s.

A solution of Eq. (5) will for a general variation in the cross section, require a numerical approach [8]. However, for a stepwise changing radius, it is possible to work out solutions by analytical means. We notice that the function $f(s)$ has to be continuous since it occurred from integrating a stepwise changing function [given by Eq. (3)], and linear in the individual tube sections as illustrated in Fig. 2. The left hand side of Eq. (5) may therefore be interpreted as the area under the graph $f(h)$ from 0 to h weighted by the section value r_h^3. With this in mind in addition to using the analytical formula for $f(h)$ [Eq.(3)] and for the area formula of a trapezoidal element, we get

$$\begin{aligned}\int_0^h r_s^3 f(s)ds &= [r_1^3 A_1]+[r_2^3 A_2]+\cdots+[r_{j-1}^3 A_{j-1}]+[r_j^3 A_h] \\ &= r_1^3\left[\frac{1}{2} f_1 l_1\right]+r_2^3\left[f_1 l_2+\frac{1}{2} f_2 l_2\right]+\cdots \\ &+ r_{j-1}^3\left[(f_1+f_2+\cdots+f_{j-2})l_{j-1}+\frac{1}{2} f_{j-1} l_{j-1}\right] \\ &+ r_j^3\left[(f_1+f_2+\cdots+f_{j-1})+\frac{1}{2}\Delta f_j\right](h-x_{j-1}) \\ &= \left[\sum_{i=1}^{j-1} r_i^3 l_i\left(\sum_{m=1}^{i-1} f_m+\frac{1}{2} f_i\right)\right]+ \\ &\quad \left[r_j^3(h-x_{j-1})\left(\sum_{i=1}^{j-1} f_i+\frac{1}{2}\Delta f_j\right)\right].\end{aligned} \tag{6}$$

From Eq. (6) we see that only the terms related to the front section or j-section, is a function of the capillary height h, while the other terms may be regarded as constants with respect to this parameter. Moreover, by inserting Eq. (6) into the left side of Eq. (5) and by substituting Δf_j from Eq. (4), we find that h and time t are related through the second order equation

$$\left[\sum_{i=1}^{j-1} r_i^3 l_i\left(\sum_{m=1}^{i-1} f_m+\frac{1}{2} f_i\right)\right]+\left(r_j^3\sum_{i=1}^{j-1} f_i\right)\Delta h_j+\frac{1}{2r_j}(\Delta h_j)^2 = kt\,. \tag{7}$$

As a short notation we have here introduced the relative height

$$\Delta h_j = h - x_{j-1}, \tag{8}$$

measured from the starting position x_{j-1} from the last section. In addition, we will also introduce the parameters

$$C_{j-1} = \textstyle\sum_{i=1}^{j-1} r_i^3 l_i\left(\sum_{m=1}^{i-1} f_m+\frac{1}{2} f_i\right) \tag{9a}$$

$$B_j = r_j^3 \textstyle\sum_{i=1}^{j-1} f_i \tag{9b}$$

$$\bar{A}_J = \frac{1}{2r_j} \tag{9c}$$

to put Eq. (7) into the quadratic form

$$C_j + B_j\Delta h_j + \bar{A}_J\Delta h_j^2 \tag{10}$$

Equation (10) is particularly interesting since many useful results may be deduced from it. The equation gives, for example, the required filling time t

$$t = \frac{C_{j-1}}{k}+\frac{B_j\Delta h_j+\overline{A_J}\,\Delta h_j^2}{k} \tag{11}$$

for all pipe section up to h, for cases where h is specified. Here the first term provides the filling

time for the first $(j-1)$ sections while the second term gives the time needed to fill up the last section up to position h.

On the other hand, if the total filling time t is known or specified, Δh_j may easily be obtained from using the quadratic solution formula on Eq. (10), to give

$$\Delta h_j(t) = \frac{-B_j + \sqrt{B_j^2 - 4\overline{A_j}(C_{j-1} - kt)}}{2\overline{A_j}} \tag{12}$$

It should be noticed that since the fluid height is a positive value, only the positive root of Eq. (10) should be considered here.

It is also possible to recalculate well known capillary formulas for tubes with a uniform radius r_U from Eq. (10). From $r_1 = r_2 = \cdots = r_j = r_U$ we find the well known equation

$$h(t) = \sqrt{2r_U kt} = \left[\sqrt{\frac{r_U \sigma \cos\delta}{2\mu}}\right]\sqrt{t} \tag{13}$$

often refereed to as the Lucas-Washburn equation [9],[10] .

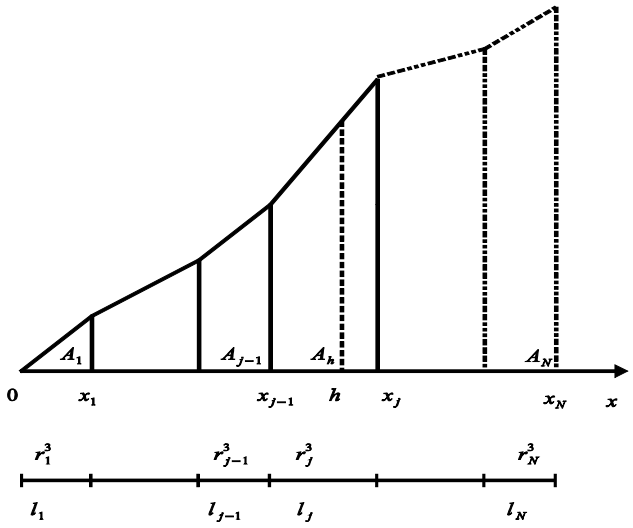

Figure 2- The areal under the graph of $f(h)$ *from 0 to* h, $A_1, \cdots, A_h$

Finally, we will show that the previously derived fluid velocity can be expressed in terms of the new notation, e.g. the $\bar{A}-$, $B-$ and $C-$terms introduced in Eq. (9). This will give us an analytical expression for the velocity as a function of time. This time relation may be found by derivation of the flow height in Eq. (12) with respect to time, which yields

$$u_{\Delta h_j}(t) = \frac{d(\Delta h_j)}{dt} = \frac{d}{dt}\left[\frac{-B_j + \sqrt{B_j^2 - 4\bar{A}_j(C_{j-1} - kt)}}{2\overline{A_j}}\right] = \frac{k}{\sqrt{B_j^2 - 4\bar{A}_j(C_{j-1} - kt)}} \qquad (14)$$

One should notice that this equation has to be identical to previous velocity expression given as a function of position u_h, for example, Eq. (1). To show this, the time t in Eq. (14) may be replaced by Eq. (11). This gives

$$u_h = \frac{k}{\sqrt{B_j^2 - 4\overline{A_j}\left(C_{j-1} - \left(C_{j-1} + B_j\Delta h_j + \overline{A_j}\Delta h_j^2\right)\right)}} = \frac{k}{B_j + 2\overline{A_j}\Delta h_j} = \frac{k}{f(h) r_h^3}$$

3 MODEL AND EXPERIMENTAL DATA

3.1 Contraction-expansion and expansion-contraction models

In order to study the influence of the pipe geometry on the absorption of water, we construct first several contraction-expansion sections (Model C) and expansion-contraction (Model E). Here the value of geometries are fixed as illustrated in Fig. 3. In addition a model with random geometries is investigated (Model R). As shown in Fig. 3, two different combinations of sections (a) and (b) give the structure of models C-E. Each combination has $(ns - N)$ sections.

When plotting the calculated absorption as (kg/m^2) vs square root time the absorption may simply be interpreted as a suction height to be compared with the results of Eqs.(12) - (14). To compare calculations with experiments where the pore volume varies depending on w/c, degree of hydration and fraction of cement paste (assuming non-porous aggregate) we could simply calculate the absorption in the form of weight. For this purpose we have calculated a mean pipe radius that we relate the degree of pore (or pipe-) filling to, for the C- and E-models, and for a random sized pore model,also taken into account the mean porosity.

For each set of models C or E, there is a corresponding model-U with the constant uniform mean volume radius r_U. We require the conservation of volume for these three models. Let V_C, V_E and V_U denote the volume for model C, model E and model U, respectively. In order to have the same volume for all three models, the radius r_U must satisfy the following condition:

$$V_C = V_E = V_U \Rightarrow \frac{1}{2}\pi(r_1^2 + r_2^2) = \pi\, r_U^2$$

or

$$r_U = \sqrt{\frac{r_1^2 + r_2^2}{2}}. \qquad (15)$$

We observe that the radius r_U depends only on the radii r_1 and r_2 but not on the section lengths l_1 and l_2.

The volume (V) of the capillary absorbed water is calculated by the following equation

$$V(t) = \sum_{i=1}^{j-1} \pi r_i^2 l_i + \pi r_j^2 \Delta h_j(t) \tag{16}$$

$\Delta h_j(t)$ is defined in Eq. (12).

The selection of data for the varying section lengths and section radii are given in Tables 1 and 2 respectively. Table 3 shows the relation between the value of radii r_1, r_2 and r_U.

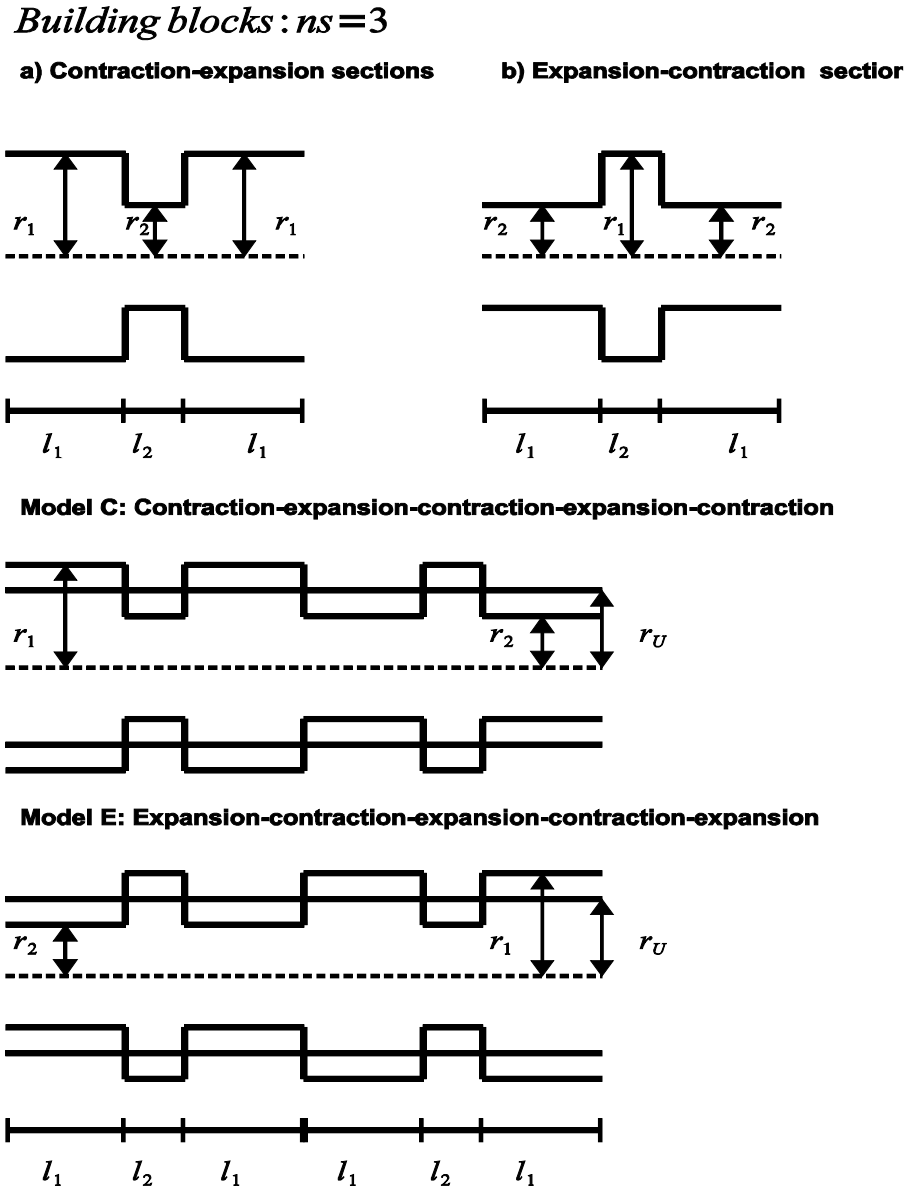

Figure 3- Model C, E with $ns = 3$, $N = 6$ *sections and Model U with constant radius*

Table 1: Variation of section length for contraction-expansion and expansion-contraction series models

N	$L(m)$	$l_1(m)$	$l_2(m)$	$l_1 : l_2$
6	0.04	0.0067	0.0067	1:1
6	0.04	0.005	0.01	1:2
6	0.04	0.008	0.004	2:1
30	0.04	0.0013	0.0013	1:1
30	0.04	0.0009	0.0018	1:2
30	0.04	0.0017	0.00086	2:1

Table 2: Variation of sections radii for contraction-expansion and expansion-contraction series models

$r_1(m)$	$r_2(m)$	$r_1 : r_2$
1×10^{-6}	0.8×10^{-6}	1:0.8
1×10^{-6}	0.5×10^{-6}	1:0.5
1×10^{-6}	0.1×10^{-6}	1:0.1

Table 3: Relation between radii (r_1, r_2) *and* r_U

$r_1(m)$	$r_2(m)$	$r_U(m)$
1×10^{-6}	0.8×10^{-6}	0.905×10^{-6}
1×10^{-6}	0.5×10^{-6}	0.79×10^{-6}
1×10^{-6}	0.1×10^{-6}	0.71×10^{-6}

3.2 Experimental data

In addition to analyzing some capillary absorption data from the literature, a series of experiments with one sided capillary absorption was performed with two different concrete qualities. Specimens were produced from ordinary portland cement (ASTM Type II/CEM I 42,5 R) with blaine specific surface 384 m^2/kg, granitic aggregate with 8 mm maximum size, 9% fines less than $0.125mm$ and 0.5% absorption and a copolymer water reducer (Sika Viscocrete) added to obtain flowable consistency. Two different mortar mixes were made with w/c = 0.45 and 0.60, respectively. Both mixes had 39 percent cement paste and 2 percent air void. Fifty litre batches were made in an 80 liter horizontal rotating paddle mixer and cylindrical specimens with diameter 100 mm and height 200 mm were cast in two layers in steel molds with slight compaction on a vibrating table between each layer. The cylinders were de-moulded after 24 hours and cured in water at 20^oC for approximately four months. Then, slices with thickness 20, 40 and 100mm where cut normal to the cylinder axis. The slices were dried at 105^oC to constant weight, air cooled to room temperature and sealed on their lateral surfaces to ensure undirectional flow of water. For each material and thickness four specimens were weighed regularly. Plots of capillary absorption in weight vs square root of time $\left(W(t) - \sqrt{t} \ : \ [kg/m^2]\right)$are shown in Fig. 4. We clearly see the vanishing nick points at increasing thickness and reduced w/c.

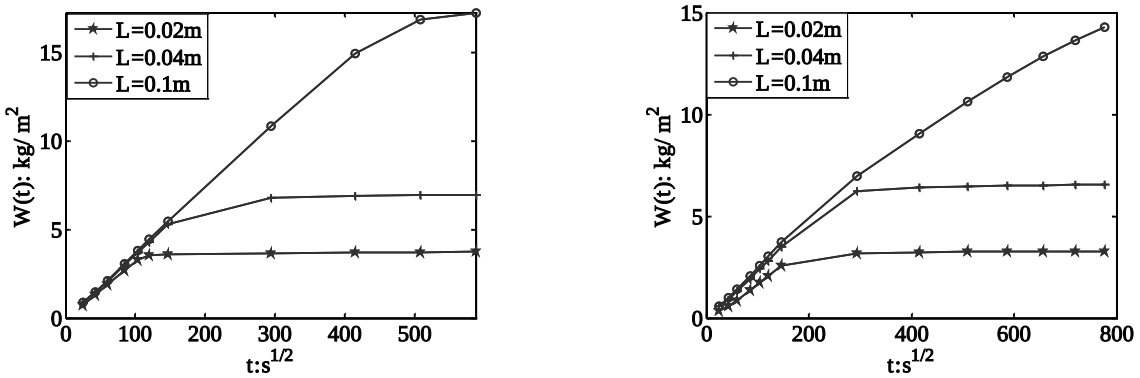

a) $w/c = 0.60$ **b)** $w/c = 0.45$

Figure 4- Experimental capillary suction for mortar specimens with ordinary Portland cement, $w/c = 0.60$ *and* 0.45*, non-porous aggregate, and different thickness* L *as* $20,40$ *and* 100 *mm.*

The suction porosities of the specimens were measured following the capillary absorption test by total immersion until constant weight and determining volume by weighing in air and in water. Then hydration was calculated based on Powers model [7] and the formulae [11] $p_{tot} = (w/c - 0.172\alpha)/(w/c + 1/\rho_c)$, where α is degree of hydration and ρ_c is particle density of cement. Finally, the capillary porosities were determined according to Powers model with the following formula by [11], $p_{cap} = (w/c - 0.415\alpha)/(w/c + 1/\rho_c)$. Tab. 4 gives the results.

Table 4 indicates around 40% fraction of capillary porosity compared to the total porosity for our specimens according to the differentiation between gelpores (where meniscii do not exist)- and capillaries based on the sorption experiments of Powers and Brownyard [7]. Compared to our previous discussion about the tensile strength of water it means that around 60% of the pore volume could be filled by other suction mechanism than capillay suction mehanisms. Our interpretation of the results then excludes the filling of the other pores which is obviously a source of error. Nevertheless we believe that the approach presented in this paper can give information about the possibility that pore necks may cause the capillary absorption anomaly as discussed in the introduction.

Table 4: Total- and capillary porosity (m^3/m^3) *and degree of hydration* α *in the mortar with* $w/c = 45$ *and 60 as measured and combination with caculated based on Power models for cement paste porosity and 39 volume* $-\%$ *cement paste in the mortar. Aggregate assumed non-absorbing.*

w/c	p_{tot}	$p_{capillary}$	α
0.45	0.16	0.064	0.78
0.60	0.18	0.0678	1.0

We have also replotted experimental data from two other studies on capillary absorption and compared these with our model. In [4] the effect of initial moisture content was investigated, whereas in [3] a continuum modelling approach based on sorptivity and Richards equation was compared with absorption and NMR-measurements.

3.3 Random size pores model

In addition to models C and E we let the value of the section radii be random and section lengths be fixed. A uniform pseudorandom function generated a uniform distribution of random values on a specified interval , $r_i \in I = [r_{min}, r_{max}]$, [12].

Let n be the number selection of random of radii $(r_i)_1^N$ and assuming a uniform random distribution of radii in the interval $[r_{min}, r_{max}]$. The following matrices V and T express the capillary suction volume and time as

$$V = \begin{pmatrix} v_{1,1} & v_{1,2} & \cdots & v_{1,N} \\ v_{2,1} & v_{2,2} & \cdots & v_{2,N} \\ \vdots & & & \vdots \\ v_{n,1} & v_{n,2} & \cdots & v_{n,N} \end{pmatrix}$$

$$T = \begin{pmatrix} t_{1,1} & t_{1,2} & \cdots & t_{1,N} \\ t_{2,1} & t_{2,2} & \cdots & t_{2,N} \\ \vdots & & & \vdots \\ t_{n,1} & t_{n,2} & \cdots & t_{n,N} \end{pmatrix}$$

where $v_{i,j}$ is the capillary suction volume as the water front reaches the end of section number j (see Eq.(16)) at the selection nummer i, $i = 1,2,...,n;\quad j = 1,2,...,N$. Hence, the corresponding suction time is $t_{i,j}$.

In practice, particularly for a random problem the mean value of V and T are most interesting. Now let $\overline{V}$ and $\overline{T}$ represent the mean value of V and T respectively. These new parameter are expressed by the following equation

$$\overline{V} = \bar{v}_j = \frac{1}{n}\sum_{i=1}^{n} v_{i,j} \quad and \quad \overline{T} = \bar{t}_j = \frac{1}{n}\sum_{i=1}^{n} t_{i,j} \quad j = 1,2,\cdots,N \tag{17}$$

Eq.(17) shows that the mean value of the matrix $\overline{V}$ is simply a row vector containing the mean value of each column $\bar{v}_j$, corresponding with the mean value of time $\bar{t}_j$. In the procedure which was presented in section 3.1, we introduced the model with uniform constant radius (Model U) which has the same capillary suction volume. Hence, if r_U is a radius to model U then the constant radius for model U is obtained from:

$$r_U = \sqrt{\frac{\bar{v}_N}{\pi L}} \tag{18}$$

where L is the length of pipe.

4 RESULTS AND DISCUSSION

The results for model capillary absorption calculated with the analytical expression (AE) presented in this section are based on density of water $\rho = 1000\ kg/m^3$, surface tension between air and water $\sigma = 0.073\ N/m$, viscosity of water $\mu = 0.001\ kg/ms$, and contact angle between concrete and air-water surface $\delta = 0$. The calculated capillary suction results are based on the time for the flow front to reach the end of the last section (e.g section N). The capillary suction experiments are based on the regular weighing of specimens stored with one side in water and using total porosity to water measured on the same concrete specimens.

Calculation of absorption is based on the weight at the time $t_i, i = 1,2,\cdots$, of the different concrete specimens that we compare the models with, or

$$W(t) = \frac{W_i}{A} \tag{19}$$

where W_i is weight of absorbed water in time step t_i (kg), either caculated with one of the Analytical models C (Contraction), E (Expansion), U (Uniform) or R (Random) or measured during capillary expansion experiments. A is area of the actual concrete specimen tested, or $A = A_U/\rho_{tot}$ for Analytical models, where A_U is the area of $U-$model and ρ_{tot} is the actual total porosity.

Note that the capillary rise in the uniform tube (model U) (Fig. 3) is a straight line function of square root of time as described by the line $\left(W(t) - \sqrt{t}\right)$. By comparing the capillary suction of the varying models with this line, we can see how strong the effect of the different geometries are on the capillary rise.

Fig. 5 shows that the varying pipe geometries have large effects on the capillary suction. For constant section length (Fig. 5(a) to (c)) it seems that the capillary rise of models C-E practically stops when $[r_1 : r_2]$ is reduced from $[1:0.8]$ to $[1:0.1]$, since models C and E used much more time to absorb as much as did model U. This is illustrated by keeping section length equal, $l_1 = l_2$. Then, the times for the three models to reach the total suction volume or capillary nick point L are $\sqrt{t_U} \approx 6.95\sqrt{s} < \sqrt{t_C} \approx 7.51\sqrt{s} < \sqrt{t_E} \approx 7.59\sqrt{s}$, when $[r_1 : r_2] = [1:0.8]$, while $\sqrt{t_U} \approx 7.44 < \sqrt{t_C} \approx 14.30 < \sqrt{t_E} \approx 14.64$, when $[r_1 : r_2] = [1:0.5]$, and $\sqrt{t_U} \approx 7.85 < \sqrt{t_C} \approx 326.46 < \sqrt{t_E} \approx 335.91$, when $[r_1 : r_2] = [1:0.1]$. The latter capillary nick point times of around 300 - 400 square-root seconds are in the same order of magnitude as experimental nick points seen on slices made of normal weigh ordinary portland cement concrete with $w/c > 0.40$ and approximately $30mm$ thickness. The flow thus seems to more or less stop when passing one or several narrow/large contraction/ expansion sections. Clearly, there is some kind of blocking phenomenon (see Fig. 5). Also, combinations of varying both section length and section radius give very interesting capillary suction curves. When $l_1 = l_2$ and the ratio of radii vary from $[r_1 : r_2] = [1:0.8]$ to $[1:0.1]$, the capillary suction curves for both models C-E are almost linear like the uniform pipe model as shown in Figs. 5 (a-b-c). On the other hand, when variation of section length is introduced, i.e. $[l_1 : l_2]$ is changed from $[1:1]$ to $[1:2]$ for $[r_1 : r_2] = [1:0.8]$, $[1:0.5]$ and $[1:0.1]$, the suction curve of model E obeys the linear behavior until the flow passes approximately 2/3 of the total suction volume, where-after the curves deviate from the linear behavior (as shown in Figs. 5 (d-e-f)). The same trend is observed for model C

where the sequence of the long and short pipe is switched for the contraction model for $[l_1 : l_2] = [1:1]$ and $[2:1]$. Apparently, the anomalous type of capillary suction curves we are interested in can be studied with both contraction and expansion models when the wide section are the longest, and are separated from each other with short, thin pipes. Reducing the radius of the small, short, pipe from 0.5:1 to 0.1:1 also makes the time scale of the analytical model similar to the time scale of capillary suction experiments shown in Figure 1 in part 1 and in the experimental data presented in the last figures of this paper.

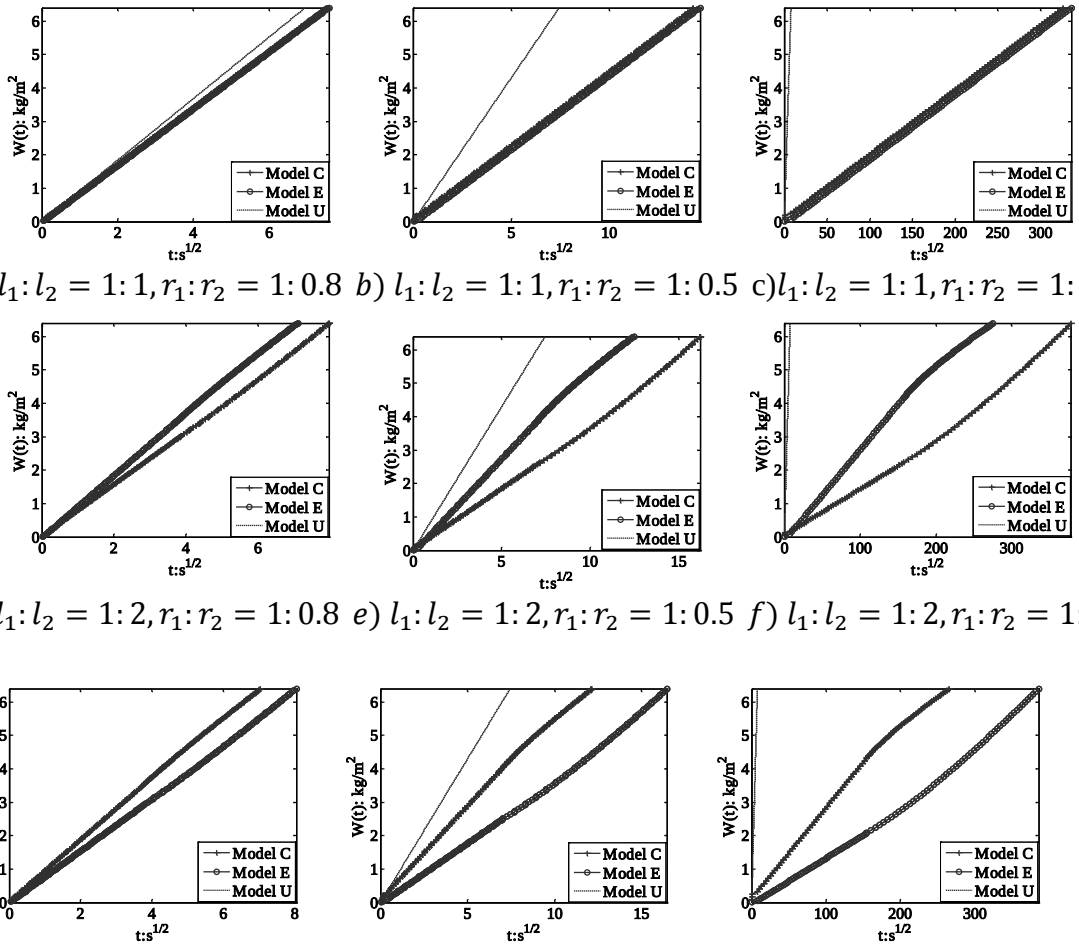

a) $l_1 : l_2 = 1:1, r_1 : r_2 = 1:0.8$ *b)* $l_1 : l_2 = 1:1, r_1 : r_2 = 1:0.5$ c)$l_1 : l_2 = 1:1, r_1 : r_2 = 1:0.1$

d) $l_1 : l_2 = 1:2, r_1 : r_2 = 1:0.8$ *e)* $l_1 : l_2 = 1:2, r_1 : r_2 = 1:0.5$ *f)* $l_1 : l_2 = 1:2, r_1 : r_2 = 1:0.1$

g) $l_1 : l_2 = 2:1, r_1 : r_2 = 1:0.8$ *h)* $l_1 : l_2 = 2:1, r_1 : r_2 = 1:0.5$ *i)* $l_1 : l_2 = 2:1, r_1 : r_2 = 1:0.1$

Figure 5- Analytical water absorption curves $\left(W(t) - \sqrt{t}\right)$ *for models C, E and U, where* $N = 30$, *and* $L = 0.04m$, *and* $\rho_{tot} = 0.16$.

Figure 6 shows the effect of the random sized pipes by comparing the capillary suction for model R and the corresponding model with constant radius (model U). The length of the large and the small pipes are $1:1$ and $1:2$, whereas the ratios of radii vary as $1:1$, $0.5:1$ and $0.1:1$. We see that, just as for the Contraction and Expansion models, there is little effect on the capillary suction compared to the uniform model by varying the radius of the small pipe as the length of the large pipe is as short as $l_1 : l_2 = 1:1$. In addition there is no effect of increased length $l_1 : l_2 = 1:2$.

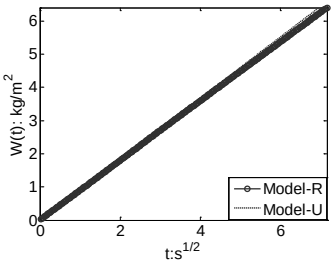

$a) l_1 : l_2 = 1:1, r_1 : r_2 = 1:0.8$

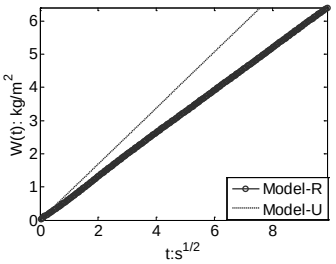

$b)\ l_1 : l_2 = 1:1, r_1 : r_2 = 1:0.5$

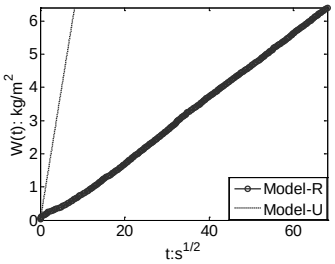

$c)\ l_1 : l_2 = 1:1, r_1 : r_2 = 1:0.1$

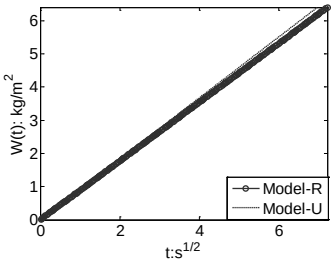

$d) l_1 : l_2 = 1:2, r_1 : r_2 = 1:0.8$

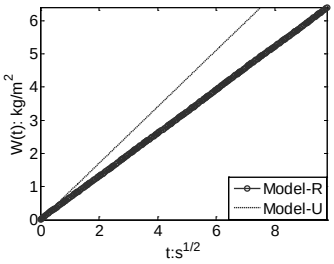

$e)\ l_1 : l_2 = 1:2, r_1 : r_2 = 1:0.5$

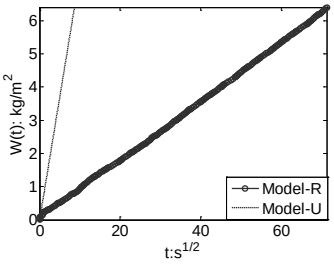

$f)\ l_1 : l_2 = 1:2, r_1 : r_2 = 1:0.1$

Figure 6- Analytical water absorption curves $\left(W(t) - \sqrt{t}\right)$ *for models R (Random) and U where* $N = 30$ *and* $n = 50$, *and* $p_{tot} = 0.16$.

We then compare the behavior observed in the AE-results with our own capillary absorption experiments as well as with the data from the literature.

Fig. 7 compares calculated capillary suction with two different pipe geometries for the $w/c = 0.60$ specimens were the ratio of radii between large and small pipes are always kept at $1:0.1$ or $1\times10^{-6} m : 0.1\times10^{-6} m$, based on the observations in Fig. 5. The main pipe geometry variable for the two plots is the length ratio between the large and the small pipes. From the plots we can see clearly how the calculated absorption approaches the measured absorption as the length ratio between the large and small pipes increases from $1:1$ to $2:1$. It is very interesting to note that the calculated capillary suction seems to give the right kind of increasing anomaly at increasing suction length, i.e at increasing specimen thickness. Apparently the increased number of necks has the right kind of effect compared to what is commonly seen in capillary suction experiments.

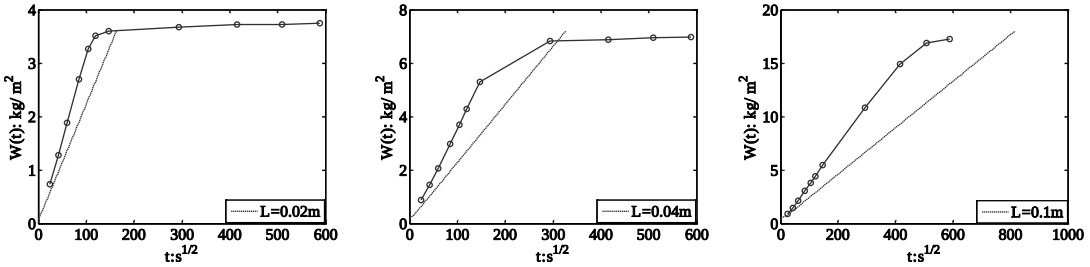

$a)\ l_1 : l_2 = 1:1, r_1 : r_2 = 1:0.1$ $b)\ l_1 : l_2 = 1:1, r_1 : r_2 = 1:0.1.$ $c)\ l_1 : l_2 = 1:1, r_1 : r_2 = 1:0.1$

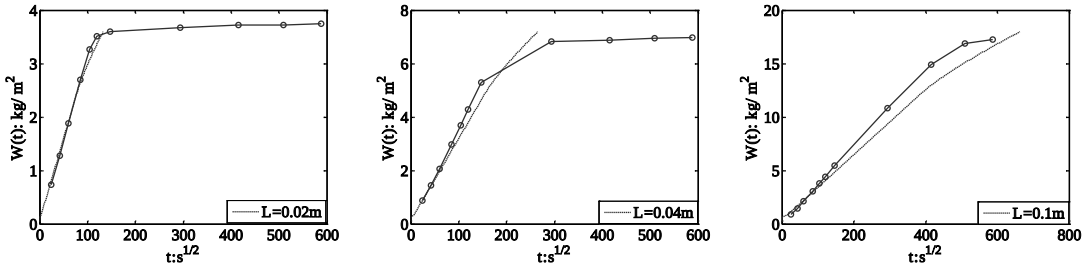

$d)\ l_1 : l_2 = 2:1, r_1 : r_2 = 1:0.1$ $e)\ l_1 : l_2 = 2:1, r_1 : r_2 = 1:0.1.$ $f)\ l_1 : l_2 = 2:1, r_1 : r_2 = 1:0.1$

Figure 7- Analytical (dashed lines, Model C) and Experimental (full lines with circles) water absorption curves $\left(W(t) - \sqrt{t}\right)$ *for* $w/c = 0.60$, *and for three different pipe/specimens length/thickness, and* $p_{tol} = 0.18$.

Fig. 8 shows the same type of plots as in Fig. 7 with Ordinary Portland Cement specimens with $w/c = 0.45$. In this plot we see that a slightly different pipe geometry with similar length of the large and small pipes fits the measured absorption best of the two investigated geometries. Possibly a somewhat larger fraction of smaller pores in $w/c = 0.45$ with less continuity compared to $w/c = 0.60$ is represented by this geometry (figure 7).

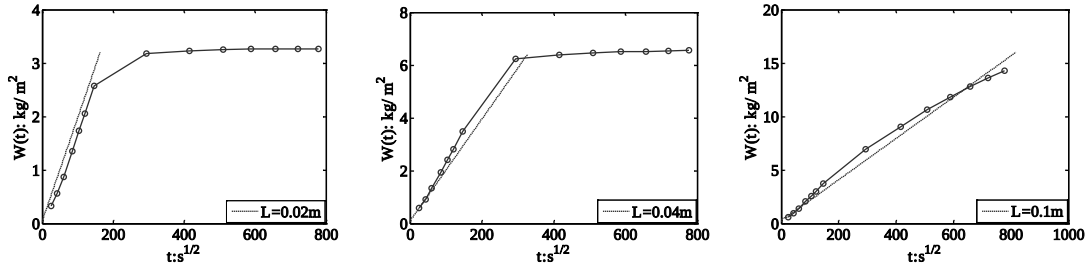

$a)\ l_1 : l_2 = 1:1, r_1 : r_2 = 1:0.1$ $b)\ l_1 : l_2 = 1:1, r_1 : r_2 = 1:0.1.$ $c)\ l_1 : l_2 = 1:1, r_1 : r_2 = 1:0.1$

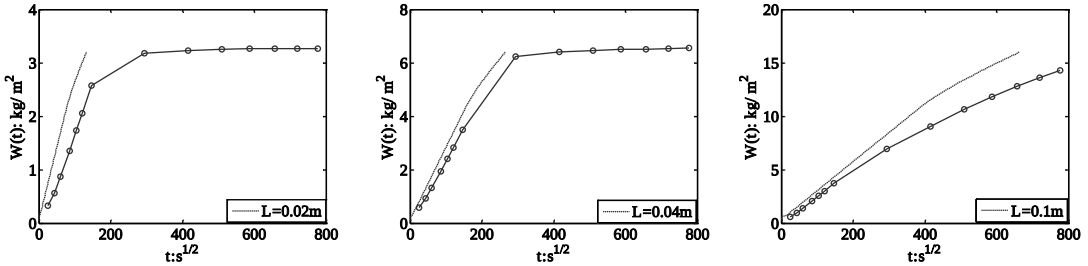

$d)\ l_1 : l_2 = 2:1, r_1 : r_2 = 1:0.1$ $e)\ l_1 : l_2 = 2:1, r_1 : r_2 = 1:0.1.$ $f)\ l_1 : l_2 = 2:1, r_1 : r_2 = 1:0.1$

Figure 8- Analytical (dashed lines, Model C) and Experimental (full lines with circles) water absorption curves $\left(W(t) - \sqrt{t}\right)$ *for* $w/c = 0.45$, *and for three different pipe/specimen length/thickness, and* $p_{tot} = 0.16$.

Fig. 9 shows experimental capillary suction data from the literature [4] together with the model. The actual concrete has $w/b = 0.40$ and two percent condensed silica fume, and so has a low fraction, if any, of capillary porosity according to Powers model. From the figure it can be seen that the changing of pipe geometry that worked successfully with high w/c in Fig. 7 with $1:0.1$ ratio between radii and a bit longer large pipe -sections is less successful. The reason could be the slow capillary suction in these specimens due to more narrow necks at $w/c = 0.45$ compared to at $w/c = 0.60$.

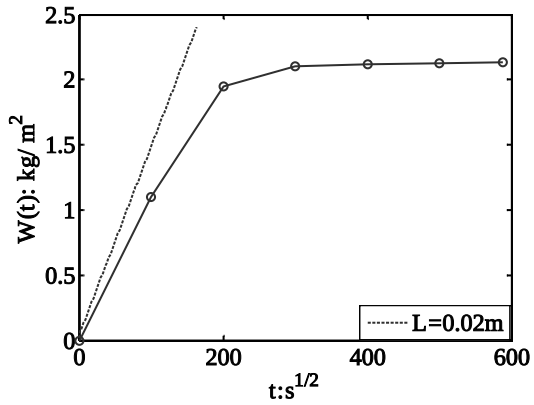

$a)\ l_1 : l_2 = 1:1, r_1 : r_2 = 1:0.1$

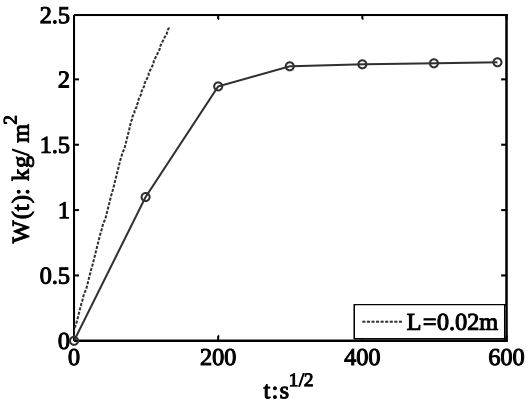

$b)\ l_1 : l_2 = 2:1, r_1 : r_2 = 1:0.1$

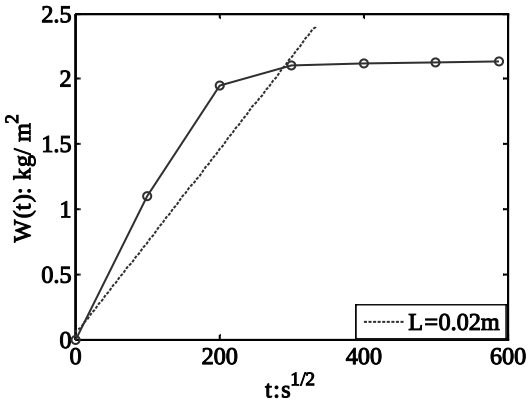

$c)\ l_1 : l_2 = 1:1, r_1 : r_2 = 1:0.07$

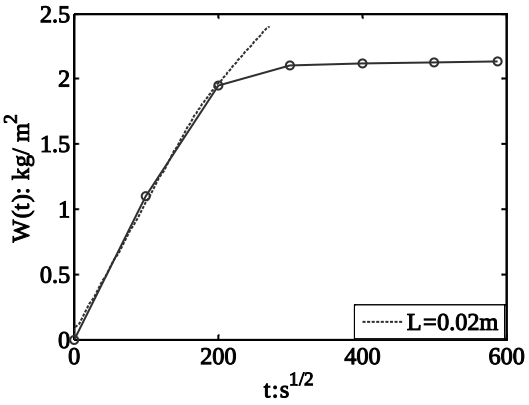

$d)\ l_1 : l_2 = 2:1, r_1 : r_2 = 1:0.07$

Figure 9- Experimental data [4] (full lines) and analytical (dashed lines) water absorption curves $\left(W(t) - \sqrt{t}\right)$ and $p_{tot} = 0.12$.

Fig. 10 shows experimental capillary suction data of ordinary portland cement mortar with *w*/*b* = 0.40 taken from [3] showing a similar tendency as in figure 9.

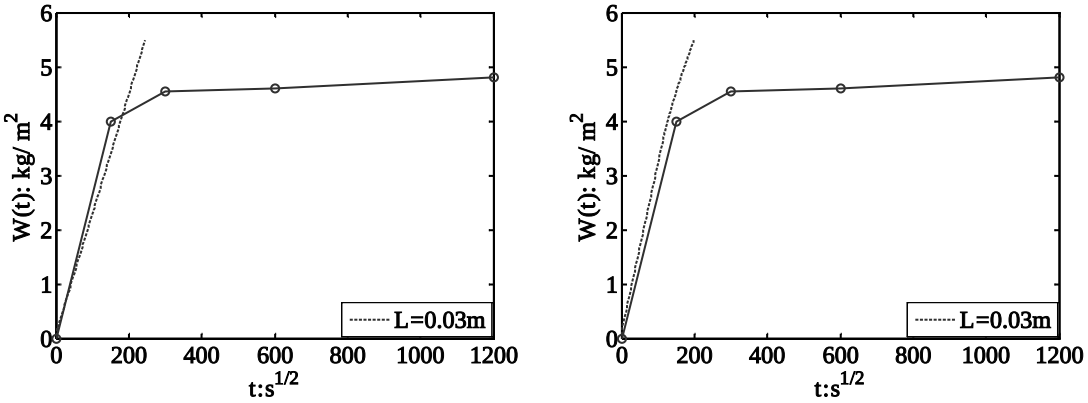

$a)\ l_1 : l_2 = 1:1, r_1 : r_2 = 1:0.1$ $b)\ l_1 : l_2 = 2:1, r_1 : r_2 = 1:0.1$

Figure 10- Experimental data [3](full lines) and analytical (dashed lines) water absorption curves $\left(W(t) - \sqrt{t}\right)$ *for slices with* $w/c = 0.40$ *and* $p_{tot} = 0.18$.

The total length of the model pipes compared to the thickness of the specimen is a matter of uncertainly. We have in most of our comparisons between calculated and experimentally measured capillary suction assumed a total pipe length equal to the thickness of the specimens. Due to factors such as entrapment of air in a network and torturousity this may be wrong and we should expect the model suction to stop before the experimental suction. However, this is not always seen, for example in the 20 mm thickness slices of own data, and also in the data [3]. Clearly more work in the calculation of the correct total absorption should be made. We believe, however, that the present investigation has shown that the kind of narrowing or pore-neck effect proposed can at least partly explain the deviation from the square root time law often seen in concrete capillary suction experiments.

The present results also demonstrate a contradiction between the restriction of capillary theory due to the tensile strength of water (minimum capillary pore size approximately $3\times10^{-7}\,m$) and the application of a sort of "effective capillary radius" which can be as low as $10^{-11}m$ when applying Eq.13, see also [2], [4], [6], [13]-[15]. This scale problem is possibly solved to a large part by the accumulated effect of repeated necks with high flow resistance, possibly together with some kind of slow diffusion mechanism filling the gel-type pores smaller than those filled by the capillary mechanism. This could be further investigated in future modelling with some sort of overlapping diffusion-loss from the water in the pipe-shaped pores into the pipe walls made of gel-material. This introduction of a multi-scale mechanism would still keep the model on a relatively simple yet realistic and sound physical basis, provied that an algorithm or computational method requiring little computational power can be developed.

Finally we should also mention that the total porosity in the model absorption was taken as total porosity to water. The filling mechanisms is, however, only active in a fraction of the pore volume. This also has take to be taken better care of in more advanced modelling, possibly by the kind of multi-scale modelling mentioned above.

5 CONCLUSIONS

Comparison of capillary suction experiments on concrete with different binder qualities and specimen thickness was made with a relatively simple pipe model consisting of a series of pipes with different diameter and length put together at regular intervals and also using random sized pipes.

The objective was to investigate to what extent the very slow capillary absorption with increasing deviation from the straight line square root of time law could be explained with narrow pore necks. Following the development and validation of the model on local flow conditions in part 1, we have here made a systematic comparison with real capillary absorption data from own experiments as well as some experimental data from the literature.

Realistic time scales for capillary filling can be obtained for series of pipes consisting of only large and small pipes of diameter in the order 1 and 0.1 microns, respectively. There has to be somewhat larger length than radius for the larger pipe in order to fit capillary suction for $w/c = 0.60$ compared to $w/c = 0.45$. The calculated capillary absorption then fits our experimentally measured absorption in slices with different thickness (20,40 and 100 mm), in line with the increased number of necks with increasing thickness and higher fraction of coarser capillary at heigh w/c . The comparison with experiments from the literature were in line with the comparisons with own experiments.

6 ACKNOWLEDGMENT

The authors would like to thank to Prof. Erik J. Sellevold at The Norwegian University of Science and Technology (NTNU) in Trondheim who suggested to model capillary absorption based on Laplace equation with multiple pipes as the starting for a model. The first author gratefully thanks Narvik University College and the university of Tromsø for the sholarship.

REFERENCES

[1] Hung, Nguyen T.; Frank, Melandsø; Stefan, Jacobsen (2009): Analytical and numerical solution for capillary suction velocity and hight in pores with multiple sizes. *Paper part 1, submitted together with this paper.*

[2] Hoff, W. D.; Hall, C.(2002): Water transport in brick, stone and concrete. Spon press London and New York. , 318p.

[3] Hazrathi , K. (1998): Etudes des mechanismes de transport de l'eau par absorption capillare dans des materiaux cimentaires conventionels et de haute performance. PhD, Laval University.

[4] Erik, J. Sellevold; Jonni, Punkki. (1994): Effects of drying procedure. Nordic Concrete Research. 15, 59--74.

[5] Hansic, L. (2005): Capillarity in concrete. PhD, University of Lubljana.

[6] Fagerlund, G. (1982): On the capillary of concrete. Nordic Concrete Research. 1, 20p.

[7] Powers, T. C.; Brownyard, T. L.(1948): Research Lab. Portland Cement Associantion. Bull. 22 .

[8] Wen-Bin Young. (2004): Analysis of capillary flows in non-uniform cross-sectional capillaries. Colloids and Surfaces A: Physicochem. Eng. 234, 123--128.

[9] Karoglou, M.; Moropoulou, A.; Giakoumaki, A.; Krokida, M.K. (2005): Capillary rise kinetics of some building materials. Colloids and Interface Science. 284, 260--264.

[10] Barbare, Nikhil; Shukla, Arun; Bose, Arijit. (2003) : Uptake and loss of water in a cenosphere-concrete composite material. Cement and Concrete Research. 33, 1681--1686.

[11] Erik J. Sellevold; Tom Farstad (2005): The PF-method-A simple way to estimate the w/c-ratio and Air content of Hardened Concrete. Mindess Symposium ConMat Conference, UBC, Vancouver Canada .

[12] Matlab versjon 7.4.0 .

[13] Garboczi, E. B. D. (1999): Computer simulation and percolation theory applied to concrete. Annual reviews of computational Physics VII, World Sc. Publ. comp. , 85--123.

[14] Fagerlund, G.(1991): Unpublished data cited by E.J Sellevold in course compendium post graduate course Concrete Structure. Norway Univ. Science and Technology.

[15] Nicos, S. Martys; Chiara, F. Ferraris (1997): Capillary transport in mortars and concrete. Cement and Concrete Research 27, 747--760.

Paper 3

Time dependent surface heat transfer in light weight arrogate cement based materials

Paper 4

Flow calculation and thermodynamics in wet frost exposure of cement based materials

Paper presented at International RILEM Symposium on Advances in Concrete through Science and Engineering 22-24 March 2004, North Western Univerity, Evanston, Illinois, USA

FLOW CALCULATION AND THERMODYNAMICS IN WET FROST EXPOSURE OF CEMENT BASED MATERIALS

Stefan Jacobsen[1], Frank Melandsø[2], Hung Thanh Nguyen[1,2]
1. Narvik University College, Norway, 2. University of Tromsø, Norway

Abstract
The calculation of moisture transport from a wet surface and into cement based materials (CBM) exposed to frost is further studied, limited to a case with continuously wet surface and constant temperature gradient dT/dx. The pressure created during phase transition of pore water to ice in the highly saturated CBM is considered a major driving force. The pressure is first calculated and analyzed using reversible thermodynamics. The pressures measured in practice and deduced theoretically vary within a rather large span. This is discussed in relation to the involved quantities (volume of unfrozen water and ice, enthalpy). Transport is calculated using d'Arcys law in the described wet frost exposure. Gradients dT/dx of various wet frost tests, as well as realistic enthalpies and volumes are used. Predicted flow varies approximately two decades using the chosen realistic values of dT/dx (20 – 100 K/m) and observed freezing temperatures (255 – 263 K). Experimental flow data from a wide variety of concretes and wet frost exposure conditions have similar values as the calculated values, indicating that the proposed approach can be used. The driving force for flow and the disruptive pressure in the degradation of the material stem from the same thermodynamic phenomena. The implication of this is that service life calculation must be based both on the freeze/thaw transport ("pumping effect") and on the subsequent degradation. Finally, further work in calculation/numerical simulation and experiments are discussed.

Key words: frost, thermodynamics, permeability/flow, cement based materials, nano porosity

1. Introduction

Most of the research on durability of building materials has been devoted to studies of their deterioration under various exposure conditions. This is mainly due to the large economic importance of too short service life of deteriorating civil engineering structures due to frost, corrosion, chemical attack etc or due to inadequate performance (barrier-, structural-, visual etc). Most research on frost action on porous building materials and particularly cement based materials has historically focused on various tests and the rate of destruction observed in these tests. Wet freeze/thaw exposure is a special exposure situation in which water is present at the material surface during frost exposure. It results in a very high transport rate of liquid into the material, a pumping effect. This accelerated absorption has been observed in many different kinds of exposure (cracking tests, scaling tests, in water, in 3 % NaCl, varying cooling rate, time of freezing etc) and CBMs (ordinary Portland cement concrete, high performance concrete, light weight aggregate concrete, recycled aggregate concrete, silica fume, fly ash) [1-5].

Fax +4776966818
E-mail: sja@hin.no

Figure 1 shows an example, observed in 2 different tests on 3 different concrete mixes tested from 5 different Nordic tests laboratories when freezing with and without access to liquid. From the figures it is clearly seen how wet freeze/thaw accelerates the increase in degree of saturation during test compared to isothermal absorption above 0 °C. The first three days are isothermal (20 °C) in both experiments.

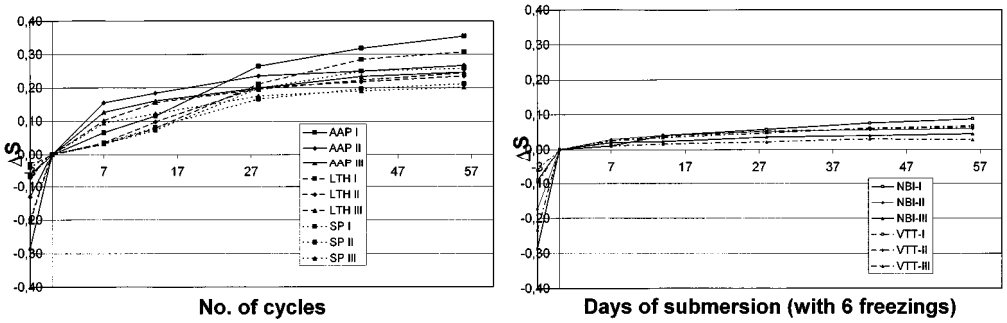

Figure 1: Increased degree of saturation vs. time for three different concretes [3]
a) wet freeze/thaw cycles b) isothermal absorption and sealed freezing

Therefore, the critical degree of saturation at which the material is deteriorating due to frost exposure [6,7] is reached faster in wet frost exposure than in isothermal absorption at temperatures above the freezing point of bulk water. Consequently, wet frost exposure is the most aggressive situation when it comes to risk of premature frost deterioration (surface damage, internal cracks/volumetric damage/loss of structural/mechanical properties) and hence low durability.

There are many approaches to study this, both experimentally and theoretically. The present paper is based on the authors own experiences, and earlier and later studies on thermodynamics and moisture transport during freezing. This includes studies on transport in frozen ground [8], the reduced frost heave by cement stabilisation [9], the correlation between frost heave and water transport in lime stabilized soil [10] as well as some newer reports on CBM, see for example [11-16].

Prior to the present approach, a calculation was made of uptake and flow during wet frost exposure in an ideal high performance concrete [4,16]. It was assumed that water in the saturated high performance hardened cement paste could flow but not freeze during wet freeze/thaw exposure. Absorption measured during wet freeze/thaw was found to be similar to calculated flow from the wet surface and into larger voids with low vapour pressure. However, this approach would limit the problem to materials without a capillary pore system containing water under capillary tension. This would exclude most CBM used in practice. Therefore, in the present paper it is assumed that a good portion of the pore water in a highly saturated cement based material can freeze at winter temperatures down to, say, -20 °C. First we calculate flow in reversible systems and compare with experimental data. Then a problem with this approach is discussed and a way further proposed.

2. Reversible thermodynamics combined with transport calculation

2.1 Pressure

At equilibrium between water and ice in a porous material we can assume that the surface tension between the two phases balances the pressure difference between them as shown by Radjy and co-workers [17]. In a sufficiently small pore with water and ice the pressure difference over a curved

Fax +4776966818
E-mail: sja@hin.no

interface may become very high. The energy and work associated with the cooling of a highly saturated porous material and subsequent phase transitions in the pore water are first calculated assuming an ideal reversible system where Gibbs free energy is unchanged on the phase transition:

$$dG = -SdT + VdP \tag{1}$$

where G = Gibbs free energy (J), S = entropy (J/K), T = temperature (K), V = volume of water (m^3) and P = pressure (Pa). It is assumed that (1) includes all work and energy change involved and follows the phase lines of the PT-diagram of ice (I)-water-vapour. It is also assumed that temperature- and pressure changes during phase transition can be ignored due to rather small changes in temperature both in terms of dT/dx and dT/dt (x: length, t: time). (At the end of the paper we discuss a new approach due to problems with these assumptions discussed in 3.1).

$$dG_i = dG_w \tag{2}$$

which gives

$$-S_i dT + V_i dP_i = -S_w dT + V_w dP_w \tag{3}$$

where subscripts i and w means ice and water. (3) can then be written as

$$(S_w - S_i)dT = V_w dP_w - V_i dP_i \tag{4}$$

and assuming a reversible equilibrium process:

$$(S_w - S_i) = \frac{\Delta H_f}{T} \tag{5}$$

where ΔH_f = enthalpy on freezing (J) and T = freezing temperature of water (K). T for pure water in porous materials like cement based materials or soils depends mainly on pore size, adhesion to pore walls or size of small particles, i.e. size and specific surface.

$$\Delta H_f = \Delta h_f \cdot w_{f,T} \cdot m_{spec} \tag{6}$$

where $w_{f,T}$ = freezeable water content (kg/kg dry material) of the porous material at temperature T (ºC) and Δh_f = heat of fusion of freezeable water (J/kg) assumed constant and m_{spec}= mass of specimen (kg). This results in Clapeyrons equation on the form:

$$V_w dP_w - V_i dP_i = \frac{\Delta H_f}{T} dT \tag{7}$$

This way of developing Clapeyrons equation can be found in various text books such as [18] and is based on the phase diagram of first order phase change. If the pressure is too high, second order phase transitions may occur and the triple point in the PT-diagram will move. However, other modifications than ice (I) require pressures above 200 MPa at the triple point [18], which at present seems unrealistic to occur in CBM.

Three possible ways of transferring additional absolute pressure (ΔP) in a highly saturated and freezing pore system can be deduced from equation (7) [19]. In the following equation (7) is integrated from T (< 273,15 K) to 273,15 K to obtain expressions for pressure generated. Firstly, if

Fax +4776966818
E-mail: sja@hin.no

the pressures of ice and unfrozen liquid are equal, $dP_w = dP_i = dP$ in equation (7) and we obtain equation (8).

$$dP = \frac{\Delta H_f dT}{(V_w - V_i)T} \Rightarrow \Delta P = \frac{\Delta H_f}{(V_w - V_i)} \ln(\frac{T}{273{,}15}) \quad (8)$$

Secondly, if the pressure of the unfrozen liquid is unchanged whereas the pressure of the ice changes, then $dP_w = 0$ in equation (7) resulting in equation (9). This case generates no liquid transport.

$$dP_i = -\frac{\Delta H_f}{V_i T} dT \Rightarrow \Delta P = \frac{\Delta H_f}{V_i} \ln(\frac{T}{273{,}15}) \quad (9)$$

Thirdly, if the pressure of ice is unchanged whereas the pressure of the unfrozen water changes, then $dP_i = 0$ in equation (7) resulting in equation (10).

$$dP_w = \frac{\Delta H_f}{V_w T} dT \Rightarrow \Delta P = \frac{\Delta H_f}{V_w} \ln(\frac{T}{273{,}15})) \quad (10)$$

Equation (8) appears most realistic since water and ice are likely to be in contact within a highly saturated porous material. By introducing La Places law for dP (se equation (13)) in equations (8) – (10) the size of the pore where the corresponding pressure is created can be deduced.

2.2 Transport

If we imagine that a unit of a CBM is cooled down homogeneously and/or without access to an external source of liquid, transport will take place internally in the pore system between unfrozen water in the smallest pores and ice according to equation (1) [20]. However, if we assume a negative gradient of temperature, dT/dx (K/m) from a wet surface and inwards, a flow may take place inwards. Figure 2 illustrates the case.

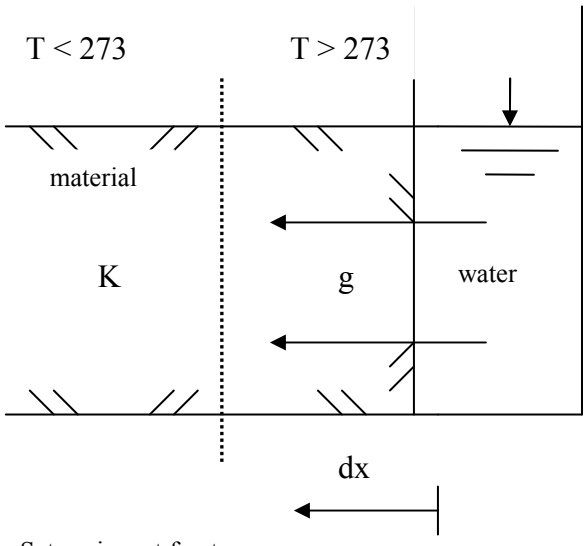

Figure 2: Set-up in wet frost exposure

Fax +4776966818
E-mail: sja@hin.no

In the further discussion the transport is assumed unidirectional mainly in the unfrozen zone of a cement based material with a wet surface and linear temperature – length gradient.

The set up of figure 2 is typical for many experimental studies on flow in wet freezing of various granular materials [21-27]. Also in the study of CBM and frost/salt exposure similar approaches where used, but with temperature below 0 °C in the salt solution [14,15] keeping the surface wet. In the studies of soil the pressure generated at the freezing site depended on transport and material. Pressures in the range 0,3 to 10 MPa were measured at the ice lens [21-23, 25, 26] whereas no such pressure measurements have been reported for CBM. In this paper we assume a cement based material with a high degree of saturation and a rather short exposure period in which steady state flow occurs. Concerning heat transfer it is for a start assumed that the major part of the flow takes place in the unfrozen part of the concrete, so that combined heat and mass transfer and Stefan-type problems are avoided. We simply assume D`Arcy flow:

$$g = K\frac{dP}{dx} \tag{11}$$

where g is steady-state flow (kg/m^2·s) and K is coefficient of permeability (kg/Pa·m·s) assumed constant with K = k/η where k = permeability (kg/m) and η = viscosity (Pa·s). (K must not be mixed with vapour permeability, δ_p, which has the same unit, but where vapour pressure is the driving force. When using vapour concentration difference as potential the vapour permeability is termed vapour diffusivity, δ_v, with the unit m^2/s). Assuming the freezing conditions of equation (8) we use dP of equation (11) obtaining:

$$g = \frac{K\Delta H_f}{(V_w - V_i)} \cdot \frac{1}{T} \cdot \frac{dT}{dx} \tag{12}$$

where g is steady-state flow through a section of temperature T. Note that we take dT to be the same as in equation (1) whereas T still is a temperature below 273,15 K of a section perpendicular to the direction of flow in figure 2. The minimum radius where ice is forming at T is found by combining equation (8) with Laplaces law, which for cylindrical pore shape is:

$$dP = -\frac{2\sigma}{r} \tag{13}$$

where σ = surface tension (water-ice: 0,031 N/m) and r = pore radius (m), the latter to be corrected for adsorbed layers. Data on σ can be found for example in [28, 29]. Experiments using two different techniques on parallel CBM specimens (low temperature calorimetry and mercury intrusion porosimetry) have given similar pore size distributions, see for example [30, 31], indicating that Laplaces law applies to meniscii in porous CBM.

3. Results and discussion

3.1 Pressure

In the following the pressures developed and the associated flow in the wet frost exposure situation of figure 2 are calculated and discussed. A few variations of parameters have been made. Then, a comparison with experimental data [2, 3, 16] is made. The parameters ΔH_f, V_w and V_i in

Fax +4776966818
E-mail: sja@hin.no

equations (8) and (10) have been varied according to table 1 to study the effect on transport as function of permeability.

Table 1: Variation of parameters in equations (8), (10) and (12)

No.	Eqn.	ΔH_f (J)	V_w (m^3)	V_i (m^3)
1	(8), (12)	Eqn. (6)	Unfrozen water (w_e-w_f)	$V_i = 1{,}089\ V_{wf}$ (V_{wf}= volume of freezeable water)
2	(8), (12)	Eqn. (6)	Total (water + ice) (w_e)	$V_i = 1{,}089\ V_{wf}$ (V_{wf}= volume of freezeable water)
3	(8), (12)	333780	0,001	0,001089
4	(10), (12)	Eqn. (6)	Unfrozen water (w_e-w_f)	-

The expression used in equations (8), (10) and (12) for freezeable water content as function of temperature down to 248 K is:

$$w_{fT} = -0{,}025 \cdot (T-273{,}15) \cdot w_e \qquad (14)$$

with T in K and w_e = evaporable water =0,06 kg/kg dry specimen and Δh_f = 333780 J/kg. Similar expressions were given in [32] for HCP. Also the amounts of ice measured using low temperature calorimetry in [30, 33, 34] (and more) would give approximately similar expressions, though not linear and shown to vary with both material (w/c, binder, age etc) and environment (ageing, water content etc). For various silts and clays non-freezeable water contents were studied in [35] giving the following type of expression for freezeable water:

$$w_{fT} = w_e - \alpha T^{\beta} \qquad (15)$$

where αT^{β} is non-freezeable water with α and β being material constants. In the calculations we assume a highly saturated well cured concrete of w/c $\approx$ 0.50, a bit less than 400 kg Portland cement per m^3 and no air entrainment. The evaporable water content of the saturated concrete is taken as 0,06 kg/kg dry material. However, depending on cement content and w/c it could be representative of many ordinary concrete qualities with capillary pore systems. Therefore we assume d'Arcy flow. In figure 3 the absolute pressures developed as function of temperature are shown based on equations (8) and (10) and the four variations of the two key parameters enthalpy and involved volumes of water and ice given in table (1).

Fax +4776966818
E-mail: sja@hin.no

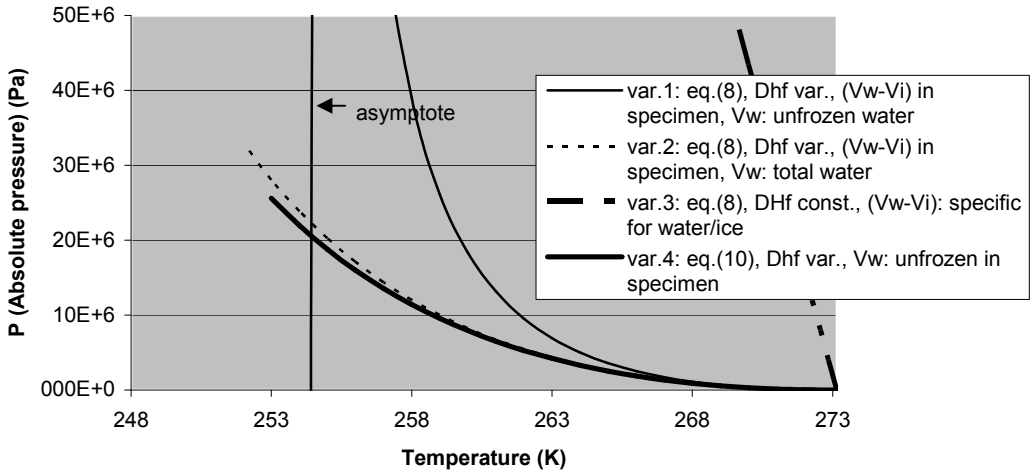

Figure 3: Absolute pressure on freezing of saturated material as function of temperature

Figure 3 shows that the calculated pressure very easily can be higher than the strength of many cement based materials even at rather moderate freezing temperatures. However, the volumes of water and ice, and heats of fusion that are used are essential to the result. The realistic material data (variation 1, 2 and 4) give a wide variety of pressures depending on the way they are used in the equations. In variation 3 we use the specific volumes of water and ice respectively as V_w and V_i in equation (8), as is normally done, [19]. This gives the highest pressure of the chosen variations.

There is also a possible anomalous behaviour in equation (8) when using variation 1 since the pressure is approaching infinity asymptotic from positive and negative side. That is, a shift from suction to pressure results when the volumes of ice and unfrozen water in the specimen are becoming equal. Whether this is physically possible in a porous material remains to be proved experimentally. If there is such an effect it would probably be in a highly saturated material where V_w and V_i are approaching during freezing. One could imagine this happening in a material that has a bit higher share of water in coarser pores compared to the share of water in very small pores. CBMs normally have a very high share of nano porosity where evaporable water in saturated specimens cannot freeze even at very low temperatures, as seen in [30, 31, 33, 34]. The calculated pressure could then increase as V_w and V_i are becoming equal as V_i is fed from V_w during freezing.

In variation 1, 2 and 4 we see that when using equation (10) the sign of the pressure is unchanged at not too low sub-zero temperatures. Whether there is a physical suction or pressure generated is something that will not be discussed further here. Transport towards the freezing site is what we see in practice (liquid uptake in wet frost exposure of cement based materials, water flow towards ice in the frost heaving of soil, vapour flow from the warm to the cold side of a house wall etc). However, we cannot eliminate the possibility that both things could happen, [19]. Here we shall only use absolute values as driving forces.

Fax +4776966818
E-mail: sja@hin.no

From figure 3 it is clear that more work is needed on which data to use for V_w, V_i and ΔH_f in the fairly simple equations developed from reversible thermodynamics and applied to highly saturated materials with high and low shares of coarse and very fine pores

During integration of equations (8) – (10) we assumed enthalpy to be constant, i.e. independent of temperature. As seen from equation (6) this is not the case. Inserting equation (14) or (15) into equation (6) and using this in equations (8)-(10) we get only a small additional linear function after integration. The variation of involved volume (V_w, V_i) is a much more important cause of the large variation of pressure in figure 3. It should also be noted that the term "enthalpy as function of temperature" used here might not be in strict accordance with that of other authors` [29, 33].

An important point to the use of the basic thermodynamics equations in section 2 of this paper is that to be able to keep the gradient situation in figure 2 energy must be continuously transferred due to transport of mass and heat, phase change, external work (changes in specimen volume), loss of heat etc. Equation (5) will in practice be like:

$$(TdS)_{idealreversible} = dQ_{war\min g} > dH_f \Rightarrow dS > \frac{dH_f}{T} \Rightarrow dS - \frac{dH_f}{T} > 0 \qquad (16)$$

In practice there can be uncontrollable accumulation of mass and change of volume (i.e unknown work performed by or on the system). This means that we probably have an irreversible process. Here we shall only state that equations (8) – (10) and (12) are simplifications based on equilibrium assumptions on the phase lines of the pT-diagram of water that may not be fully applicable in a transient situation with mass-and heat transfer. Some implications of this for better modelling are discussed in the next section.

3.2 Transport calculations

Figure 4 shows flow through a section with temperature T = 255 and 263 K and dT/dx = 20 and 100 K/m, as function of permeability. The enthalpy and volumes of variation 1 above have been used. It is seen how transport through a section of temperature T increases with increasing temperature gradient (dT/dx), inverse temperature and d'Arcy's permeability coefficient, as predicted by eqn. (12). The effect of enthalpy and volume involved on pressure was discussed in the previous section.

Fax +4776966818
E-mail: sja@hin.no

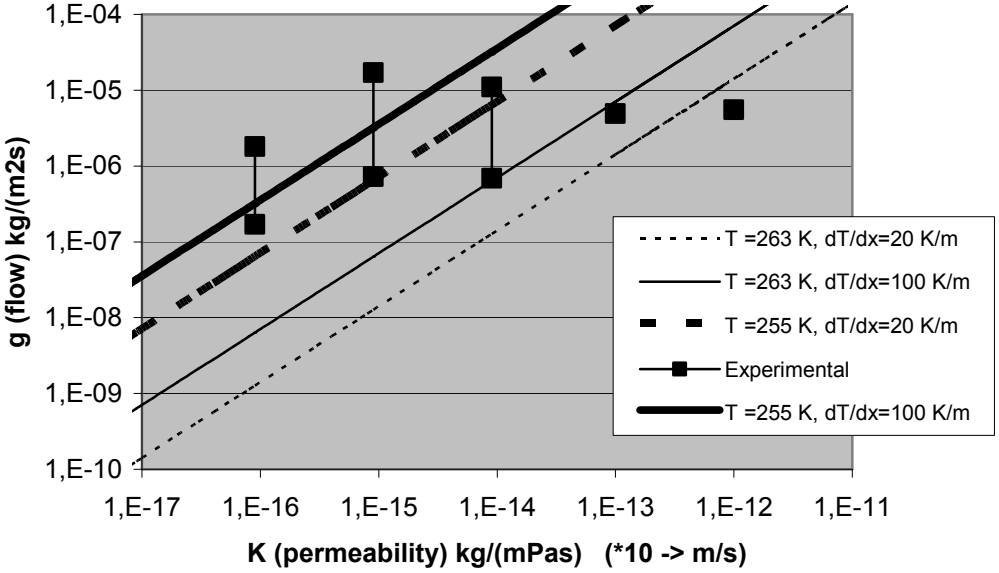

Figure 4 Transport through a section of temperature T in wet frost exposure using equation (12) and variation 1 of table 1 and figure 3. Experimental values are min and max of table 3

When observing figure 4 it is also important to keep in mind that since flow through a given section depends on temperature, the global flow into the specimen will not be steady state but increase inside the specimen as we move towards a sinking temperature below 0 °C. However, at the same time the permeability will be reduced by ice formation. Laboratory measurements of permeability in soil showed that K dropped 4 – 6 orders of magnitude in relatively permeable materials when frozen [36-38]. Most of the drop in permeability due to freezing occurred just below zero. The accumulated resulting flow into the wet end will be difficult to predict. The closer we get to the wet side the lower is the pressure and the higher is the permeability. In addition there is the simultaneous phase transition and heat flow. Also this problem will have to be dealt with using better models, see section 3.5.

3.3 Flow measured in wet frost exposure of concrete

Table 2 shows some characteristics of the experiments we have used data from. The flow and material data of table 3, also plotted in figure 4, were measured in four different wet frost exposure laboratory test conditions with varying gradients (dT/dx), number of cycles, wet period, pure water or salt etc [2, 3, 4, 16]. From figure 4 and table 3 we see that the experimental values are in the same range as the calculated values. However, the trend flow versus permeability is not very pronounced compared to in the model. It appears that a wide range of estimated permeabilities (K) (four decades) has a low influence on variation in observed flow (two decades). Note that the experimental values of the parameters of eq. (12); dT/dx, T, ΔH_f (i.e. w_f) and K vary considerably within the experiments. The largest numerical error is probably in the permeabilities, which are estimates based on [39]. For lower temperatures (255 K) and high dT/dx the calculation fits better for materials with low K. For a saturated material, low K normally would mean low w_f and that ice formation should affect K less than in materials with high w_f. For higher temperatures (263 K) and

Fax +4776966818
E-mail: sja@hin.no

low dT/dx the calculation fits better for materials with higher K (and consequently high w_f). Figure 4 is an indication that the present approach can be used, rather than an attempt of curve-fitting.

Table 2: Characteristics of wet frost exposure. T_{min} = 255 K in all cases.

Test method	**dT/dx (K/m)**	**Reference**	**Period wet freezing (% of time)**
ASTM C666 A	90 (measured)	[40]	5 (estimate)
SS 13 72 44	20 (measured)	[41]	12 (estimate)
CDF set-up	30-50 = 40 (measured)	[42]	10 (estimate)
Wet version of SS 13 72 44	10 (estimate)	[15]	100 (known)

Table 3: Flow data (based on weighing), w_e and w_f . K estimate based on [39]

Material *	**Ref.**	**g** kg/(m^2*s)			**W_e** (g/g$_{dry}$)	**$W_{f\text{-}10}$** (heat)	**K** kg/(m·Pa·s)
		ASTMC666 (90 K/m)	SS137244 (20 K/m)	CDF (40 K/m)			
067-00	[3]		5,5 * 10 $^{-6}$		0,076		~ 10 $^{-12}$
048-00			4,9 * 10 $^{-6}$		0,062		~ 10 $^{-13}$
040-00	[2]	4,5 * 10 $^{-6}$	1,9 * 10 $^{-6}$		0,054	0,004	~ 10 $^{-14}$
040-05		6,8 * 10 $^{-6}$	4 * 10 $^{-6}$	1,1* 10 $^{-5}$	0,058	0,004	
040-05A		1,8 * 10 $^{-6}$	6,9 * 10 $^{-7}$	4,1 *10 $^{-6}$	0,06		
035-08		4,8 * 10 $^{-6}$	4,8 * 10 $^{-6}$	1,7 * 10 $^{-5}$	0,058	0,001	~ 10 $^{-15}$
035-08A		2,5 * 10 $^{-6}$	7,6 * 10 $^{-7}$		0,065		
035-08L		1 * 10 $^{-6}$	7,2 * 10 $^{-7}$		0,089		
035-08Ls		2,5 * 10 $^{-6}$	3,9 * 10 $^{-6}$		0,185		
030-08		1,7 * 10 $^{-7}$			0,048	0,0018	~ 10 $^{-16}$
030-08L		1,8 * 10 $^{-6}$	4,8 * 10 $^{-7}$				
040-00A1	[15]						~ 10 $^{-14}$
040-00A3			3,6 -8,3				-
048-00							~ 5*
048-00A			*10 $^{-7}$				10 $^{-12}$
055-00A							

*: w/c and % silica fume, A: air entrainment, L/Ls: dry and saturated light weight aggregate

In addition to these data a couple of other studies have been performed in Scandinavia the last years on liquid uptake during wet frost exposure. In [14] thin concrete slices (app. 5 mm) were submerged into salt solutions at constant sub-zero temperature for 6 - 14 hours. The slices were weighed regularly during exposure. The slices must however be expected to have reached uniform temperature so that dT/dx ≈ 0. The measured weights calculated as steady state flow rates were in the lower range of table 3: ≈ 8*10^{-7} - 6*10^{-6} kg/(m^{2}s).

In [15] however, wet frost absorption measurements were performed in a similar manner but during a cooling and heating cycle (5 mm thick discs, dT/dt ≈ 10 K/h). A temperature gradient dT/dx therefore existed in these specimens, probably a bit less than 10 K/m. It was observed that liquid uptake increased as the temperature was lowered and that most of the liquid absorbed during freezing was expelled again during warming. Also in [43] with cyclic tests according to [44] some (but not all) of the water taken up was expelled during thawing, possibly as a consequence of the cyclic reversing of dT/dx. Another factor in the data of table 2 and 3 is the presence of salt in some

Fax +4776966818
E-mail: sja@hin.no

of the experiments. In brief, salt on the surface will reduce the free energy of the surface liquid and thus the potential for flow towards the ice. However, salt will also reduce the free energy and thus RH of solution in the pore system, which may increase the potential for transport. Salt on the surface will also increase the period of wet frost exposure. Salt on the surface may therefore increase transport compared to water.

3.4 Implications for service life

Even though a bit beyond the topic of this paper it should be mentioned that the pressure at a given subzero temperature can be both driving force for flow and destruction when surpassing the material strength. Therefore the pumping mechanism and the destruction mechanism are linked. It may then not be right to define frost damage as a function of two separated phenomena, i.e. first the water uptake and then the destruction on subsequent freezing when the critical degree of saturation is surpassed [6, 7]. In case of parallel processes we then will have to look into service life models where the destruction phase is included in the practical service life. A conceptual model for frost deterioration has been presented [45, 46]. Equations and material parameters for calculations can also be found in [12].

3.5 Implications for further modelling

As mentioned in section 2 there are new ways that can be used for calculation. Molecular simulation and modelling studies have been used in the study of ion-transport in cement based materials [47] and other porous media [48]. Also in the study of phase transitions within porous solids this numerical technique has recently been used for improved basic understanding [49, 50]. We hope to take advantage of some of this progress in our further study of mass transfer models in cement based materials under wet freezing conditions.

3.6 Implications for further experiments

Based on the presented model an experiment like in the set-up in figure 2 should be carried out to study effect of various parameters. By appropriate choice of material, thickness and temperatures it should be possible to observe non-destructive flow. Measurements of flow, moisture (destructive or non-destructive) and temperature distribution and mechanical behaviour would be data for both input and verification.

Table 4 gives an idea of practical temperatures, T, gradients, dT/dx and dimensions. The set-up could also be useful in the simultaneous study of redistribution of dissolved ions, contaminants etc due to freezing [27].

Table 4: Temperature (T), gradient (dT/dx) and depth (dx) below wet surface

		Depth (m) to T from wet surface of 275 K		
		T = 268 K	T = 263 K	T = 258 K
30		0,233	0,40	0,566
100	dT/dx	0,07	0,12	0,17
200	(K/m)	0,035	0,06	0,085
400		0,0175	0,03	0,0425

From table 4 we see that a practical length of a specimen would be in the order of 3 – 20 cm which is what is often used in frost heave tests. In a highly saturated material with not too low permeability it should be possible to register additional flow due to freezing in specimens of this size. A comparison with flow at isothermal conditions should always be performed to separate the flow mechanisms. It is believed that more work in the field of studies like [51] is needed.

Fax +4776966818
E-mail: sja@hin.no

4. Conclusions

The presented calculations based on simple reversible thermodynamics and comparisons with experimental data on flow during wet freeze/thaw indicate that the pressure created on freezing can cause the flow observed in experiments. However, the involved quantities (volume of water and ice, freezeable water, enthalpy) have a major effect on the calculated pressure and flow.

Service life modelling should take this into account since both driving pressure for transport and degrading pressure as the critical degree of saturation is surpassed are due to the same mechanism.

Improved models based on numerical modelling are needed. They should take into account an irreversible thermodynamic process involving both mass and heat transfer as well as mechanical response.

Some practical considerations on temperature gradient and depth below wet surface indicate that flow during wet frost exposure can be obtained in static wet frost experiments on specimens in the order of 3 – 20 cm thickness.

5. References

1. Jacobsen S. and Sellevold E.J., 'Frost/salt scaling testing of concrete – importance of absorption during test', Nordic Concrete Research Publication 14 (1) (1994) 26-44.
2. Jacobsen S., Dr.Ing. thesis 101, Norwegian Inst. Of Technology, Trondheim ISBN 82.7119-851-3 (1995) 286 p.
3. Jacobsen S., Bager D., Kukko H., Tang L. and Nordstrøm K., 'Measurement of internal cracking as dilation in the SS 137244 frost test', Nordtest project 1389-98, Norw. Build. Res. Project report 250 ISBN 82-536-0645-1 (1999) 26 p./5 app.
4. Jacobsen S., 'Liquid uptake mechanisms in wet freeze/thaw: review and modelling', in 'Frost damage in Concrete', RILEM PRO 25, ISBN 2-912143-31-4, D.Janssen, M.Setzer, M.Snyder (eds.) (2002) 41-51
5. Jacobsen S. and Lahus O.: 'High volume fly ash RCC for dams: freezing and thawing durability', in ACI Special Publication SP202 (2002) 17 p.
6. Whiteside T.M and Sweet H.S., 'Effect of mortar saturation in concrete freezing/and thawing tests' Proc. HRB 30 (1950) 204-216
7. Fagerlund G., 'Degré critique de saturation – un outil pour l'estimation de la résistance au gel des matériaux des constructions', Matériaux et constructions 23 (4) (1971) 271-285
8. Perfect E., Groenevelt P.H., Kay B.D., 'Transport phenomena in frozen porous media' Transport Processes in Porous Media, J.Bear and Y.M.Corapcioglu (eds.) Kluwer Academic Publishers, Netherlands (1991) 243-270
9. Springenschmid R., 'Bodenstabilisierung mit zement', Tagungsberichte der arbeitsgruppe untergrundforschung Wien, 23 (1963) 121-140
10. Jessberger H., 'Bodenfrost', Strassenbau und strassenverkehrstech., Bonn 125 (1971) 179 p.
11. Zuber B. and Marchand J., 'Modeling the deterioration of hydrated cement systems exposed to frost action part 1: description of the mathematical model' Cem Con Res 30 (2000) 1929-1939
12. Setzer M., 'Micro ice lens formation and frost damage', ref. as [4] (2002) 1-16
13. Setzer M., 'Micro-ice-lens formation in porous solid',J Coll Interface Sci 243 (2001) 193-201
14. Lindmark S., 'Mechanisms of salt frost scaling' Dr.th.Lund Sweden TVBM1017 (1998) 266 p
15. Tange Hasholdt M., 'Experimental investigation of water uptake during cyclic freeze/thaw action', Dr.thesis part 3, DTI-Aalborg University, ISBN 87-7756-701-3 (2002) 39 p.

Fax +4776966818
E-mail: sja@hin.no

16. Jacobsen S., Calculating liquid transport into HPC during wet freeze/thaw, submitted to CCR (2000/2003) 12 p.
17. Radjy F.F.: 'Freezing and frost damage', Lecture notes Sellevold E.J et al Building Materials, Technical University of Denmark, Building Materials Laboratory (august 1971) 45 p.
18. Zemansky, M.W., 'Heat and Thermodynamics' 4th ed, McGraw Hill (1957) 484 p.
19. Sæthersdal R., 'Frost susceptibility of soil', Frost i jord 17 (1976) 125-151
20. Powers T.C., Helmuth R.A., Theory of volume changes in hardened Portland cement paste during freezing' Proc. HRB 32 (1953)285-297
21. Radd, F.J, Oertle D.H. Experimental pressure studies on frost heave mechanisms and the growth fusion behavour of ice in soils and glaciers Rep no.515-4-2-66, Conoco, Ponca City Oklahoma
22. Williams P.J.,'Pore pressure at a penetrating frost line and their prediction' Norw. Geot. Inst. Publ. 72 (1967) 51-72
23. Hoekstra P., 'Water movement and freezing pressures', Soil Sci Soc. Amer Proc 33 (1969) 512-518
24. Watanabe K. and Mitsoguchi M., 'Ice configuration near a growing ice lens in a freezing porous medium consisting of micro glass particles', J Cryst Growth 213 (2000) 135-140
25. Sutherland, H.B and Gaskin, P.N.,'Pore water and heaving pressures developed in partially frozen soils' 2nd Int. Permafrost Conf. Proc. Washington D.C (1973) 409-419
26. McGaw, R., Berg R.L, Ingersoll J.W., 'An investigation of transient processes in an advancing zone of freezing' 4th Int. Permafrost Conf. Proc. Nat.Ac.Pres Wash.DC (1983) 821-825
27. Gay, G and Azouni, M.A, 'Experimental study of the redistribution of heavy metals contaminants in coarse-grained soils by unidirectional freezing' Cold Regions Science and Technology 37 (2003) 151-157
28. Hesstvedt E., 'The Interfacial Energy Ice/Water', Norw. Geot. Inst. Publ.56 (1964) 7-10
29. Hansen E.W., Gran H.C, Sellevold E.J. 'Heat of fusion and surface tension of solids confined in porous materials derived from a combined use of NMR and calorimetry', J. Phys. Chem. B 101 (1997) 7027-7032
30. Sellevold E.J., Bager D.H., 'Low temperature calorimetry as a pore structure probe', 7th Int. Congr. Chem. Of Cement Vol.IV (1980) 394-399
31. Jacobsen S., Sellevold E.J., Matala S, 'Frost durability of High Strength Concrete: Effect of internal cracking on ice-formation, Cem and Concr Res 26 (6) (1996) 919-931
32. Powers T.C, Brownyard T.L., 'Studies of the physical properties of hardened portland cement paste, PCA Bull. 22, Skokie Ill. (1948)
33. le Sage de Fontenay C., Sellevold E.J., ASTM STP 691 (1980) 425-438
34. Bager D.H., Sellevold E.J., Cem Conc Res 16 (1986) 835-844
35. Anderson D.M and Tice A.R., 'Predicting unfrozen water contents in frozen soils', Highway Res. Rec 393 (1972) 12-18
36. Burt T.P and Williams P.J., 'Hydraulic conductivity in frozen soils', Earth Surface Processes 1 (1976) 349-360
37. Horiguchi K. and Miller R.D., 'Experimental studies with frozen soil in an "ice sandwich" permeamater' Cold Regions Science and Technology 3 (1980) 177-183
38. Horiguchi K.and Miller R.D, 'Hydraulic conductivity functions of of frozen materials' 4th Int. Permafrost Conf. Proc. Nat.Ac.Pres Wash.DC (1983) 504-508
39. Herholdt A et al. 'Beton Bogen' (The concrete book) Aalborg Portland 2nd ed Denmark (1985) 731 p.
40. Jacobsen S. and Sellevold E.J, 'Self healing of high strength concrete after deterioration by freeze/thaw', Cem Con Res 26 (1) (1996) 55-62

Fax +4776966818
E-mail: sja@hin.no

41. Petersson P.E. 'Concrete salt frost durability – test methods', Concrete and frost, Danish Concrete Association Publ.no.22 (1985) 307-328
42. Hartmann V., Optimising and calibration of frost salt scaling testing of concrete CDF-test Dr.Ing dissertation Universität GH Essen (1993) 128 p.
43. Rønning T.F., 'Freeze/thaw resistance of concrete. Effect of: curing conditions, moisture exchange and Materials', Dr.ing thesis 2001:4, Norwegian University of Science and Technology (2001) 11 ch/9 app
44. Swedish Standard SS 13 72 44, 'concrete testing – hardened concrete – scaling at freezing', CEN TC 51/WG12/TG4 European reference test "Test methods for the freeze/thaw resistance of concrete – part 1 scaling" (2000)
45. Bager D.H and Jacobsen S., 'A conceptual model for the freeze/thaw damage of concrete' in 'Frost resistance of building materials' K Fridh (ed) Proc 3rd Nordic res seminar, Lund Sweden rep TVBM-3087 (1999) 1-18
46. Bager D.H and Jacobsen S., 'A model for the destructive mechanism in concrete caused by freeze/thaw action', ref. as [4] (2002) 17-40
47. Kirkpatrick R.J.:, Yu, P., Kalinichev A.: 'Chloride binding to cement phases: exchange isotherm, ^{35}Cl NMR and molecular dynamics modelling studies', in Materials Science of Concrete Special Volume on Calcium Hydroxide in Concrete, Jan Skalny et al (ed) The American Ceramic Society (2001) 77-92
48. Martys, N.S., Chen H.: 'Simulation of multicomponent fluids in complex three-dimensional geometries by the lattice Bolzmann method', Physical review E 53 (1) (1996) 743-750
49. Brennan, J.K. and Dong W.: 'Molecular simulation of the vapour-liquid phase behaviour of Lennard-Jones mixtures in porous solids', Physical review E 67, 031503 (2003) 1-6
50. Radhakrishnan, R., Gubbins K.E., Sliwinska-Bartkowiak, M.: 'Global phase diagrams for freezing in porous media', Journal of Chemical physics 116 (3) (2002) 1147-1155
51. Kaufmann J. 'Experimental identification of damage mechanisms in cementitious porous materials on phase transition of pore solution under frost deicing salt attack', EMPA-EPFL These no 2037 (1999) 193 p.

6. Acknowledgement

Thanks to Professor Erik J. Sellevold at The Norwegian University of Science and Technology for comments and a helpful discussion on the nature of pressure during freezing.

Fax +4776966818
E-mail: sja@hin.no

ISBN xxx-xx-xxxx-xxx-x